

CONTRACT NO. NAS 2-2600

APPLICATION OF GALLIUM-ARSENIDE SOLAR CELLS TO SOLAR PROBE POWER SYSTEMS

FINAL REPORT

GPO PRICE \$ _____

CFSTI PRICE(S) \$ _____

Hard copy (HC) \$3.00

Microfiche (MF) .75

653 July 65

Prepared for

NATIONAL AERONAUTICS AND SPACE ADMINISTRATION
AMES RESEARCH CENTER
MOFFETT FIELD, CALIFORNIA

FACILITY FORM 602

N66 36101

(ACCESSION NUMBER)

88

(PAGES)

CR-69537

(NASA CR OR TMX OR AD NUMBER)

(THRU)

1

(CODE)

03

(CATEGORY)

By the

ASTRO-ELECTRONICS DIVISION
DEFENSE ELECTRONIC PRODUCTS
RADIO CORPORATION OF AMERICA
PRINCETON, NEW JERSEY



AED R-2817-1

2nd Issue: February 1, 1966

CONTRACT NO. NAS 2-2600

APPLICATION OF GALLIUM-ARSENIDE SOLAR CELLS TO SOLAR PROBE POWER SYSTEMS

FINAL REPORT

Prepared for

**NATIONAL AERONAUTICS AND SPACE ADMINISTRATION
AMES RESEARCH CENTER
MOFFETT FIELD, CALIFORNIA**

By the

**ASTRO-ELECTRONICS DIVISION
DEFENSE ELECTRONIC PRODUCTS
RADIO CORPORATION OF AMERICA
PRINCETON, NEW JERSEY**



AED R-2817-1

2nd Issue: February 1, 1966

TABLE OF CONTENTS

Section		Page
I	INTRODUCTION AND SUMMARY	1
	A. Summary	6
	B. Conclusions and Recommendations	7
II	SOLAR-CELL DEGRADATION FACTORS	11
	A. Degradation Due to Thermal Environment.	11
	B. Degradation Due to Charged-Particle Irradiation.	11
	C. Degradation Due to Ultraviolet Irradiation	16
	D. Degradation Due to Micrometeorite Environment.	17
	E. Degradation Due to Solar Wind.	17
III	CALCULATION OF I-V CURVE CHARACTERISTICS FOR SILICON AND GALLIUM-ARSENIDE SOLAR CELLS	19
	A. Introduction.	19
	B. Air-Mass-Zero Short-Circuit Current	21
	C. Air-Mass-Zero Maximum Power Current.	22
	D. Air-Mass-Zero Open-Circuit Voltage	23
	E. Air-Mass-Zero Maximum Power Voltage	24
	F. Summary of Results	24
	G. Effect of Solar Cell Mismatch on Output Power	25
	H. Off-Normal Incidence Operation of Solar Cells	32
	I. Conclusions.	32
IV	THERMAL CONTROL METHODS	33
	A. Temperature Control Techniques for Near-Earth Trajectories	33
	B. Thermal Control by Tilting the Solar Array with Respect to the Sun Vector.	34
	C. Thermal Control Using a Deployable Sun Shield.	37

TABLE OF CONTENTS (Continued)

Section		Page
IV	D. Thermal Control of Spinning Cylindrical Array by Varying the Array Packing Fraction.	46
	E. Thermal Control Using a Hybrid System of Array Tilting and Cylindrical Mirror.	49
V	SOLAR-ARRAY PARAMETERS FOR THE FOUR SOLAR PROBE MISSIONS	57
	A. Solar-Array Parameters for the 0.4-AU Mission	57
	B. Solar-Array Parameters for the 0.51-AU Mission	60
	C. Solar-Array Parameters for the 0.291-AU Mission	62
	D. Solar-Array Parameters for the 0.09-AU Mission	64
	E. Summary of Array Parameters for the Four Solar Missions	66
VI	DEVELOPMENT PLAN FOR THE GALLIUM-ARSENIDE SOLAR ARRAY.	69
	A. Phase I: Investigation of Solar-Cell and Solar- Cell-Assembly Characteristics	70
	B. Phase II: Device and Materials Development	73
	C. Phase III: Solar Panel Design, Development and Test	74
	D. Phase IV: Design, Fabrication and Test of Flight-Model Solar-Array System	76
	REFERENCES AND BIBLIOGRAPHY	79
APPENDIX		
	OPTIMUM GRID SPACING.	A-1

LIST OF ILLUSTRATIONS

Figure		Page
1	Solar Probe Trajectory for 0.4-AU-Perihelion	2
2	Solar Probe Trajectory for 0.51-AU-Perihelion	3
3	Solar Probe Trajectory for 0.291-AU-Perihelion	4
4	Solar Probe Trajectory for 0.09-AU-Perihelion	5
5	Air-Mass-Zero Conversion Efficiency of Gallium-Arsenide and Silicon Cells as a Function of Temperature	12
6	Omnidirectional Solar Proton Environment in the Vicinity of the Earth	12
7	Silicon Solar Cell Parameter Degradation Versus Proton Flux	15
8	Gallium-Arsenide Solar Cell Parameter Degradation Versus Proton Flux	15
9	I-V Curves for 0.4-AU Mission	30
10	I-V Curves for 0.51-AU Mission	30
11	Predicted I-V Curves for 8.6 Percent Efficient Gallium- Arsenide Solar Cell at 10-Sun Intensity	31
12	Predicted I-V Curves for 8.6 Percent Efficient Gallium- Arsenide Solar Cell at 5-Sun Intensity	31
13	Solar Intensity Versus Orbit Time for Sun-Earth Elliptical Orbits	35
14	Thermal Analysis Model of Flat Array with One Axis Rotation with Respect to Sun Vector	36
15	Array Temperature as a Function of Tilt Angle (θ) and Solar Intensity for Silicon or GaAs Cells, $\left(\frac{\bar{\alpha}}{\bar{\epsilon}}\right)_{\text{cell}} = 0.7$. . .	38
16	Array Temperature as a Function of Tilt Angle (θ) and Solar Intensity for Silicon or GaAs Cells, $\left(\frac{\bar{\alpha}}{\bar{\epsilon}}\right)_{\text{cell}} = 1.1$. . .	39
17	Array Power Output as a Function of Tilt Angle and Solar Intensity for Gallium-Arsenide Cells, $\left(\frac{\bar{\alpha}}{\bar{\epsilon}}\right)_{\text{cell}} = 0.7$. . .	40

LIST OF ILLUSTRATIONS (Continued)

Figure		Page
18	Array Power Output as a Function of Tilt Angle and Solar Intensity for Gallium-Arsenide Cells, $\left(\frac{\bar{\alpha}}{\bar{\epsilon}}\right)_{\text{cell}} = 1.1$	40
19	Thermal Analysis Model of Flat Array with Deployable, Intensity-Reducing Sun Shield	41
20	Array Temperature for Silicon or GaAs Cells as a Function of Solar Intensity, Configuration Factor and Number of Shield Layers (Eight-Percent Shield-Hole Area)	42
21	Array Temperature for Silicon or GaAs Cells as a Function of Solar Intensity, Configuration Factor and Number of Shield Layers (Ten-Percent Shield-Hole Area)	43
22	Array Power Output for Gallium-Arsenide Cells as a Function of Solar Intensity, Configuration Factor and Number of Shield Layers (Eight-Percent Shield-Hole Area)	44
23	Array Power Output for Gallium-Arsenide Cells as a Function of Solar Intensity, Configuration Factor, and Number of Shield Layers (Ten-Percent Shield-Hole Area)	45
24	Configuration Factor as a Function of Normalized Spacing Distance Between Solar-Cell Array and Sun Shield	46
25	Thermal Analysis Model of Spinning Cylindrical Array	47
26	Array Temperature for Silicon or GaAs Cells as a Function of Solar Intensity and Packing Fraction (β) on a Spinning Cylindrical Array	48
27	Array Power Output for Gallium-Arsenide Cells as a Function of Solar Intensity and Packing Fraction (β) on a Spinning Cylindrical Array	49
28	Cylindrical Mirror Geometry	51
29	Cylindrical Mirror Cooling Method	52
30	Cylindrical Mirror Positioning Diagram	54
31	Array Power Output for Hybrid Gallium-Arsenide Cell System as a Function of Solar Intensity and Array Tilt Angle, $\left(\frac{\bar{\alpha}}{\bar{\epsilon}}\right)_{\text{cell}} = 0.7$	55

LIST OF ILLUSTRATIONS (Continued)

Figure		Page
32	Array Power Output for Hybrid Gallium-Arsenide System as a Function of Solar Intensity and Array Angle, $\left(\frac{\bar{\alpha}}{\bar{\epsilon}}\right)_{\text{cell}} = 1.1 \dots\dots\dots$	56
33	Maximum Power Output of Silicon and Gallium-Arsenide Solar Cells Versus Orbit Time for 0.4-AU Extended Pioneer Trajectory	58
34	Maximum Power Output of Silicon and Gallium-Arsenide Solar Cells Versus Orbit Time for 0.51-AU Advanced Pioneer Trajectory	61
35	Maximum Power Output of Silicon and Gallium-Arsenide Solar Cells Versus Orbit Time for 0.291-AU Advanced Pioneer Trajectory	63
36	Maximum Power Output of Gallium-Arsenide Solar Cells Versus Orbit Time for 0.09-AU Advanced Pioneer Trajectory	65

LIST OF TABLES

Table No.		Page
1.	I-V Curve Characteristics at Beginning of Missions	20
2	Temperature Shift Parameters	20
3	I-V Curve Characteristics for 0.09-AU Mission	26
4	I-V Curve Characteristics for 0.291-AU Mission	27
5	I-V Curve Characteristics for 0.4-AU Mission	28
6	I-V Curve Characteristics for 0.51-AU Mission	29
7	Thermal Properties of Various Solar-Cell Array Construction Materials	37
8	Silicon and Gallium-Arsenide Solar-Cell Array Parameters for Minimum Output of 55 Watts During 0.4-AU Mission . .	59
9	Array Area as a Function of Distance of Closest Sun Approaches for GaAs and Silicon Solar-Cell Spinning Cylindrical Arrays	59
10	Silicon, Gallium Arsenide, and Hybrid Solar-Cell Array Parameters for Minimum Output of 285 Watts During 0.51-AU Mission	61
11	Silicon, Gallium-Arsenide, and Hybrid Solar-Cell Array Parameters for Minimum Output of 285 Watts During 0.291-AU Mission	63
12	Gallium-Arsenide Solar-Cell Array Parameters for Minimum Output of 285 Watts During 0.09-AU Mission . . .	65
13	System Characteristics of Silicon, Gallium-Arsenide, and Hybrid Solar-Cell Arrays for the Four Solar-Probe Missions	68
14	Development Plan Schedule	77

SECTION I

INTRODUCTION AND SUMMARY

36101

This is the final report of a six-month study performed for the NASA-Ames Research Center by the Astro-Electronics Division of RCA, under Contract NAS 2-2600. The study was undertaken to establish the "power system applications of gallium-arsenide solar cells for solar probe missions." The major purposes of the study were to determine whether silicon or gallium-arsenide solar cells are at all applicable to solar-probe missions, and to establish the weight, area, and cost requirements for using such solar cells in solar probe missions. (The specific missions considered involved solar probe trajectories approaching to within 0.4 AU*, 0.51 AU, 0.291 AU, and 0.09 AU of the Sun. Trajectories for these missions are presented in Figures 1 through 4, respectively.)

The results of this study indicate that, with the use of suitable temperature-control techniques, gallium-arsenide solar cells will be a practical source for missions with solar approach distances down to 0.07 AU. Closer approaches will be feasible only if area, weight, or cost can be increased beyond those limits which presently appear practical.

As solar cell temperature tends to rise with decreasing perihelion, an important part of the effort involved conceptual design of reliable, lightweight, temperature control systems. For each temperature control technique considered, three different types of solar array designs were developed, to independently minimize weight, area, and cost per unit of power. Selected temperature control techniques were considered to correlate system design with distance from the Sun, establishing practical limits for the minimum perihelion. (There is no theoretical limit on perihelion; the minimum distances developed in this analysis are based on practical weight and space limitations.)

All findings of this study are based upon practical weight, area, and cost considerations for each of the four solar-probe trajectories. However, as realistic values of solar-array temperatures are ultimately dependent upon spacecraft configuration and thermal design, the thermal considerations presented in this report are subject to modification as required to reflect the specifics of power system and spacecraft design.

* AU = "astronomical unit." One AU is defined as the mean distance from the Earth to the Sun.

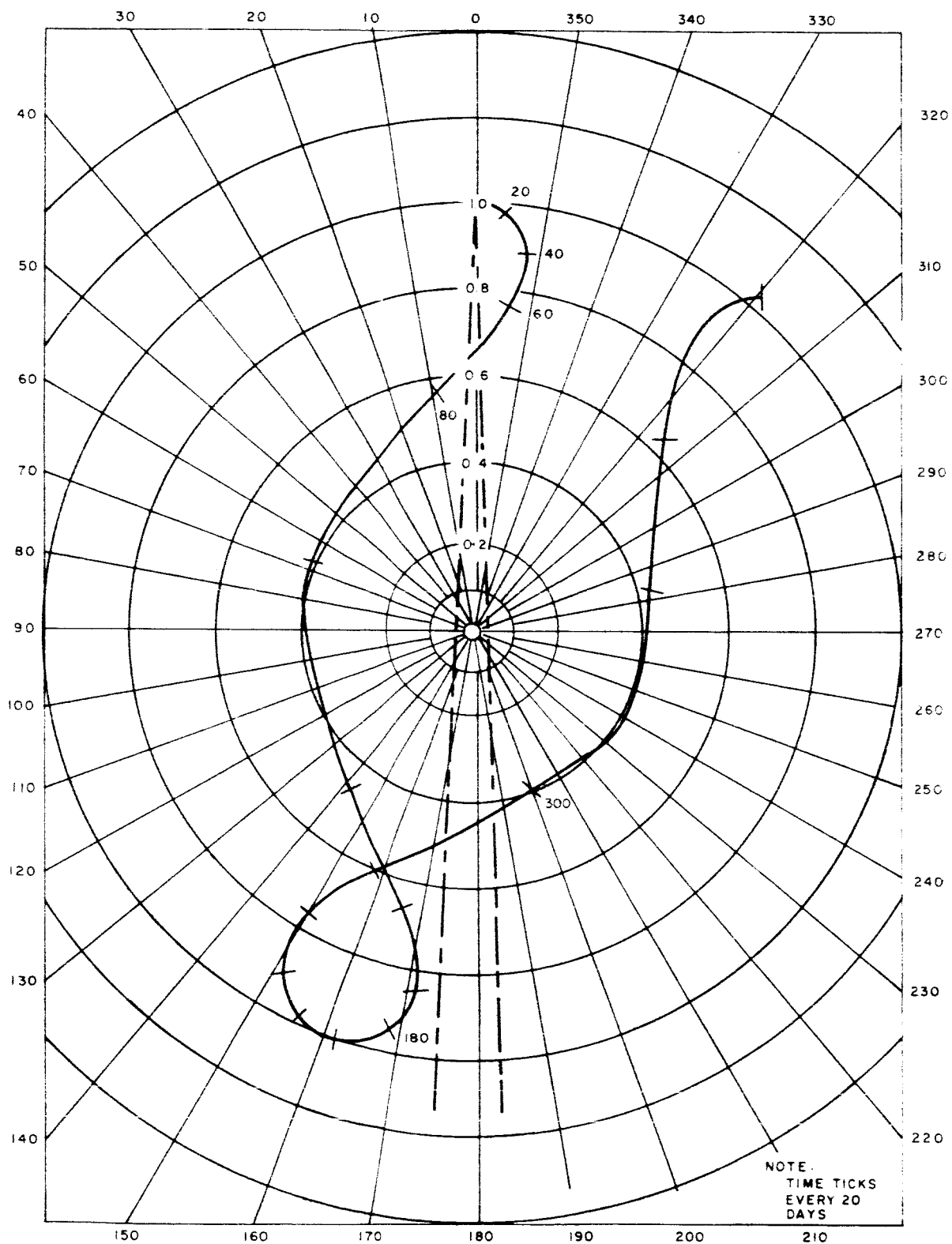


Figure 1. Solar Probe Trajectory for 0.4-AU Perihelion

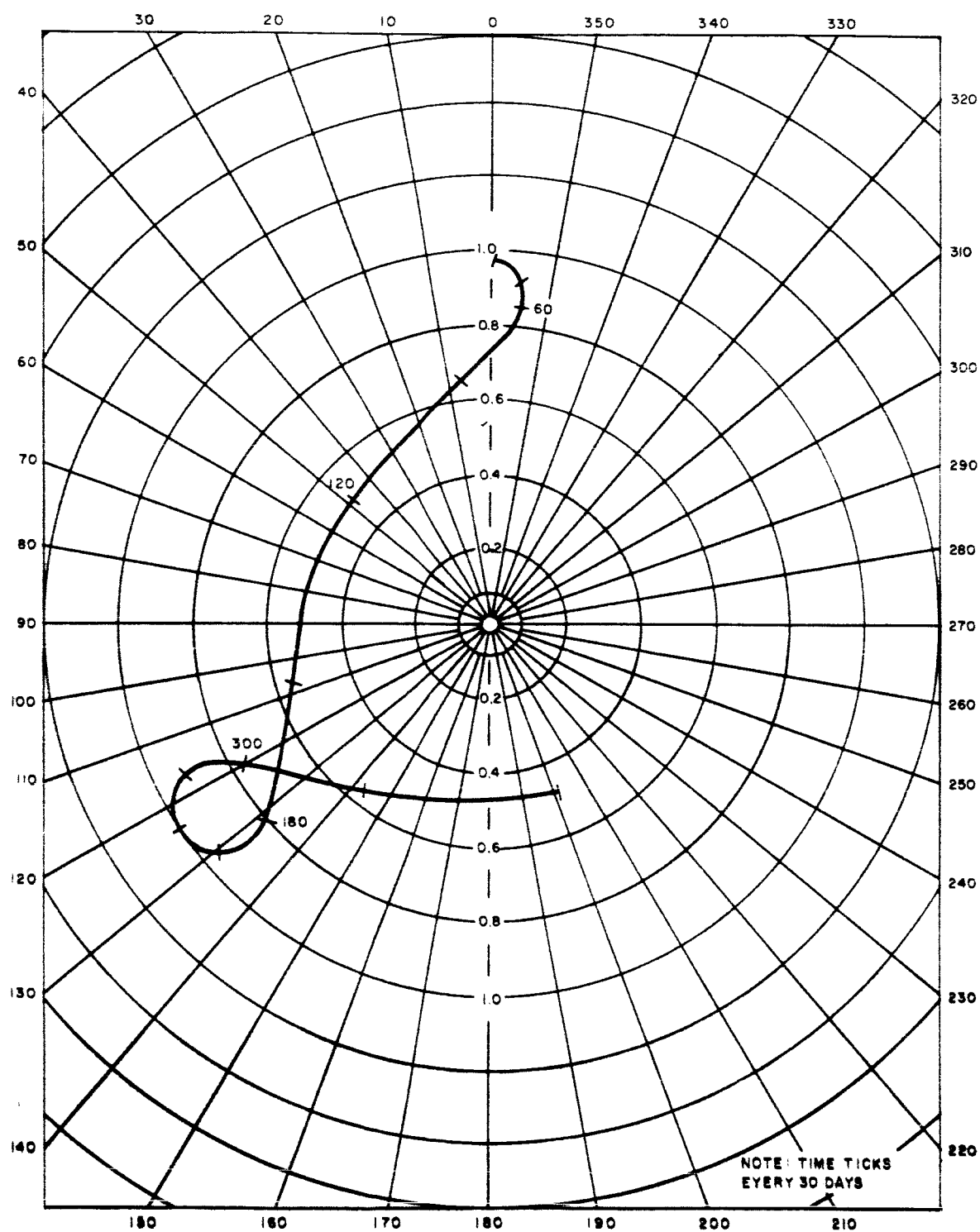


Figure 2. Solar Probe Trajectory for 0.51-AU Perihelion

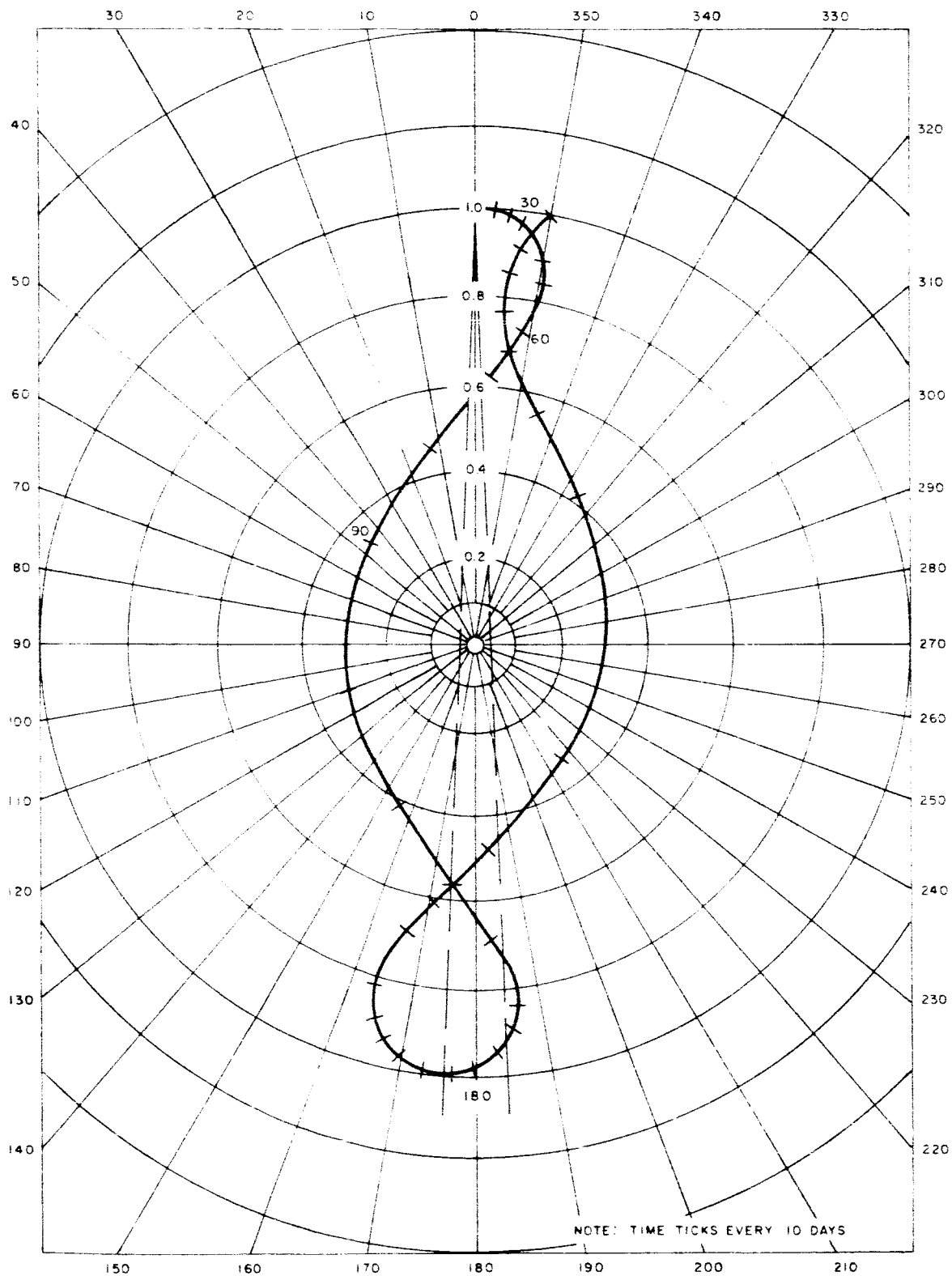


Figure 3. Solar Probe Trajectory for 0.291-AU Perihelion

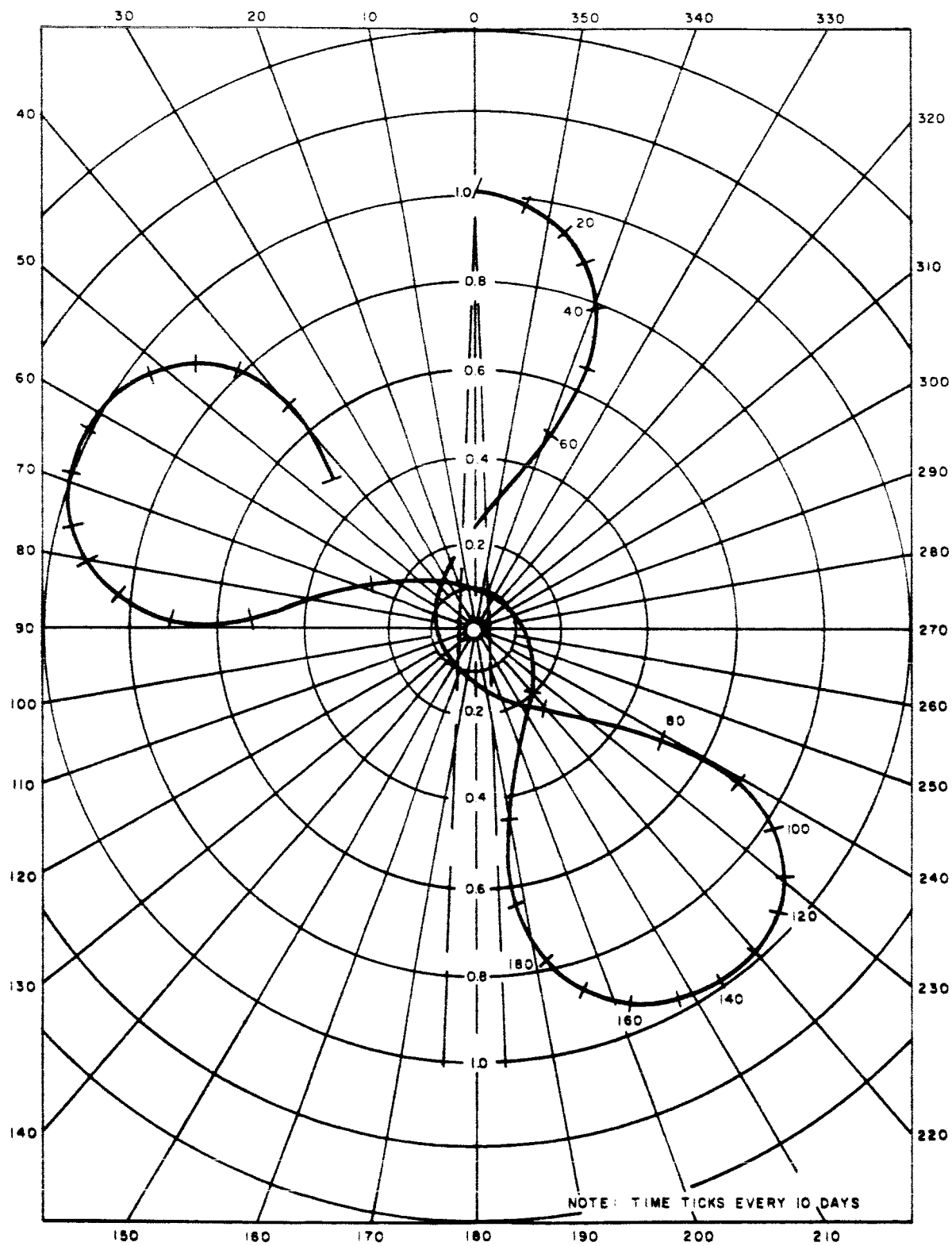


Figure 4. Solar Probe Trajectory for 0.09-AU Perihelion

A. SUMMARY

As noted earlier, the specific missions considered in this study involved perihelions from 0.51 to 0.09 AU. A design requirement was that the solar array provide a continuous power output, not falling below a specified level, for the entire duration of each of these missions. Thus, the possibility of varying the system duty cycle to fit the mission profile was not considered. However, such a possibility must be kept in mind. The solar cell output will slowly vary as the spacecraft approaches the Sun, and a saving in array area could be realized by matching the system power requirements to these variations.

An important part of the study involved analyzing the effects of environmental factors on solar cell operation. Specific factors considered for each of the four trajectories were high temperature, electron and proton irradiation, ultraviolet irradiation, micrometeorite bombardment, and solar wind. Charged-particle flux encountered for each trajectory was calculated and converted to a damage equivalent of normally incident 17.6-Mev proton flux. Output characteristics of gallium-arsenide and silicon solar cells were calculated as functions of mono-energetic flux.

The efficiencies of both gallium-arsenide and silicon solar cells were determined as functions of operating temperature and irradiance. (This analysis was based upon characteristics of typical state-of-the-art cells, extrapolating the current-temperature and voltage-temperature coefficients to conditions of high illumination intensity.) The effects of variations in solar-cell base resistivity and spectral response, and the effects of non-normal illumination incidence, were also considered.

Based on the analyses described above, electrical output versus time was plotted for each of the four selected trajectories, for both gallium-arsenide and silicon solar cells. The following solar array characteristics were determined:

- Perihelion power;
- Power-to-area ratio;
- Power-to-weight ratio;
- Power-to-cost ratio.

Thermal analyses were performed to develop several (general) temperature control techniques applicable to use in solar probe missions. Four methods of array deployment were considered, each of which provides a lower operating temperature than would a flat array oriented normal to the sun vector:

- (1) Tilting the array with respect to the sun vector;
- (2) Deploying a sun shield to reduce the intensity of incident radiation;
- (3) Reducing the packing factor (ratio of solar cell area to total array area); and
- (4) Tilting the array away from the Sun and using a cylindrical mirror to reflect the incident irradiation onto the array.

Both gallium-arsenide and silicon solar-cell arrays were designed for missions having 0.4*, 0.51**, and 0.291** AU perihelions. The minimum perihelion was calculated for the array design to be used in the Extended Pioneer (a spinning, cylindrical array). Hybrid arrays, consisting of both gallium-arsenide and silicon solar cells, were designed for the missions having 0.51-AU and 0.291-AU perihelions. Because of the severe temperatures anticipated, only a gallium-arsenide array was designed for the mission having a 0.09** AU perihelion. Temperature control techniques are required for silicon solar-cell arrays at the 0.291-AU perihelion and for gallium-arsenide solar-cell arrays at the 0.09-AU perihelion.

B. CONCLUSIONS AND RECOMMENDATIONS

The results of this study show that a solar cell array is a feasible power source for solar probe missions. The most severe environmental constraints imposed by the four missions considered (solar probe trajectories with perihelions of 0.4, 0.51, 0.291, and 0.09-AU, respectively) will be the high temperatures induced by proximity to the Sun. As high temperatures decrease solar-cell output, a thermal control system must be used for silicon solar-cell arrays at the 0.291-AU perihelion and gallium-arsenide solar-cell arrays at the 0.09-AU perihelion. Because of the greater temperature sensitivity of silicon solar cells, their use is precluded for the 0.09-AU mission.

If a 9-mil glass covering is provided, charged-particle radiation should produce no damage in a gallium-arsenide solar cell for any of the four missions considered. However, substantial radiation effects are anticipated for the silicon solar cells. For a 0.2-AU perihelion (the minimum perihelion for a silicon solar-cell array), charged-particle radiation would reduce the output of silicon cells by from 30 to 35 percent.

Because of the extremely wide range of array operating voltages (caused by the severe temperature excursions experienced along the trajectory), maximum power-point tracking must be used for every array. Such a tracking technique would cause the array power to be supplied at that voltage at which power output

* Extended Pioneer (Spin-stabilized Vehicle)

** Advanced Pioneer (Sun-oriented Vehicle)

is maximum, matching the power system requirements to the array characteristics at each point in time.

The assumptions made to perform the solar-cell power calculations reflect the uncertainty regarding photovoltaic energy conversion processes in the near-Sun environment. Gallium-arsenide solar cells appear very attractive for solar probes if the assumptions concerning high-intensity current generation and cell efficiency, linearity of temperature coefficients up to 575°K, and stable solar-cell performance during long periods of high-temperature operation are valid. However, before development can proceed, further experimental work must be carried out to test these assumptions.

Annealing of charged-particle irradiation damage in silicon at high temperatures (375 to 475°K) would considerably improve the array efficiency for those missions where high temperature does not preclude the use of silicon solar cells. Precise annealing rates as functions of temperature and damage types and rates also remain to be determined in subsequent programs.

Thermal control techniques are essential to near-Sun approaches with solar-cell arrays. The techniques considered in this study will reduce the operating temperature of the array by as much as 400°K from that experienced for a flat, normally oriented array.

Considerable experimental data must be obtained for both silicon and gallium-arsenide solar cells before a specific design of a solar array is attempted. Based on the information gathered during this study, further testing is recommended to determine:

- ◆ Ultraviolet irradiation degradation of the solar cell, cover glass, and cover-glass adhesive, expressed as a function of solar irradiance and temperature.
- ◆ Effects of high temperature on the stability of solar-cell operation, efficiency of energy conversion, functions of all array materials, and annealing of electron and proton irradiation degradation.
- ◆ Effects of high solar irradiance on the short-circuit current, open-circuit voltage, and output characteristics of solar cells, and the optimum grid contact configuration.
- ◆ Effectiveness of the temperature-control techniques described in this report.

In addition to these tests, it is further recommended that the gallium-arsenide solar-cell production facility at the Electronic Components and Devices Division of RCA be reestablished. This facility, which produced the high-efficiency gallium-arsenide cells analyzed during this study, is currently dismantled and the cognizant personnel have been reassigned. The successful development of the gallium-arsenide solar-cell arrays is dependent upon reestablishing this facility. This effort is defined in Phase II of the Development Plan.*

* As defined in the Development Plan, Section VI of this report.

SECTION II

SOLAR-CELL DEGRADATION FACTORS

Environmental factors which tend to degrade the power output of both silicon and gallium-arsenide solar cells will be encountered in the four solar-probe missions. A discussion of the thermal, charged-particle irradiation, ultraviolet irradiation, micrometeorite bombardment and solar wind environmental factors is presented in the following paragraphs. With the exception of the thermal factor, each of these environmental factors is cumulative and is not reversible.

A. DEGRADATION DUE TO THERMAL ENVIRONMENT

The primary degrading effect on solar-cell power output is the decrease in cell efficiency with increasing temperatures. Figure 5 shows the relationship of silicon and gallium-arsenide conversion efficiency as a function of cell temperature and equivalent solar intensity. At air-mass-zero efficiencies of 10.5 percent for silicon and 8.6 percent for gallium arsenide (measured at 300° K), these curves indicate that silicon cells retain their higher efficiencies until a temperature level of 380° K is reached. For higher temperatures, the gallium-arsenide cells are superior. Zero efficiency is reached at a temperature of 486° K for silicon while gallium arsenide does not reach zero efficiency until 560° K. The thermal effect noted here is instantaneous, noncumulative and reversible. Secondary thermal degrading effects also result due to the materials used for thermal and power optimization. Materials having low solar-absorptivity used on thermal control areas are subject to permanent degradation by ultraviolet irradiation, charged-particle irradiation, and micrometeorites. This degradation produces an increase in the array temperature. Multilayer optical filters bonded to the solar cell are temperature sensitive in that the cutoff points and the transmission level shift with temperature. The construction of the solar array must be such as to minimize thermal gradients between the cells and the substrate, especially for the high solar-constant missions, or serious degradations can result.

B. DEGRADATION DUE TO CHARGED-PARTICLE IRRADIATION

The charged-particle radiation environment that the solar cells will experience is assumed to consist primarily of solar-flare protons. This assumption is based on the information (shown in Figure 6) provided by the NASA-ARC solar-flare model. The flare particle count is specified as 8.5×10^{10} protons/cm²/year, at energies greater than 20 Mev and isotropic at 1 AU (solar-flare protons received in the vicinity of the Earth).

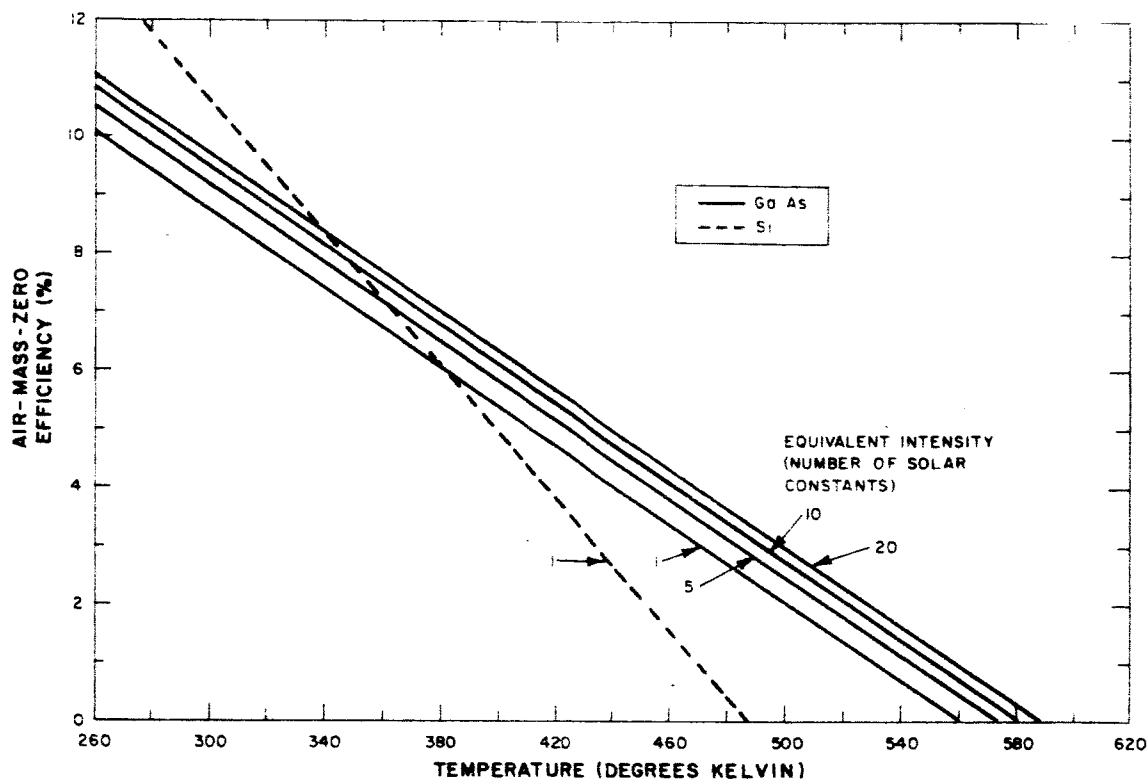


Figure 5. Air-Mass-Zero Conversion Efficiency of Gallium-Arsenide and Silicon Cells as a Function of Temperature

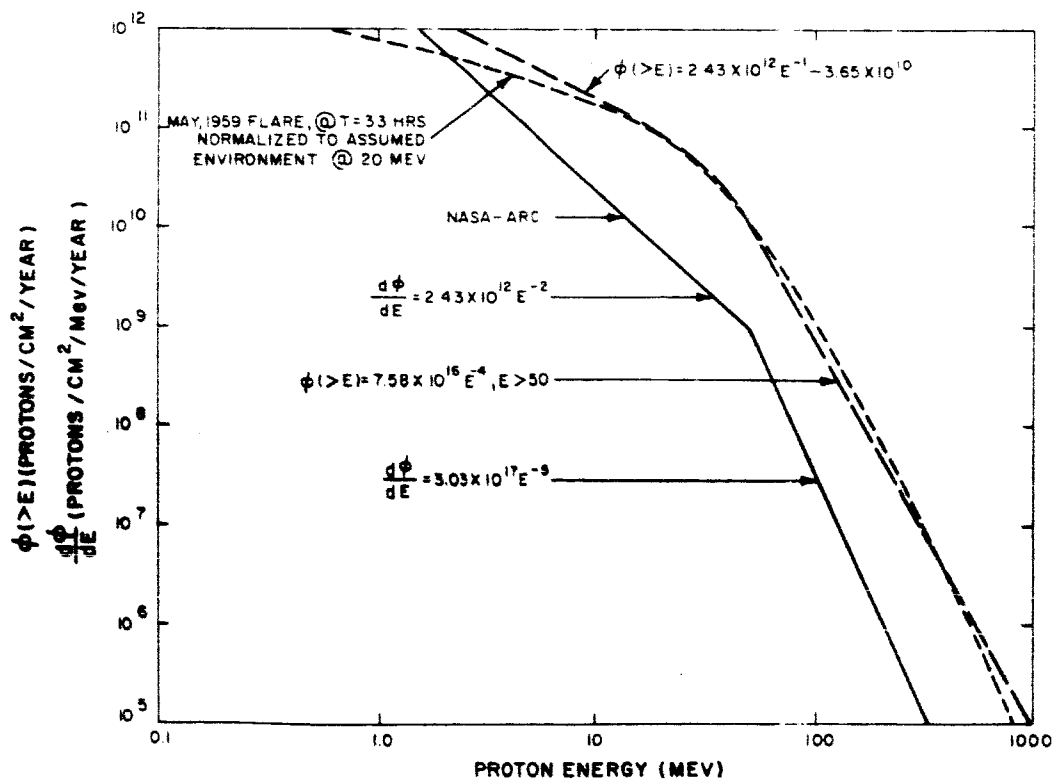


Figure 6. Omnidirectional Solar Proton Environment in the Vicinity of the Earth

Assuming that the yearly dose given in Figure 6 is the result of continuous emission from the Sun throughout the year, the dose received by the solar cells at any given time as a function of vehicle trajectory is computed by applying the $1/R^2$ law where R is the sun-probe distance in AU.

From Figures 1 through 4 it can be seen that the probe trajectories are in a system of coordinates where the earth-sun line is held fixed to show the relative positions of the Sun-Earth and the solar probe at all points of the orbit. The total radiation dose encountered by a solar probe at any given time in orbit is determined as a function of the sun-probe distance and the appropriate multiplying factors that can be applied to the yearly earth proton fluxes given in Figure 6. This is expressed as:

$$\text{Orbit dose} = (\text{yearly earth dose})(\text{multiplying factor}) \text{ proton/cm}^2$$

The charged particles encountered by the solar cells during the course of their trajectory toward the Sun are responsible for degradation of the solar-cell operational parameters; these are short-circuit current (I_{SC}), maximum-power current (I_{pm}), maximum-power voltage (V_{pm}), and open-circuit voltage (V_{oc}).

The total cumulative 17.6 Mev proton normally incident damage-equivalent flux density, ϕ_T , has been calculated for each of the four solar-probe trajectories at 20-day intervals, using the following data:

- A calculated flux multiplying factor A, which relates flux density to probe distance from the Sun,
- The annual flux rate for earth orbit for protons with energy greater than 5 Mev, ϕ_γ ,¹
- The omnidirectional infinite backshielding correction factor,² and
- A damage factor based on the proton damage curve.³

The damage-equivalent 17.6-Mev proton flux is chosen as the common flux measure in comparing the radiation damage effects on the silicon solar cell and the gallium-arsenide solar cell because of limitations on test time in the cyclotron used for proton testing.⁴ The total 17.6-Mev flux (ϕ_T) is calculated as the product of the four factors:

$$\phi_T = A \times \Theta_m \times K_d \times \phi_\gamma$$

where

- A is the flux multiplying factor,
- Θ_m is the omnidirectional factor,
- K_d is the 17.6-Mev proton equivalent damage factor and
- ϕ_γ is the encountered flux.

From the proton energy-range relationship it is known that approximately 9 mils of fused silica will stop protons with energies below 5 Mev. This thickness of glass shielding was selected for both the silicon and gallium-arsenide cells for the four missions under consideration because protons with energies below 5 Mev cause a disproportionately large amount of damage to the solar cells.

The expression for ϕ_T is valid with the following assumptions:

- (1) The damage caused by each proton in the 5- to 60-Mev range is equivalent to that caused by a 17.6-Mev particle. This range of energies encompasses 99 percent of the vehicle-encountered protons.
- (2) The solar cell is assumed to have infinite backshielding. Since the solar cell will be traveling toward the Sun, which is the source of protons, practically all the damage will be caused by particles impinging on the light-active surface of the solar cell.

A review of the data source articles⁴ shows that these assumptions are reasonable for the solar cells and the missions being considered.

Having obtained the damage-equivalent 17.6-Mev proton fluxes, the irradiation degradation of the solar-cell current and voltage parameters are plotted as a function of total encountered 17.6-Mev particles per cm^2 for low-resistivity, n-on-p silicon solar cells (Figure 7) and p-on-n gallium-arsenide solar cells (Figure 8). For the four missions being considered, the highest value of integrated 17.6-Mev proton flux dosage is less than 2.5×10^{12} protons/ cm^2 ; therefore, negligible radiation damage is experienced by the cover-glassed gallium-arsenide solar cell. Significant damage is produced by this flux on the cover-glassed silicon solar cells as shown in the degraded values of their output characteristics (presented later in this report).

A reduction in the number of particles per unit area encountered by the solar probes will be affected by the solar-cell array cooling techniques described in Section IV. Since the encountered flux is essentially unidirectional, rotating the solar-cell panels away from normal solar incidence will reduce the encountered flux by the cosine of the off-normal angle. This will also cause the charged particles to see an effectively thicker cover-glass shielding. The result will be a lower damage rate of the solar-cell output power; the amount of damage may be determined after the off-normal angle versus time in orbit has been specified.

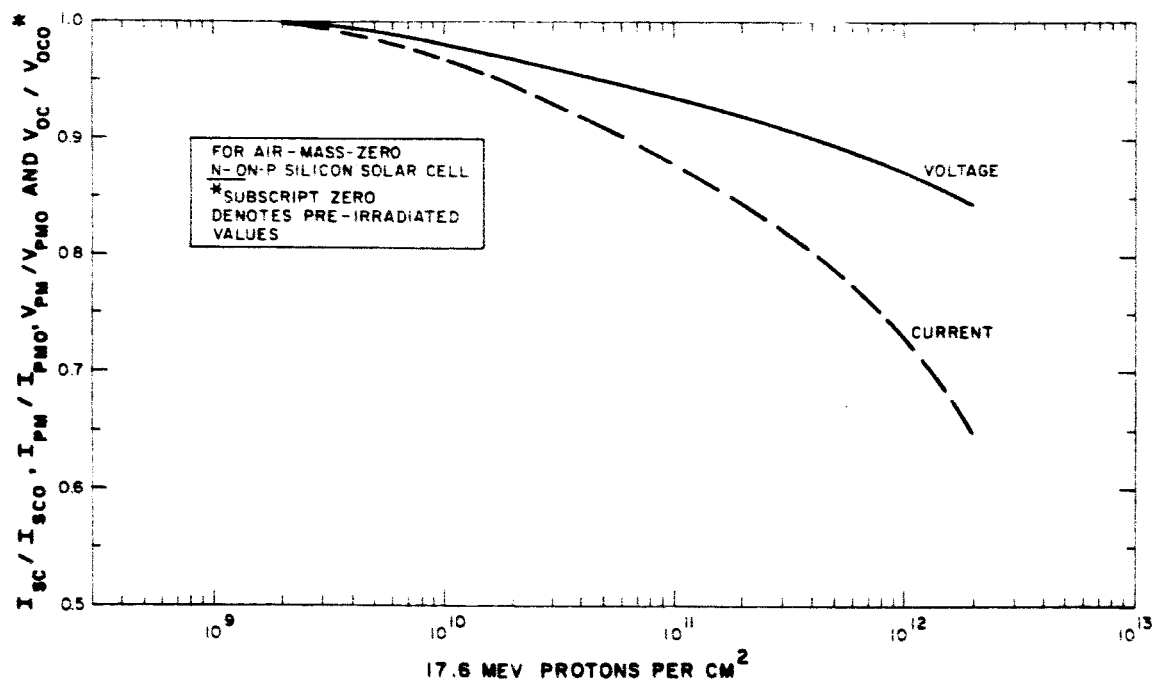


Figure 7. Silicon Solar Cell Parameter Degradation Versus Proton Flux

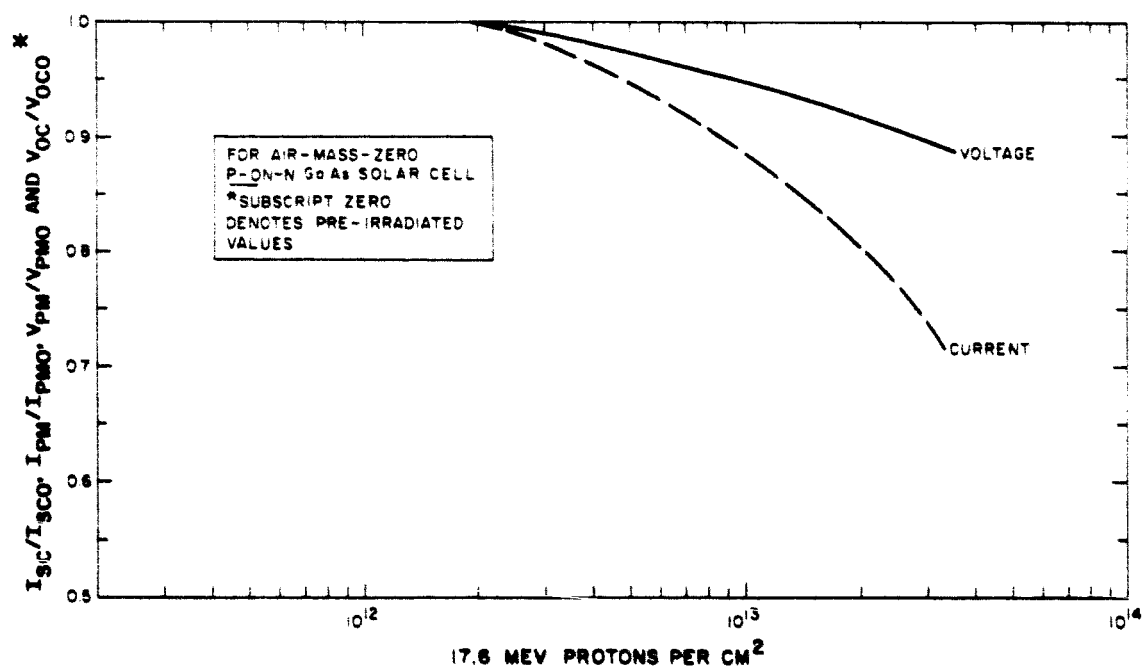


Figure 8. Gallium-Arsenide Solar Cell Parameter Degradation Versus Proton Flux

In the array cooling technique utilizing an intensity-reducing sun shield, the density and thickness of the perforated metallic shield will contribute to the shielding of the solar cells. If the sun shield is only one or two mils thick, its protection is negligible, but ten or more mils of shielding will reduce the charged-particle radiation damage to the solar cells by a significant amount.

The technique which tilts the solar-cell panel surface-normal vector at right angles to the incident solar irradiance and reflects energy to the cells by means of a mirror will almost completely eliminate the damage to the solar cells from charged-particle irradiation. This results from the fact that the cells are geometrically shielded and that high-energy protons are not reflected from the mirror surface.

C. DEGRADATION DUE TO ULTRAVIOLET IRRADIATION

At low values of solar flux (1 sun), extensive testing of the solar cell assembly (consisting of a transparent adhesive, filters, fused silica covers, and silicon solar cells) has led to confidence in reliable prediction of performance of such assemblies for near-earth missions. However, test data for near-sun missions are either sparse or nonexistent and therefore confidence in predicting performance is low.

Transparent adhesive systems undergo photochemical decomposition as a result of ultraviolet exposure which changes the optical properties of the solar-cell assemblies. This results in a reduction of transmitted light and an attendant increase in the adhesive absorptivity which increases solar-cell operating temperature. The selection of an adhesive must include the consideration of its resistance to ultraviolet irradiation. Adhesive systems such as the silicones, which have a minimal absorption of ultraviolet photons, provide a minimum degradation of optical properties. To give the adhesive system protection from ultraviolet exposure, filters evaporated on glass covers are used. These filters are commonly of the blue-red type; it is the blue cutoff end of the filter which affords the protection.

Filters exposed to ultraviolet irradiation, show an initial decrease in their transmission properties. The bulk of this effect occurs during the first 20 hours in sunlight, either in vacuum or in the atmosphere. The effect amounts to a five-percent decrease in transmission, which does not significantly change after the first 20 hours. Testing has confirmed this conclusion for periods up to a simulated 4-years sunlight exposure at one-sun distance.

Glass subjected to ultraviolet radiation will brown due to "solarization" (color-center recombinations due to impurities contained in a given glass composition). However, since the solar-cell covers now being used are the high-purity fused silica glass, the changes in transmissive properties will be negligible in the 2000-4000 Å ultraviolet region.

Unfortunately, most of the ultraviolet radiation tests have been conducted in the spectral range from 2000-4000 Å, whereas at close distances to the Sun, the solar-cell assembly will be subjected to the extreme ultraviolet spectrum of the Sun (284 Å, 304 Å, and 335 Å; at the mean solar irradiance of 304 Å the energy density is 3×10^{-8} w/cm²). In addition to the consideration of wavelength, the effects of the long-term ultraviolet radiation on cover glass, filters, transparent adhesives and solar cells are unknown.

D. DEGRADATION DUE TO MICROMETEORITE ENVIRONMENT

Calculated results of solar-cell micrometeorite damage based on estimates of the micrometeorite particle flux and velocity distribution as functions of distance from the Sun indicates very little effect on solar-cell degradation (approximately one percent loss per year). However, due to uncertainties in the flux and velocity distribution of the micrometeorite environment, the degradation of solar-cell surfaces may be much higher. Therefore, a micrometeorite degradation factor of 0.95 (believed to be conservative) is used in estimating the solar-cell performance.

E. DEGRADATION DUE TO SOLAR WIND

The solar cells will be subjected to a continuous flux of solar wind plasma. Solar wind plasma consists of low-energy protons of about 500-ev energy levels and having a density of 50 protons/cm³. In addition to the low-energy protons, the solar wind plasma probably consists of approximately 15 percent alpha-particles, 0.1 percent oxygen and carbon ions, 0.01 percent nitrogen and silicon ions, and 0.001 percent magnesium, sulfur, and iron ions.

The average velocity of the plasma for quiet conditions is about 600 km/sec and the particle flux is 2×10^8 protons/cm². For the solar-flare conditions occurring on the average of twice per month and lasting 20,000 seconds in the worst year of the eleven-year cycle, the flux increases by one order of magnitude, the particle velocity increases to 1000 km/sec, and the particle energy increases from 1 to 5 kev. Since protons up to 40 kev will be completely absorbed by 0.235 micron of silicon dioxide, the resulting damage to solar cells with 9 mils of fused silica is insignificant.

SECTION III

CALCULATION OF I-V CURVE CHARACTERISTICS FOR SILICON AND GALLIUM-ARSENIDE SOLAR CELLS

A. INTRODUCTION

Calculations were made to determine the relative performance of n-on-p, silicon solar-cells and p-on-n, gallium-arsenide solar cells for the four solar probe missions (0.51, 0.40, 0.291, and 0.09 AU). In making the performance calculations, it was necessary because of lack of test data to omit two degradation factors from the calculations. These are the ultraviolet irradiation degradation and the irreversible thermal degradation of the solar cell, cover glass, and cover-glass adhesive assembly. It is known that the ultraviolet radiation at a one sun environment can produce up to about 5 percent degradation in silicon solar-cell current, but ultraviolet testing at higher intensities has not been reported and a reasonable estimate of the damage due to intensities of up to 120 suns cannot presently be made. In a final report prepared under NASA Contract NAS5-9006, a loss in efficiency of gallium-arsenide solar cells after storage at high temperatures (200-250°C) is reported.⁵ However, this data is not sufficient to allow the selection of a high-temperature degradation design factor. It is realized that either of these factors, ultraviolet damage or high-temperature degradation, can severely limit the use of solar cells for the solar-probe missions, and the need for further testing is required.

Two approximations were required in order to predict both the silicon and gallium-arsenide solar-cell characteristics for the solar-probe missions. The first approximation requires that the low temperature ($< 375^{\circ}\text{K}$) and low-intensity (one sun) performance data for the silicon solar cells be extrapolated to the high temperature ($375^{\circ}\text{K} < T < 475^{\circ}\text{K}$) and high intensity (10 suns and above) ranges. The second approximation requires a similar type of extrapolation to describe the gallium-arsenide solar-cell operating characteristics for the missions. These approximations are necessary because very little test data exists for gallium-arsenide cells, and silicon cell test data is limited over 375°K and above one-sun intensity.

The 303°K air-mass-zero I-V curve characteristics used for the 1×2 cm, cover-glassed solar cells at the beginning of each of the four missions (0 days) are given in Table 1.

TABLE 1. I-V CURVE CHARACTERISTICS AT BEGINNING OF MISSIONS

	I _{sc} (ma)	I _{pm} (ma)	V _{pm} (mv)	V _{oc} (mv)	Efficiency (Air Mass Zero) (%)	P _{max} (mw)
Silicon	63.0	57.5	460	580	10.5	26.4
Gallium Arsenide	33.8	30.2	720	910	8.6	21.7
Values include a 5-percent cover-glass loss factor						

These selected values are representative of approximately the best ten percent of the present product.^{6, 7} The characteristics for the gallium-arsenide cell were taken from the referenced report⁶ air-mass-one data and changed to air-mass-zero values with the spectral correction factor of 1.17.

The temperature shift parameters used for the I-V curve characteristic calculations are given in Table 2.

TABLE 2. TEMPERATURE SHIFT PARAMETERS

	dI _{sc} /dT (ma/°K)	dV _{oc} /dT (mv/°K)	dV _{pm} /dT (mv/°K)
Silicon	0.04	-2.5	-2.5
Gallium Arsenide	0.03	-2.8	-2.8

The temperature shift for I_{pm} is obtained with the equation

$$\frac{I_{sc}}{I_{pm}} = 1.07 + (T-273) \times 10^{-3}$$

where T is temperature in degrees Kelvin. The silicon temperature-shift parameters and the I_{sc}/I_{pm} relationship were obtained from reference 7. The gallium-arsenide temperature-shift parameters were taken from reference 6.

The general procedure used to calculate the I-V curve characteristics of the solar cells as they trace the trajectories of the solar probes are described in the following four paragraphs.

B. AIR-MASS-ZERO SHORT-CIRCUIT CURRENT (AMO I_{sc})

This characteristic is calculated for each 20-day interval. The procedure consists of three steps, each of which takes into account one of the three major environmental factors that affect the cell. These are the radiation, the cell temperature, and the illumination intensity.

Step 1. Radiation Correction on AMO I_{sc}

This is done by entering the curves (Figures 7 and 8) of normalized AMO short-circuit current versus flux of 17.6-Mev protons with the flux (ϕ_T) at the beginning of each of the 20-day intervals and applying the normalized current obtained to the 303°K unbombarded value of AMO short-circuit current. The correction is given by the equation

$$AMO I_{scR} = \gamma AMO I_{sc}$$

where the subscript R designates a radiation-correction value and γ is the normalized current obtained from the radiation degradation curve.

Step 2. Temperature Correction on AMO I_{scR}

Temperature correction for the short-circuit current is performed with the equation

$$AMO I_{scRT} = AMO I_{scR} + (T-303) \frac{dI_{sc}}{dT} .$$

In this equation, T is the temperature in °K, the subscript T designates temperature-corrected value, and $\frac{dI_{sc}}{dT}$ is the short-circuit current temperature sensitivity. The sensitivities used are 0.04 ma/°K for silicon cells and 0.03 ma/°K for gallium-arsenide cells. The value for silicon is an approximation of the AMO $\frac{dI_{sc}}{dT}$ taken from ComSat study test results.⁷ This value is for a lightly bombarded solar cell and is approximately 0.06 percent I_{sc} per °K. The gallium-arsenide value is calculated from data in reference 6.

Step 3. Illumination Intensity Correction on AMO $I_{sc_{RT}}$

Correction for illumination intensity is based on the assumptions that the Sun's intensity is inversely proportional to the square of the distance from the cell to the Sun. The first approximation assumes that the Sun is a point source; this is valid as long as the nearest approach is greater than 8 to 10 solar diameters. The nearest approach is 8 million miles, approximately ten diameters. For the initial analysis it is also assumed that the short-circuit current is directly proportional to the Sun's intensity, although it is known that with increasing intensity the series-cell resistance ultimately causes the I_{sc} to saturate. However, at 10 to 15 suns which is the limiting normal intensity for thermal reasons, the departure from proportionality may be small with current production cells.

The expression which incorporates variable illumination is

$$AMO I_{sc_{TRS}} = \frac{R_{se}^2}{R^2} AMO I_{sc_{TR}}$$

where the subscript S designates illumination corrected, R_{se} is the distance from the Sun to the Earth and R is the distance from the Sun to the solar cell.

C. AIR-MASS-ZERO MAXIMUM POWER CURRENT ($AMO I_{pm}$)

The maximum power current is obtained for each 20-day interval. Calculations are made using the corrected short-circuit current ($AMO I_{sc_{TRS}}$) and the current distortion factor. The distortion factor, in the ratio of the short-circuit current to the maximum power current, is defined in the equation

$$D = 1.07 + (T-273) \times 10^{-3}$$

where T is the temperature in $^{\circ}K$.

The maximum power current is

$$AMO I_{pm_{TRS}} = \frac{AMO I_{sc_{TRS}}}{D}$$

The distortion factor used was obtained on a group of RCA 10-ohm-cm, n-on-p, silicon solar cells over the temperature range of 253 to 343 $^{\circ}K$. Its use here represents an approximation which appears to be reasonable for low series-resistance versions of both solar cell types.

D. AIR-MASS-ZERO OPEN-CIRCUIT VOLTAGE (AMO V_{oc})

This characteristic is calculated in the same manner as the short-circuit current; the procedure consists of three steps which take into account the effects of radiation, temperature, and illumination intensity.

Step 1. Radiation Correction on AMO V_{oc}

The correction for radiation is made by entering the curves (Figures 7 and 8) of normalized AMO open-circuit voltage versus flux of 17.6-mev protons with the flux (ϕ_T) for each of the 20-day intervals and applying the normalized V_{oc} obtained to the 303°K unbombarded value of AMO open-circuit voltage. The correction is given by the equation

$$AMO V_{ocR} = \alpha AMO V_{oc}$$

where the subscript R designates radiation corrected and α is the fractional ratio for the voltage.

Step 2. Temperature Correction on AMO V_{ocR}

The temperature correction is made using the equation

$$AMO V_{ocRT} = AMO V_{ocR} + (T-303) \frac{dV_{oc}}{dT}$$

where the subscript T designates temperature corrected, T is the temperature in °K and $\frac{dV_{oc}}{dT}$ is the open-circuit voltage temperature sensitivity. The sensitivity used are minus 2.5 mv/°K for silicon and minus 2.8 mv/°K for gallium arsenide. The silicon value is a worst case approximation for low resistivity solar cells. The gallium-arsenide value is taken from the report⁶ referred to previously.

Step 3. Illumination Intensity Correction on AMO V_{ocRT}

Correction for illumination intensity is made using the equation

$$AMO V_{ocRTS} = AMO V_{ocRT} + \frac{aKT}{q} \ln \left(\frac{AMO I_{scTRS}}{AMO I_{scTR}} \right)$$

where a is a multiplier, K is Boltzmann's constant, T is the absolute temperature in degrees Centigrade and q is the basic electronic charge. The only

assumption made (over and above those used in the short-circuit current calculations) is with regard to the multiplier a . Calculations for ComSat silicon solar cells gave a value of 1 for a . On this basis the value of 1 was used for all calculations on both silicon and gallium-arsenide cells.

E. AIR-MASS-ZERO MAXIMUM POWER VOLTAGE (AMO V_{pm})

The maximum power voltage is calculated using the equation

$$AMO V_{pmRTS} = AMO V_{ocRTS} (AMO V_{oc} - AMO V_{pm})$$

where $AMO V_{oc}$ and $AMO V_{pm}$ are the values for the unbombarded solar cell under one sun at a temperature of 303°K.

The assumptions made are: (1) that the solar cells series resistance does not change with temperature and radiation, and (2) that it decreases with increasing illumination (short-circuit current). Tests on un-irradiated silicon solar cells (Nimbus and ComSat programs) and gallium-arsenide solar cells show that temperature does not materially affect series resistance. Output characteristics of silicon solar cells show that this is essentially true for post-irradiated cells. For variable illumination intensity, tests show that the series resistance of current production silicon solar cells decreases with increasing illumination up to four or five suns.

F. SUMMARY OF RESULTS

The corrected results obtained for the I-V curve characteristics of both cell types are listed in Tables 3 through 6. In the 0.09-AU calculations, the solar-cell temperature is limited by controlling the intercepted solar intensity. For example, if the maximum desired temperature is 573°K which is obtained with a normally incident illumination of 15 suns, the same temperature may be maintained when the normally incident illumination is 20 suns by the use of an appropriate temperature-controlling technique. Silicon cell temperature is limited to 468°K.

The temperature used in the solar-cell characteristic calculations were obtained from the equation

$$T = \left(\frac{\bar{\alpha}_{eff} S}{\bar{\epsilon}_{eff} N \sigma} \right)^{1/4}$$

where

$$\frac{\bar{\alpha}_{\text{eff}}}{\bar{\epsilon}_{\text{eff}}} = 0.95$$

N = 4 (Extended Pioneer, spin-stabilized vehicle),

= 2 (Advanced Pioneer, sun-oriented array),

σ = Stefan-Boltzmann constant,

T = temperature, and

S = solar constant.

Output characteristics (I-V curves) for the silicon and gallium-arsenide solar cells are shown in Figures 9 and 10. These curves represent the closest sun approach conditions for the cells in the 0.4 and 0.51 AU missions, respectively. Figures 11 and 12 are predicted I-V characteristic curves for the gallium-arsenide solar cell for temperatures of 375 to 525°K at equivalent solar illumination intensities of 10 and 5 suns, respectively.

G. EFFECT OF SOLAR CELL MISMATCH ON OUTPUT POWER

The spread in cell-to-cell output characteristics caused by variations in the base resistivity and variations in the spectral response characteristics is known for silicon solar cells. At this point in the development of gallium-arsenide cells it can be assumed that their spread is like that of silicon.

Base resistivity of silicon cells can be controlled during production such that this parameter will vary between 1 and 2 ohm-centimeters for a low-resistivity cell and, typically, between 7 and 13 ohm-centimeters for a nominal 10 ohm-centimeter cell. The high-resistivity cells are superior in radiation resistance and have a greater short-circuit current output and a lower open-circuit voltage output than the low-resistivity cell at room temperature conditions. The room temperature maximum power is approximately the same for both high- and low-resistivity cells, but at elevated temperatures the low-resistivity cell exhibits greater power because of the smaller value of its voltage-temperature coefficient.

Spectral response variations in silicon solar cells of a given base resistivity can cause a difference in current output of ± 3 to 4 percent under tungsten illumination. "Blue-shifted" cells (i.e., cells whose spectral response is relatively greater in the shorter wavelength region of the solar spectrum) exhibit higher output power after exposure to charged-particle irradiation than do the normal, or "red-shifted", solar cells. For this reason solar-cell manufacturers strive to obtain blue-shifted cells during production runs.

TABLE 3. I-V CURVE CHARACTERISTICS FOR 0.09-AU MISSION

Days After Launch	Cumulative Proton Flux* $\phi_T \times 10^{11}$ (p/cm ²)	I _{sc} (ma)		I _{pm} (ma)		V _{pm} (mv)		V _{oc} (mv)		Temp. (°K)
		GaAs	Si	GaAs	Si	GaAs	Si	GaAs	Si	
0	-----	34.5	64.1	30.8	57.1	647	395	837	515	329
20	0.071	38.5	70.0	34.0	61.9	619	362	809	482	339
40	0.166	54.4	95.5	46.8	82.3	548	208	738	412	369
55	-----	104.5	178.0	85.4	145.1	394	---	584	---	433
59	-----	139.5	234.5	111.0	186.5	318	---	508	---	465
60	0.381	166.5	---	127.5	---	195	---	385	---	513
61	-----	194.0	---	142.0	---	79	---	269	---	573
70	-----	194.0	---	142.0	---	79	---	269	---	573
80	5.040	154.2	223.0	123.0	177.5	227	51	417	171	463
100	5.224	50.4	73.0	43.8	63.3	569	261	759	381	361
120	5.340	36.7	53.0	32.7	47.2	644	326	834	446	331
140	5.410	34.4	49.8	29.4	44.6	658	338	848	458	325
160	5.470	38.3	55.1	33.9	48.8	628	310	818	430	337
180	5.580	56.0	80.5	48.0	69.0	532	215	722	335	375
200	5.800	195.0	---	152.0	---	256	---	446	---	493
205	-----	194.0	---	142.0	---	79	---	269	---	573
220	10.84	194.0	---	142.0	---	79	---	269	---	573
222	-----	194.0	---	142.0	---	79	---	269	---	573
240	11.47	72.2	97.2	60.8	82.0	485	177	675	297	395
260	11.59	42.7	57.3	37.6	50.4	616	289	806	409	343
280	11.65	34.5	46.2	30.8	41.3	653	323	843	443	327
300	11.72	37.5	50.0	33.3	44.4	638	309	828	429	333
320	11.80	52.5	70.0	45.3	60.4	553	234	743	354	367
340	11.90	168.0	---	132.9	---	304	---	494	---	473

*17.6 Mev

Notes: In this probe, the solar array was tilted off-normal from sun vector to limit maximum array temperature to 573°K for gallium arsenide.

Characteristics given are corrected for radiation, temperature, and illumination.

TABLE 4. I-V CURVE CHARACTERISTICS FOR 0.291-AU MISSION

Days After Launch	Cumulative Proton Flux* $\phi_T \times 10^{11}$ (p/cm ²)	I _{sc} (ma)		I _{pm} (ma)		V _{pm} (mv)		V _{oc} (mv)		Temp. (°K)
		GaAs	Si	GaAs	Si	GaAs	Si	GaAs	Si	
0	-----	34.5	64.0	30.8	57.1	650	398	840	518	328
20	0.066	35.6	64.7	31.6	57.5	643	382	833	502	327
40	0.138	44.0	79.1	38.5	69.3	598	341	788	461	349
60	0.238	68.1	118.0	57.3	99.4	478	226	668	346	397
75	-----	135.0	227.0	107.5	181.0	322	85	512	205	463
80	0.450	180.5	300.0	141.0	213.0	263	---	453	---	489
90	-----	372.0	---	275.0	---	111	---	301	---	559
98	-----	460.0	---	328.0	---	21**	---	169	---	611
100	1.075	449.0	---	322.0	---	30**	---	190	---	603
116	-----	142.0	223.0	113.0	177.5	324	70	514	190	463
120	1.500	127.5	200.0	103.1	162.0	379	117	569	237	441
140	1.650	51.3	80.7	44.4	69.9	566	277	756	397	362
160	1.750	40.0	62.7	35.4	55.4	623	327	813	447	339
180	1.810	35.3	55.5	31.4	49.6	645	347	835	467	330
200	1.890	37.4	58.7	30.2	52.2	641	342	831	462	332
220	1.950	44.0	68.5	38.5	60.0	598	304	788	424	349
240	2.040	80.7	125.0	68.6	106.3	520	235	710	355	383
260	2.160	126.0	193.0	102.0	156.2	371	104	561	224	444
264	-----	142.0	216.0	113.0	172.0	324	61	514	181	463
280	2.460	375.0	---	273.0	---	44**	---	234	---	583
296	-----	173.0	259.0	138.0	206.0	332	65	522	185	463
300	3.100	125.0	187.0	101.0	151.5	378	108	568	228	441
320	3.380	61.4	92.0	52.7	79.0	341	244	531	364	373
340	3.500	42.2	63.3	37.2	55.8	620	312	810	432	341

*17.6 Mev

**Linear distortion factor approximation breaks down at the higher temperatures; experimental values required for meaningful estimates.

Characteristics given are corrected for radiation, temperature, and illumination.

TABLE 5. I-V CURVE CHARACTERISTICS FOR 0.4-AU MISSION

Days After Launch	Cumulative Proton Flux* $\phi_T \times 10^{11}$ (p/cm ²)	I _{sc} (ma)		I _{pm} (ma)		V _{pm} (mv)		V _{oc} (mv)		Temp. (°K)
		GaAs	Si	GaAs	Si	GaAs	Si	GaAs	Si	
0	-----	33.0	62.0	30.8	58.0	790	525	980	645	277
20	0.065	34.4	63.2	32.1	59.1	783	507	973	627	280
40	0.138	41.9	77.4	38.7	71.6	776	493	966	613	291
60	0.238	58.4	104.5	53.4	94.2	705	429	895	549	314
80	0.400	108.5	185.5	95.4	163.0	625	351	815	471	350
100	0.775	247.5	405.5	203.0	332.0	430	175	620	295	432
120	1.200	173.5	280.0	144.5	235.0	494	223	684	343	403
140	1.390	77.4	125.0	68.5	111.0	658	365	848	485	334
160	1.510	46.7	75.8	42.8	69.5	742	436	932	556	298
180	1.560	36.8	59.6	34.4	55.7	782	472	972	592	281
200	1.640	33.0	53.3	30.8	49.8	795	485	985	605	275
220	1.700	34.3	55.5	32.1	51.8	791	479	981	599	277

Note: Characteristics given are corrected for radiation, temperature, and illumination.

* 17.6 Mev

TABLE 6. I-V CURVE CHARACTERISTICS FOR 0.51-AU MISSION

Days After Launch	Cumulative Proton Flux* $\phi_T \times 10^{11}$ (p/cm ²)	I _{sc} (ma)		I _{pm} (ma)		V _{pm} (mv)		V _{oc} (mv)		Temp. (°K)
		GaAs	Si	GaAs	Si	GaAs	Si	GaAs	Si	
0	-----	34.5	64.0	30.8	57.2	750	398	840	518	328
20	0.066	35.2	63.6	31.4	56.7	745	385	835	505	326
40	0.138	37.6	66.8	33.3	59.0	627	363	817	483	337
60	0.212	47.2	82.5	41.2	72.0	589	326	779	446	353
80	0.312	66.2	114.0	56.4	97.2	525	265	715	385	383
100	0.463	93.0	155.5	76.1	127.5	411	159	601	279	418
120	0.700	152.0	244.5	121.0	195.0	323	77	513	197	468
140	1.000	144.5	232.0	116.5	187.0	364	110	554	230	453
160	1.190	89.6	145.0	74.6	121.0	461	191	651	311	408
180	1.310	53.4	86.3	46.2	74.6	360	277	750	397	565
200	1.400	38.1	61.5	33.7	55.4	626	333	816	453	338
220	1.470	33.3	53.0	29.7	47.3	648	351	838	471	329
240	1.550	33.2	52.7	29.7	47.1	654	355	844	475	327
260	1.550	36.1	57.2	32.1	50.8	638	342	828	462	333
280	1.670	45.0	71.0	39.5	62.4	605	313	795	433	347
300	1.760	60.5	94.6	51.8	81.0	533	248	723	368	373
320	1.870	91.0	108.0	75.2	108.0	430	183	620	267	411
340	1.960	137.5	212.0	111.2	172.0	381	113	571	233	456
360	2.080	139.0	217.0	111.5	170.0	344	82	534	202	468
Note: Characteristics given are corrected for radiation, temperature, and illumination. * 17.6 Mev										

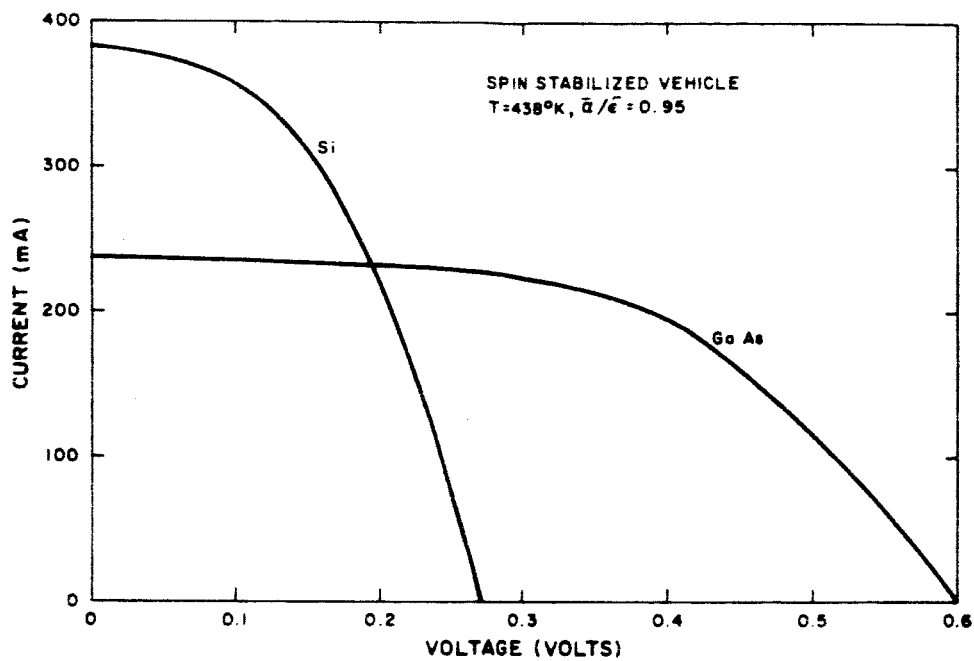


Figure 9. I-V Curves for 0.4-AU Mission

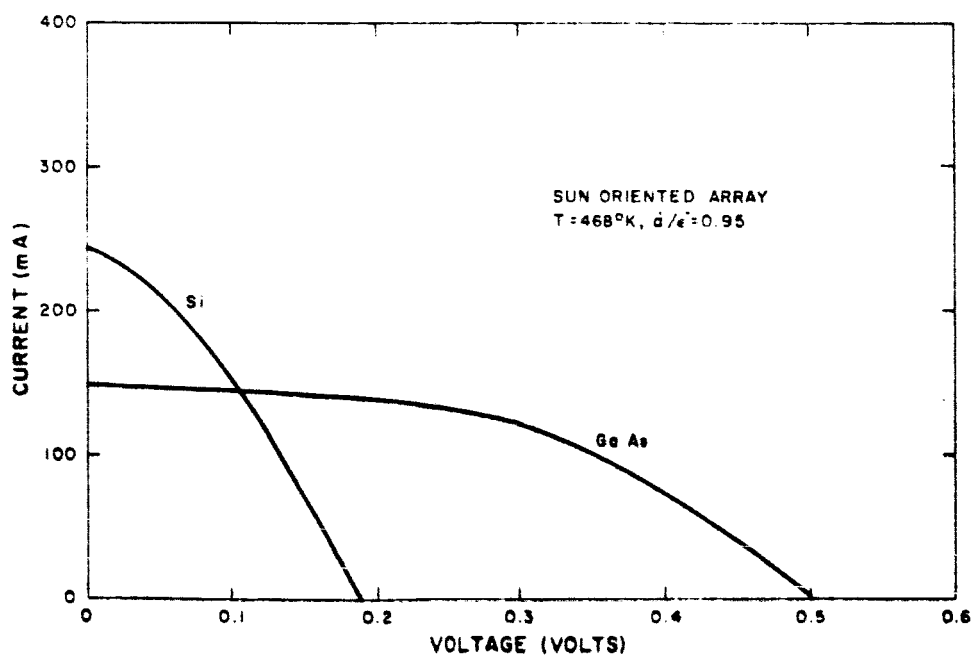


Figure 10. I-V Curves for 0.51-AU Mission

H. OFF-NORMAL INCIDENCE OPERATION OF SOLAR CELLS

One of the solar-cell array cooling techniques described later in the report involves tilting a flat solar panel with respect to the incident solar illumination. The current output of cover-glassed silicon cells has been measured as a function of angle of incidence of illumination. The relationship is a cosine function for angles up to about 60° off-normal incidence and may be approximated by the cosine function of an angle $(1 + N) \theta$ where N varies from 0.05 to 0.10 for angles greater than 60° . Angle of incidence data have not been reported for gallium-arsenide solar cells, therefore it will be assumed that the current output of these cells also varies as the cosine of the off-normal incidence angle.

I. CONCLUSIONS

Inspection of the tabulated I-V curve characteristics and the plotted I-V curves makes evident the superior performance of the gallium-arsenide solar cell at higher temperatures. Also evident is the extreme power degradation due to high temperatures. Mechanical techniques which will lower the operating temperature of the solar cells from that experienced by a thermally-uncontrolled solar-cell array are a necessity for the 0.291-AU silicon mission and the 0.09-AU gallium-arsenide mission. The same or similar cooling techniques would, of course, increase the power conversion efficiency for missions where the temperature is not high enough to completely eliminate the power output from the solar array.

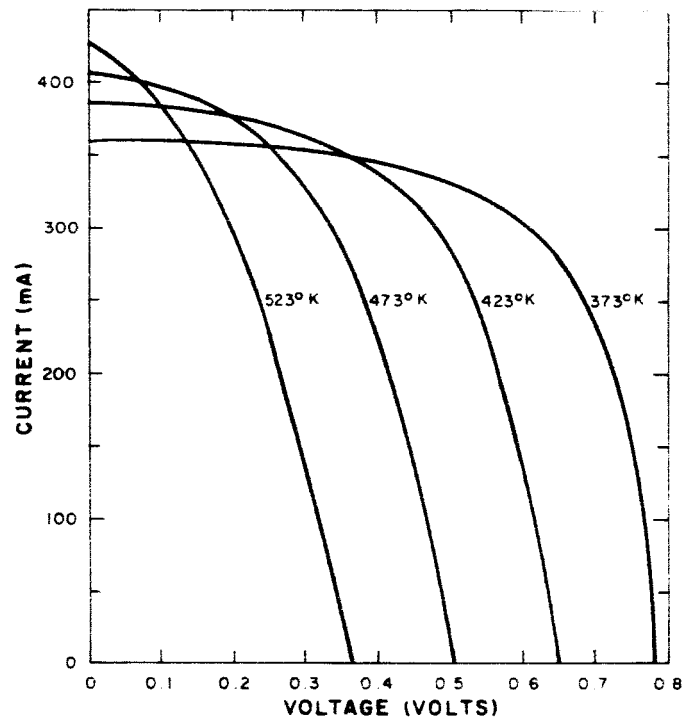


Figure 11. Predicted I-V Curves for 8.6 Percent Efficient Gallium-Arsenide Solar Cell at 10-Sun Intensity

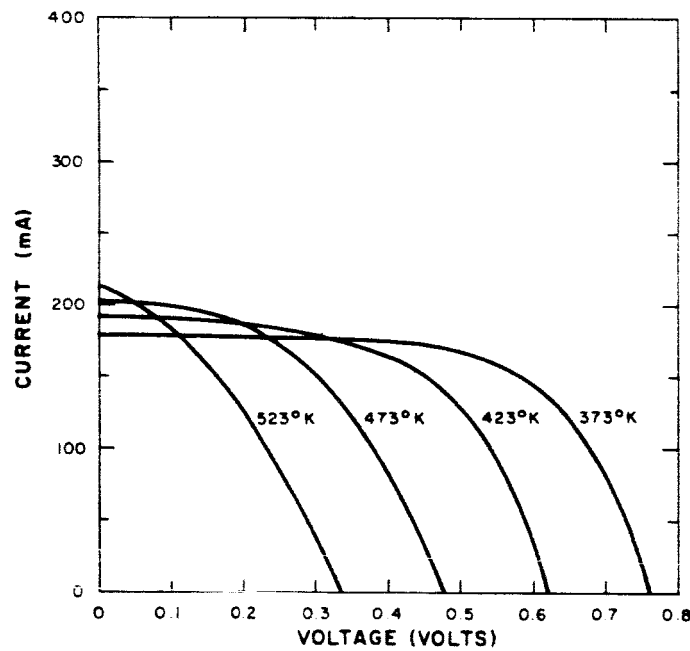


Figure 12. Predicted I-V Curves for 8.6 Percent Efficient Gallium-Arsenide Solar Cell at 5-Sun Intensity

SECTION IV

THERMAL CONTROL METHODS

Thermal control of the solar-cell array is required to maintain array construction materials within an acceptable design temperature range, and to maintain a temperature range for the solar cells which results in the desired array power output. Since the array materials may be capable of withstanding temperatures much higher than that at which the cell efficiency reaches zero, the thermal analysis was performed primarily for the purpose of producing the desired array power. The assumption was made that the array materials are not affected by the resulting temperatures. The results of the thermal analysis may be used for the selection of solar array systems based upon trade-off considerations of power, cost, area, materials and other appropriate factors.

A. TEMPERATURE CONTROL TECHNIQUES FOR NEAR-EARTH TRAJECTORIES

At near-Earth trajectories, solar-cell array temperatures (for non-spinning arrays) have been minimized by the use of three techniques:

- (1) The application of a low solar absorptivity ($\bar{\alpha}$), high-emissivity ($\bar{\epsilon}$) finish such as a white paint on the panel rear surface in order to maximize heat rejection and minimize absorption of any incident solar energy.
- (2) The application of a thin, fused-silica cover to the bare solar cell to obtain high effective cell emissivity and particle irradiation protection.
- (3) The application of a low solar absorptivity, high-emissivity finish to the cell side of the array in the areas not covered by cells.

Often the silica covers used on the bare solar cells are coated with multilayer interference films. The multilayer coating serves three purposes: (1) to maximize solar energy transmission over the response range of the cell, (2) to protect the bonding cement and cell from ultraviolet energy, and (3) to lower the cell temperature by dropping the absorptivity through selective reflection of solar energy outside the response range of the cell.

Two types of glass filter covers have been widely used for silicon cells whose response range is from 0.4 to 1.1 microns. Blue filters reject the ultraviolet portion of the solar spectrum below 0.4 micron. Blue-red filters also reject

the solar energy spectrum below 0.4 micron, and, in addition, reject infrared energy between 1.0 and 1.5 microns. Since the thermal improvement achieved by the use of blue-red filters is often offset by their higher cost and reduced transmission, blue filters are more commonly used. The response range for gallium-arsenide cells is from 0.4 to 0.9 micron; blue-red filters for use with these cells therefore require a narrower bandpass design in order to obtain optimum thermal characteristics. Glass filter covers normally have an additional coating on the exposed face which minimizes reflection of solar energy by the glass over the cell response wavelength range. A comparison of the thermal properties of various cell, filter glass combinations is given in Table 7.

The use of special finishes on the inactive areas of the cell side of the array is related to the array packing fraction β (the ratio of total cell area to total array area) which, in practice, is rarely greater than 0.9. White paint or Rokide finishes have been frequently used to coat the inactive area; these have an $\bar{\alpha}$ of 0.15 at best. A more recent development is the use of a second-surface mirror. This type of finish consists of metallic silver, vapor-deposited on one surface of fused silica. The silver is overcoated by a vapor-deposited layer of inconel. The material is bonded to the inactive array areas with the silver side down. The solar absorptivity of the second-surface mirror is from 0.05 to 0.10, a considerable improvement over white paint.

While the techniques used for near-earth trajectories remain useful, additional thermal control techniques are required to maintain acceptable array temperatures as the vehicle approaches the Sun and the solar constant increases. Several methods of thermal control have been studied for sun-vehicle distances varying from 1.0 to 0.09 AU. Four such thermal control methods are presented in the following paragraphs. Figure 13 illustrates the relationship of solar intensity versus time from launch for sun-earth elliptical trajectories of 0.51, 0.4, 0.291 and 0.09 AU perihelions.

B. THERMAL CONTROL BY TILTING THE SOLAR ARRAY WITH RESPECT TO THE SUN VECTOR

Figure 14 illustrates the thermal analysis model of a flat array which can be tilted with respect to the Sun. The tilt angle (θ) is defined as the angle between the panel normal and the sun vector. Thermal calculations were performed varying the following three parameters:

- Tilt angle
- AU from Sun (or number of solar constants)
- ($\bar{\alpha}/\bar{\epsilon}$) value for the solar cell.

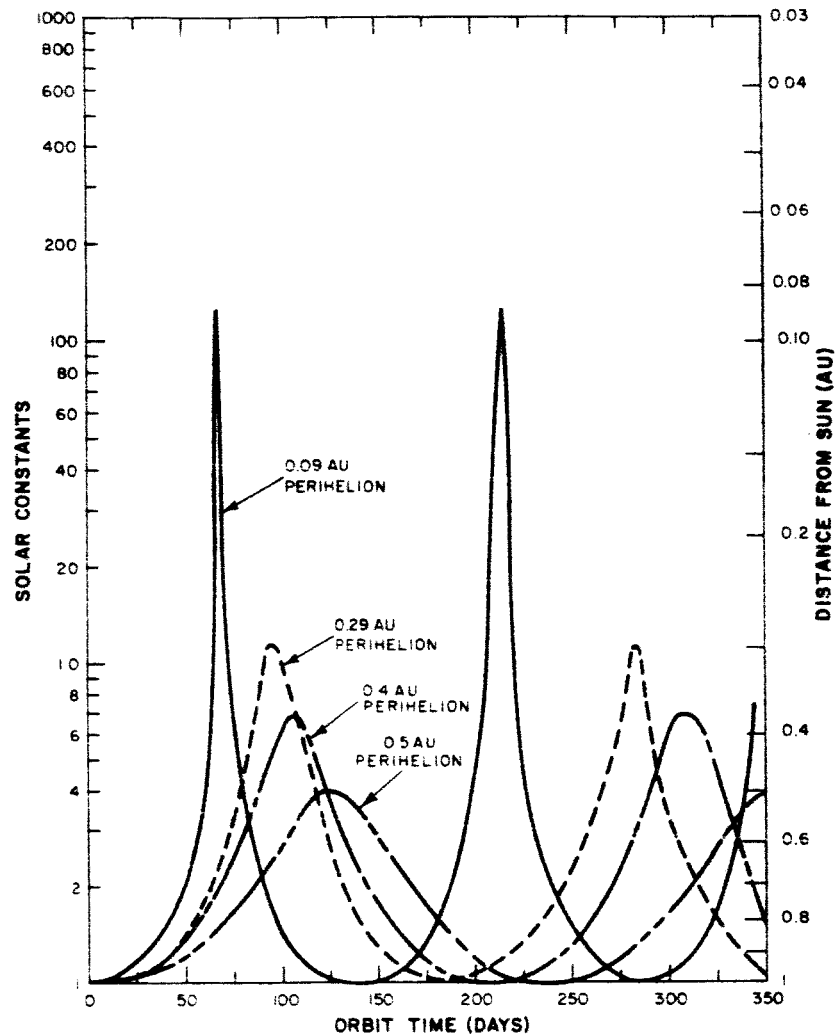


Figure 13. Solar Intensity Versus Orbit Time for Sun-Earth Elliptical Orbits

Two $(\bar{\alpha}/\bar{\epsilon})$ values were selected; 0.7 as representative of a narrow bandpass blue-red filtered cell, and 1.1 as representative of a cell covered with glass having an anti-reflective coating. These values characterize the extreme bounds of $(\bar{\alpha}/\bar{\epsilon})$ values for state-of-the-art glass-covered cells.

Figures 15 and 16 show array temperature as a function of number of solar constants. Figures 17 and 18 show array power output per unit cell area as a function of number of solar constants. The temperature curves indicate that as the tilt angle increases, the temperature decreases; the most significant reductions resulting for tilt angles of 60° and greater. The power output curves indicate that as the tilt angle is increased, the power output is reduced in the range of 1 to 10 solar constants. Above 10 solar constants and over specific ranges of tilt angle,

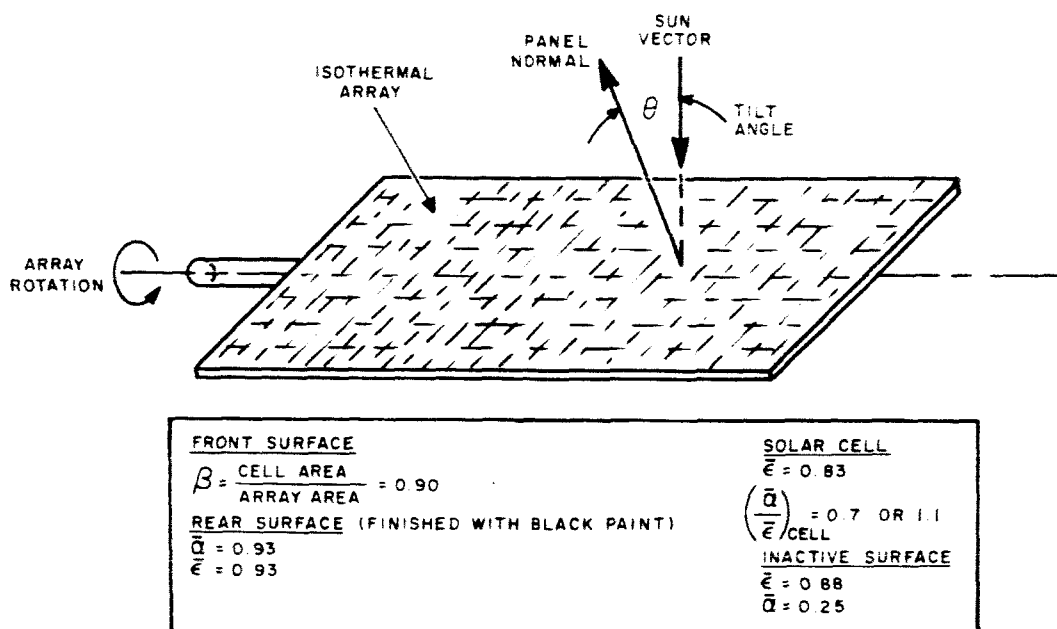


Figure 14. Thermal Analysis Model of Flat Array with One Axis Rotation with Respect to Sun Vector

power output increases as the tilt angle increases. It should be noted that these power values, which are based on I_{sc} being $\cos \theta$ dependent, are optimistic at the higher tilt angles since reflection may lower the power output to zero at $\theta \approx 85^\circ$, depending on filter characteristics.

The calculations were performed assuming that the $\bar{\alpha}$ of the array is not a function of the tilt angle. However, even black paint exhibits angle dependency to some extent. Solar cells with multilayer interference coatings are angle sensitive. Measurements of $\bar{\alpha}$ at angles approaching 90° are very difficult to perform accurately. In order to perform the 0.09-AU mission, tilt angles of 80° and higher would be required. Therefore, the following factors should be considered for design application of the tilting array:

- As the number of multilayer interference layers applied to the cell cover glass increase, the $\bar{\alpha}$ dependence upon angle becomes greater. More design information is required on $\bar{\alpha}$ values for filtered cells at angles greater than 60° .
- Automatic positioning of the array at the desired angle might be accomplished by sensing array temperature, cell voltage, or current, or array power output. If temperature were used

as the controlling parameter, the power output would be directly related to the results of the thermal calculations. These are dependent upon the accuracy of $\bar{\alpha}$ as a function of θ . Environmental proof testing of the array would require a Johnson-matched, collimated solar source.

- If operation at the maximum power output is desired, the array design materials must withstand temperatures up to 550°K without degradation.
- The configuration of the payload/solar-panel system must be such as to minimize the exchange of reflected solar energy, especially at high solar-constant values.

TABLE 7. THERMAL PROPERTIES OF VARIOUS SOLAR-CELL ARRAY CONSTRUCTION MATERIALS

Identification	Solar Absorptivity ($\bar{\alpha}$)	Thermal Emissivity ($\bar{\epsilon}$)
White Paint	0.15 to 0.25	0.87
White Vitreous Enamel	0.25	0.88
Black Epoxy Paint	0.93	0.93
Bare Silicon Solar Cell	0.81	0.40
Narrow Bandpass Blue-Red Filter on Gallium-Arsenide Cell	0.62	0.83
Solar Cell with Blue Filter	0.78	0.83
Silicon Cell with Blue-Red Filter	0.68	0.83
Second-Surface Mirror (fused silica with vacuum-deposited silver)	0.05 to 0.10	0.83

C. THERMAL CONTROL USING A DEPLOYABLE SUN SHIELD

Figure 19 illustrates the thermal analysis model of the sun-shield configuration. The system consists of a fixed-position solar-cell array normally oriented to the Sun, and a multilayer, metallic-foil sun shield which can be deployed parallel to the array when required. The sun shield is composed of "n" layers of thin metallic foil (such as titanium to withstand the high temperature application) which are physically separated to produce the insulation effect desired. The shield is perforated with a regular hole pattern that permits a fixed

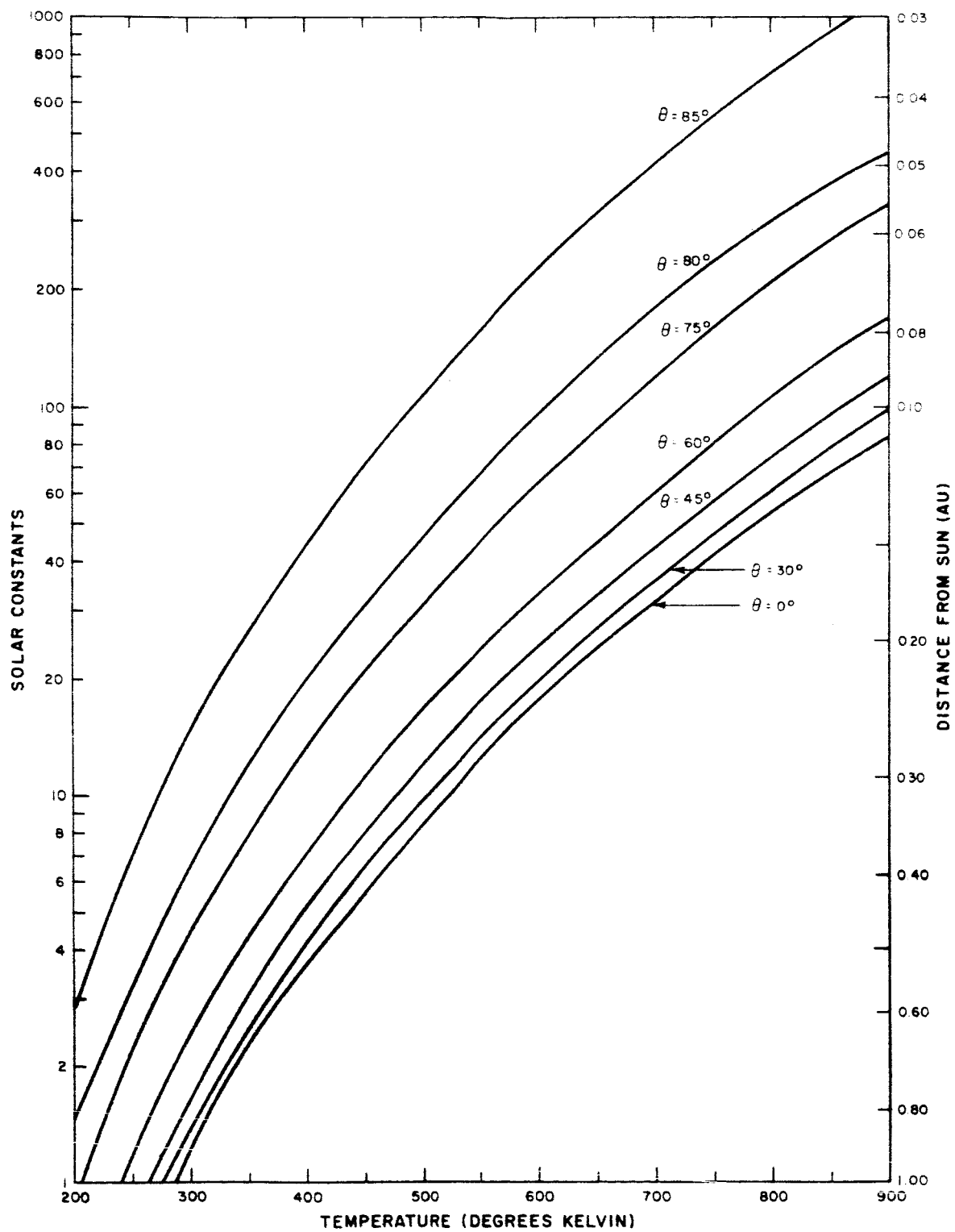


Figure 15. Array Temperature as a Function of Tilt Angle (θ) and Solar Intensity for Silicon or GaAs Cells, $\left(\frac{\bar{\alpha}}{\bar{\epsilon}}\right)_{\text{cell}} = 0.7$

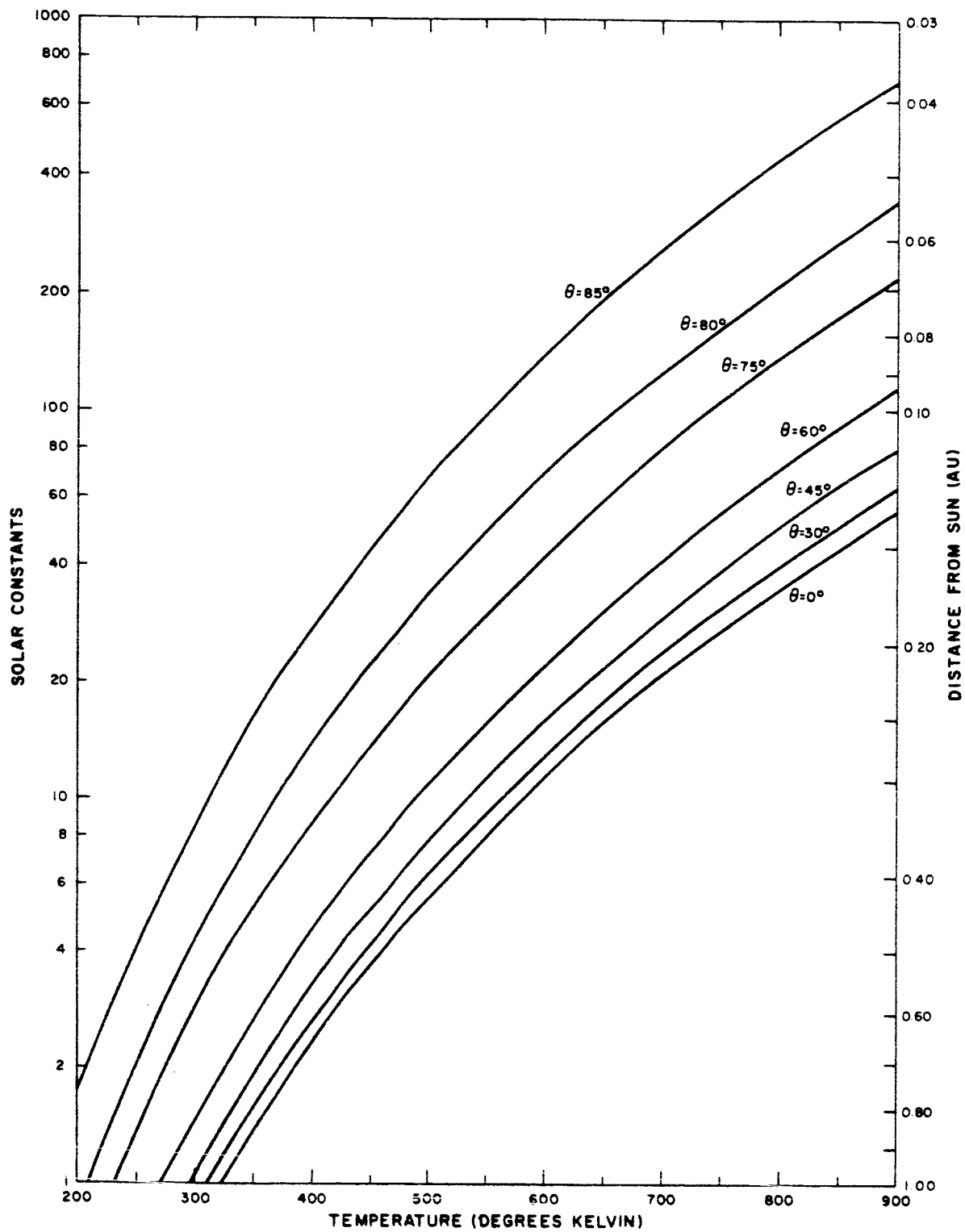


Figure 16. Array Temperature as a Function of Tilt Angle (θ) and Solar Intensity for Silicon or GaAs Cells, $\left(\frac{\alpha}{\epsilon}\right)_{\text{cell}} = 1.1$

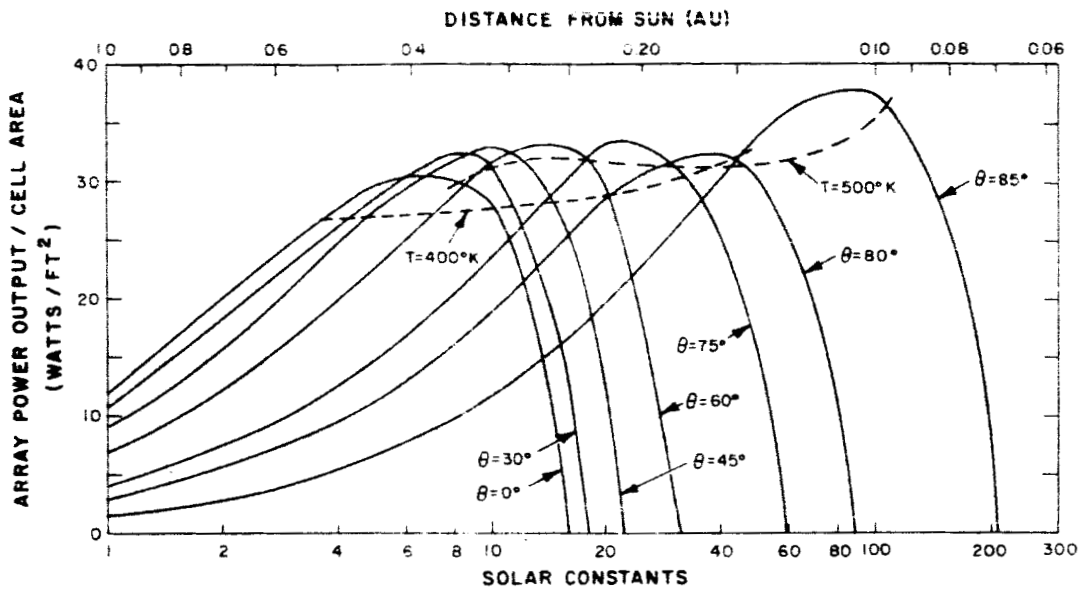


Figure 17. Array Power Output as a Function of Tilt Angle and Solar Intensity for Gallium Arsenide Cells, $\left(\frac{\bar{\alpha}}{\bar{\epsilon}}\right)_{\text{cell}} = 0.7$

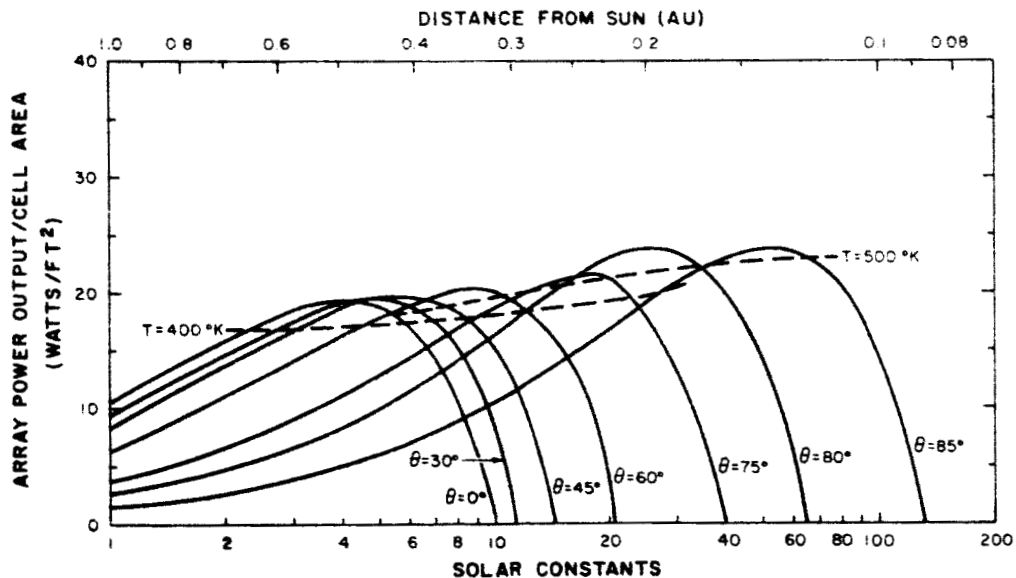


Figure 18. Array Power Output as a Function of Tilt Angle and Solar Intensity for Gallium-Arsenide Cells, $\left(\frac{\bar{\alpha}}{\bar{\epsilon}}\right)_{\text{cell}} = 1.1$

percentage of solar energy to be passed to the solar array. Nearly uniform illumination of the array at reduced solar intensity is achieved by proper relationship of the hole size and spacing, and by displacement distance of the deployed shield from the array.

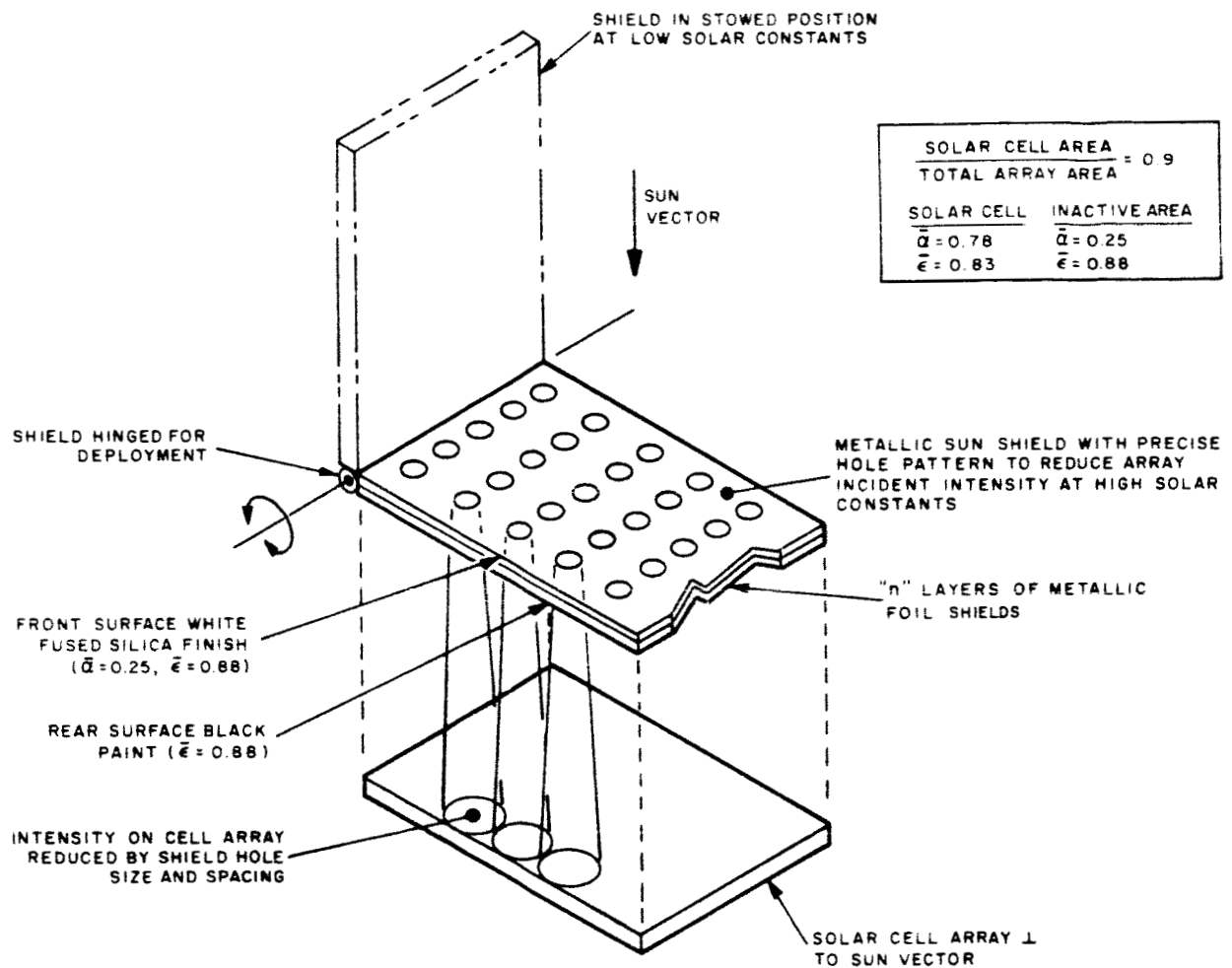


Figure 19. Thermal Analysis Model of Flat Array with Deployable, Intensity-Reducing Sun Shield

The sun shield remains in the stowed position until the power output of the sun-oriented array begins to drop due to the increasing temperature at higher solar constants (refer to Figures 17 and 18; Figure 17 indicates a deployment intensity of 8.4 solar constants for a selected design point of 500°K). At this time, the shield is deployed parallel to the panel and the effective array illumination is reduced. Figures 20 and 21 show array temperature as a function of number of solar constants, and Figures 22 and 23 show array power output per solar-cell area for the deployed shield configuration. A series of curves are displayed which are functions of: (1) configuration factor (ϕ) between array and sun shield, (2) number of sun-shield foil layers (n), and (3) percentage of sun-shield hole area which passes solar energy to the array. Configuration factor is defined as the percentage of thermal energy leaving the array that strikes the sun shield. Figure 24 illustrates the relationship of ϕ with array size and array/sun-shield spacing.

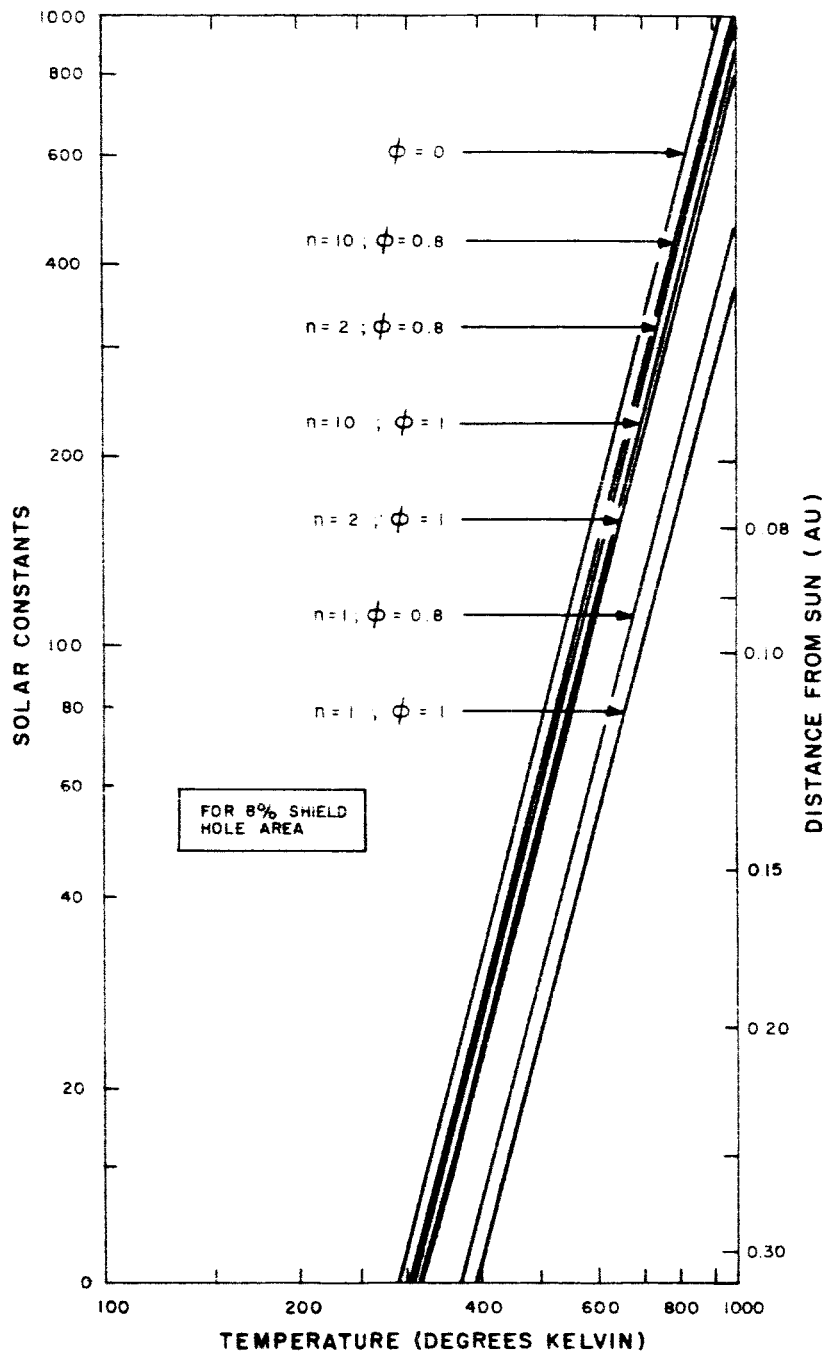


Figure 20. Array Temperature for Silicon or GaAs Cells as a Function of Solar Intensity, Configuration Factor and Number of Shield Layers (Eight-Percent Shield-Hole Area)

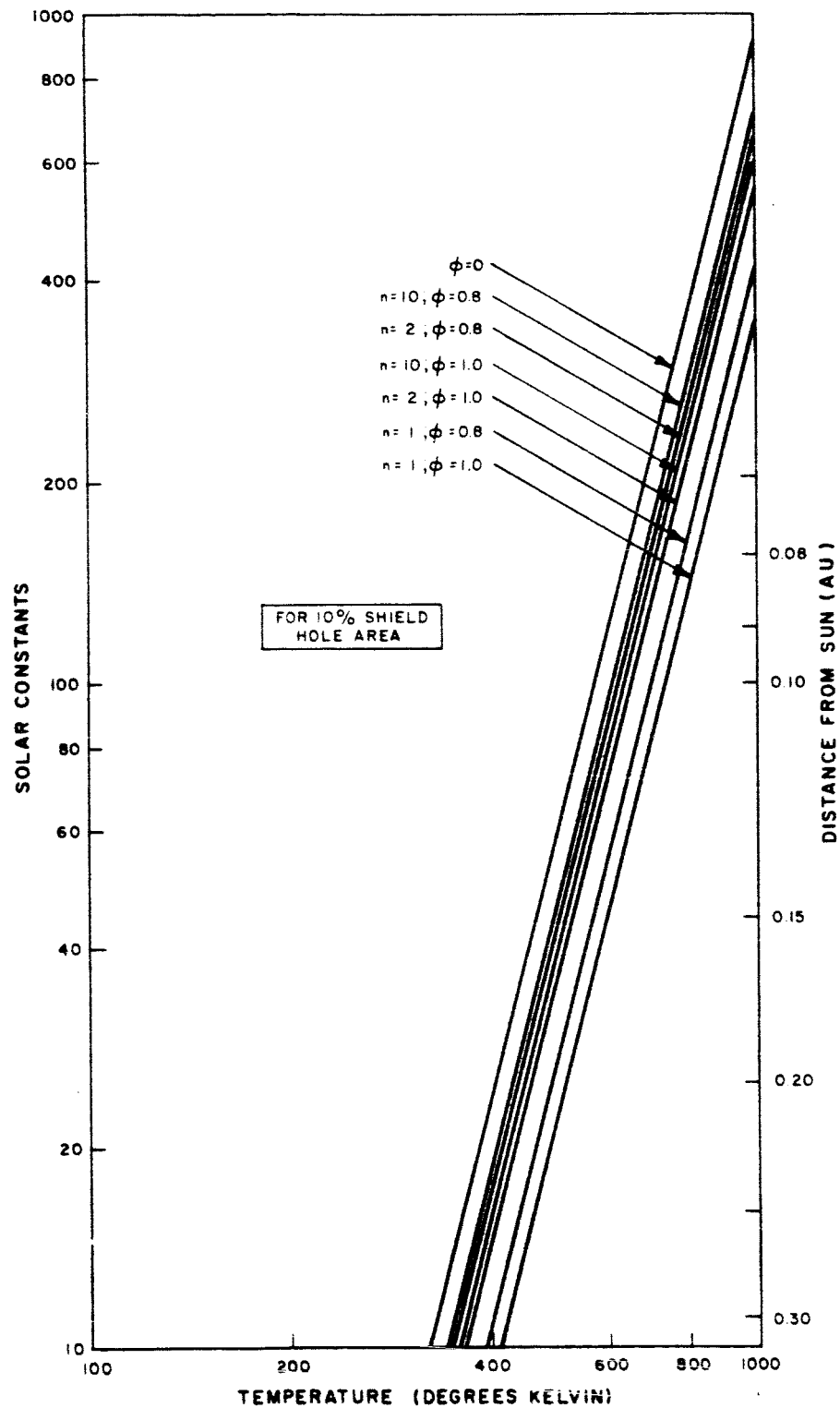


Figure 21. Array Temperature for Silicon or GaAs Cells as a Function of Solar Intensity, Configuration Factor and Number of Shield Layers (Ten-Percent Shield-Hole Area)

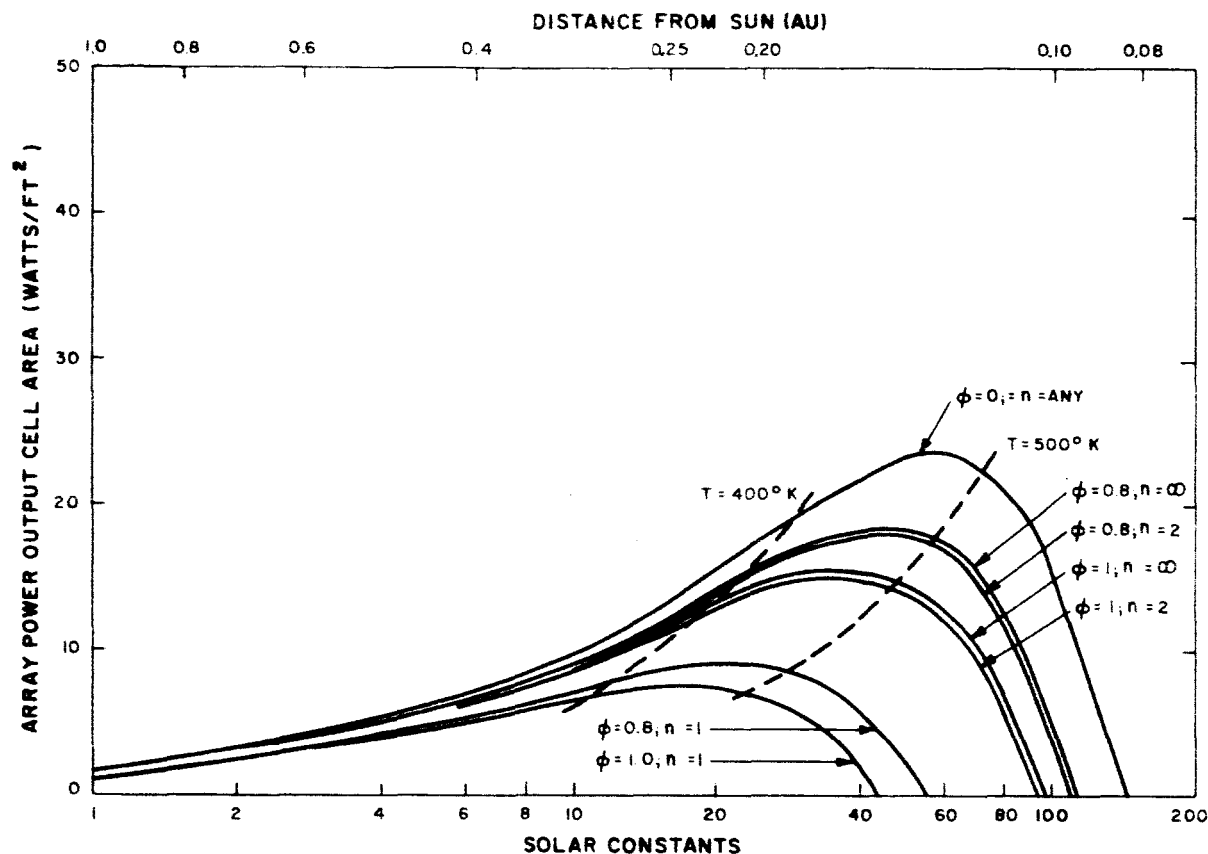


Figure 22. Array Power Output for Gallium-Arsenide Cells as a Function of Solar Intensity, Configuration Factor, and Number of Shield Layers (Eight-Percent Shield-Hole Area)

The general trends of the temperature and power output curves are as follows:

- Temperature decreases and power output increases as the sun-shield/array spacing distance is increased (decreasing ϕ).
- Temperature decreases and power output increases as the number of sun-shield layers (n) increase. Ten shield layers produce nearly the same results as an infinite number of shields.
- As the percentage of hole area in the shield is increased, more power output is produced up to approximately 40 solar constants. For solar constant values higher than 40, the higher percentage hole case produces less power output.
- Decreasing ϕ is more effective than increasing n .

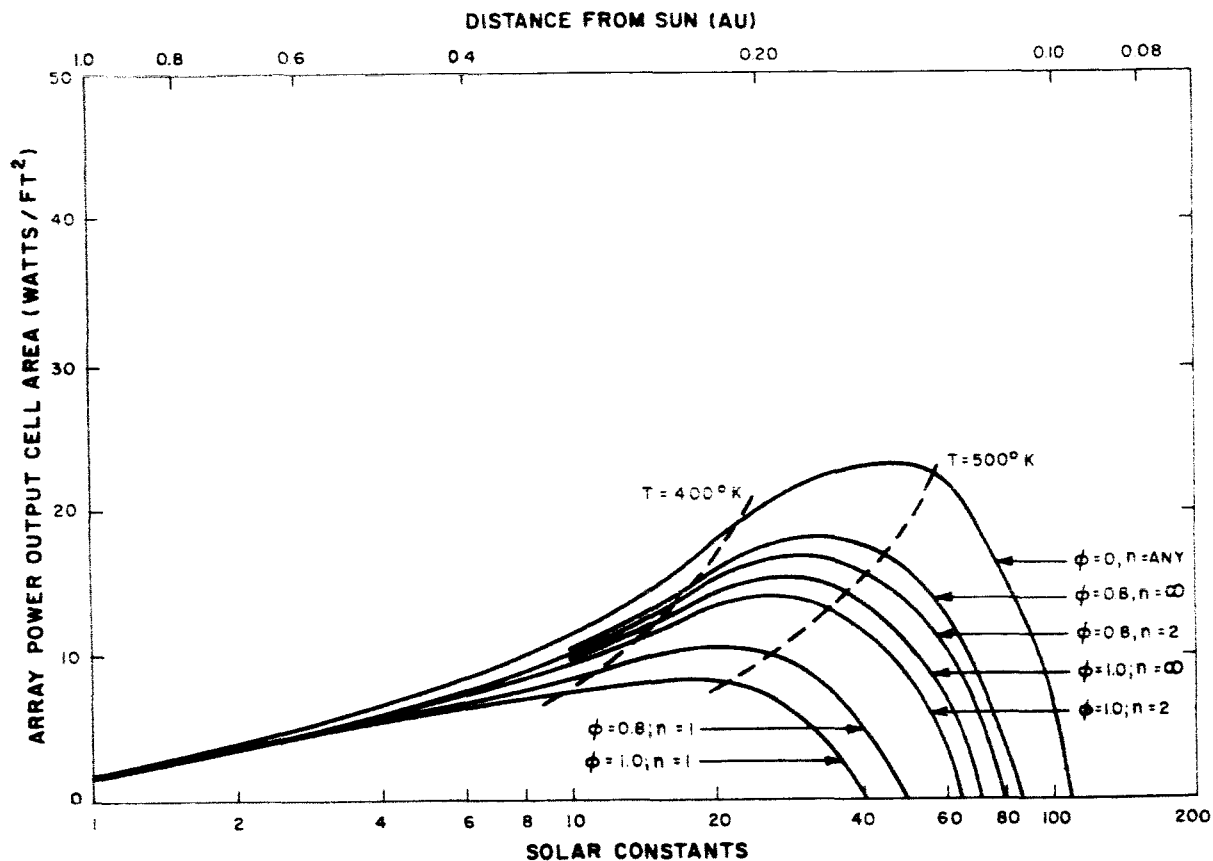


Figure 23. Array Power Output for Gallium-Arsenide Cells as a Function of Solar Intensity, Configuration Factor, and Number of Shield Layers (Ten-Percent Shield-Hole Area)

The deploying shield design has several advantages over the tilting array design. One significant advantage is the elimination of the angle of incidence problem, all thermal calculations being performed for normally oriented surfaces. However, analytical and experimental investigations on sun-shield hole design would be required to insure that the proper illumination level is achieved at the array, and that no intense solar spotting results. At high solar-constant values, patterns of bright spots and shadows may produce undesirable thermal gradients on the array. Overlapping of the incident solar energy from the shield's holes is desired to produce approximate uniform illumination. The increasing de-collimation of the Sun's rays at increasing solar constant positions helps obtain uniformity of illumination on the solar array if the total thickness of shields is not large relative to hole size and thermal gradients through the stack of shields do not cause significant misalignment.

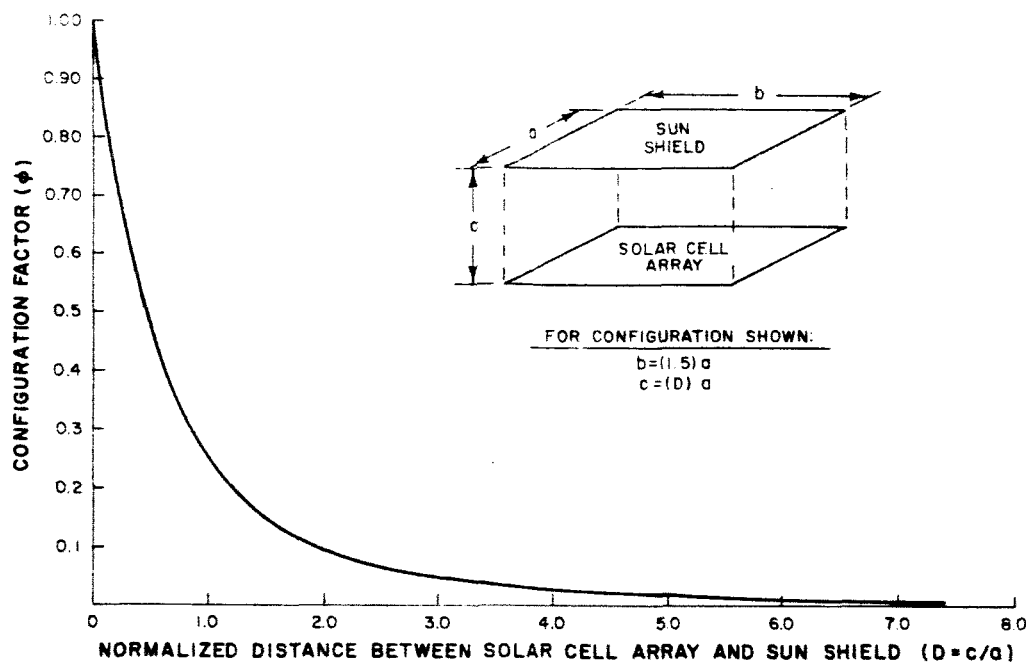


Figure 24. Configuration Factor as a Function of Normalized Spacing Distance Between Solar-Cell Array and Sun Shield

D. THERMAL CONTROL OF SPINNING CYLINDRICAL ARRAY BY VARYING THE ARRAY PACKING FRACTION

Figure 25 shows the thermal-analysis model of a spinning cylindrical array. The vehicle is spin-stabilized* so that the spin axis is maintained perpendicular to the sun vector. Only the lateral area of the cylinder is used for the cell array, leaving the top and bottom surfaces available for internal thermal control of the vehicle. Blue-filter gallium-arsenide solar cells are used and the inactive array area is covered with second-surface mirrors (a low α , high ϵ finish). The inside surface of the array is thermally insulated from the vehicle interior.

Calculations were performed to determine array temperature (Figure 26) and array power output (Figure 27) as a function of number of solar constants and packing fraction (β), the ratio of solar cell area to total array area. The curves show that as β is decreased (less solar cells, more second-surface mirrors), temperature and power output per total array area decrease until approximately 7 solar constants. For solar constant values greater than 7, the power output generally increases as β is decreased. However, the level of available maximum power continually declines for decreasing β . The curve clearly shows both the advantage and disadvantage of decreasing the packing

*Extended Pioneer

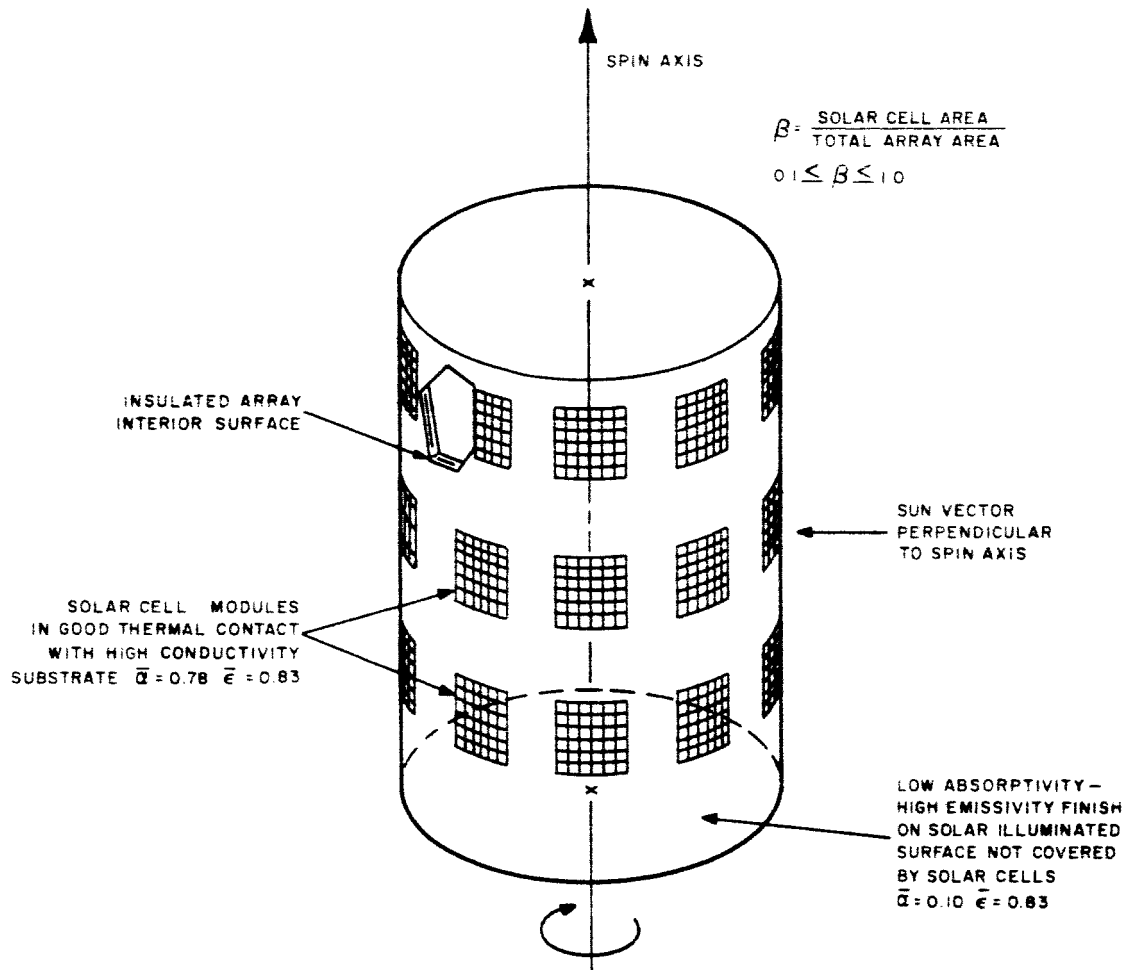


Figure 25. Thermal Analysis Model of Spinning Cylindrical Array

fraction. The advantage is obtaining array power output at high solar-constant values (beyond 0.3 AU); the disadvantage is reduced power output at near-earth positions for the low β values. The cylindrical array is the simplest thermal-control system investigated and compares favorably with the flat arrays if limited power is required at near-earth positions. If a system were devised to obtain a high packing fraction at near-earth positions and a low packing fraction at near-sun positions, the cylindrical array would be more attractive. One way to accomplish this objective would be to design small cell modules with one side of high β , and the other side of low β . The modules would be inset into cavities on the vehicle side and would rotate 180° upon command at the desired trajectory position.

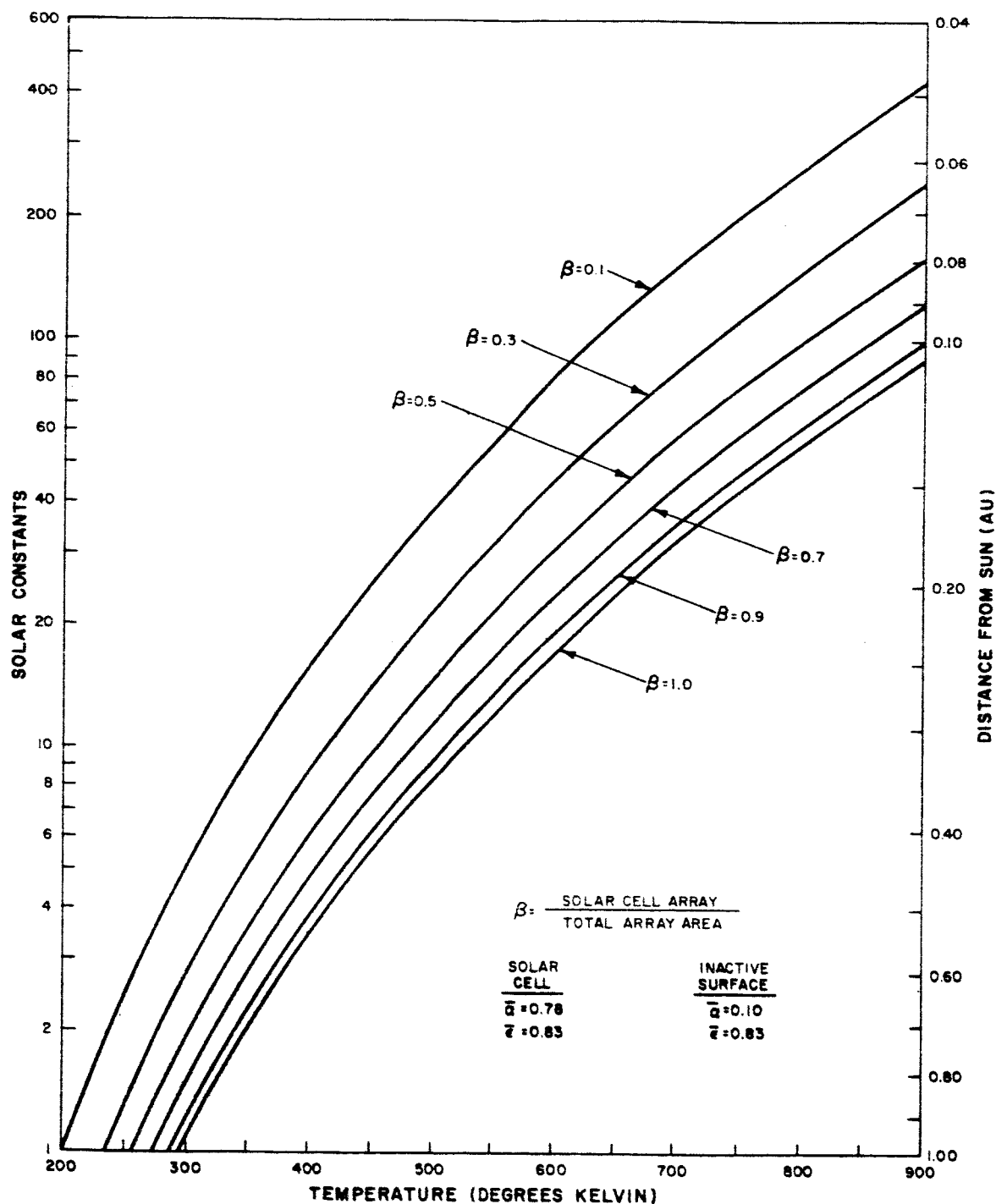


Figure 26. Array Temperature for Silicon or GaAs Cells as a Function of Solar Intensity and Packing Fraction (β) on a Spinning Cylindrical Array

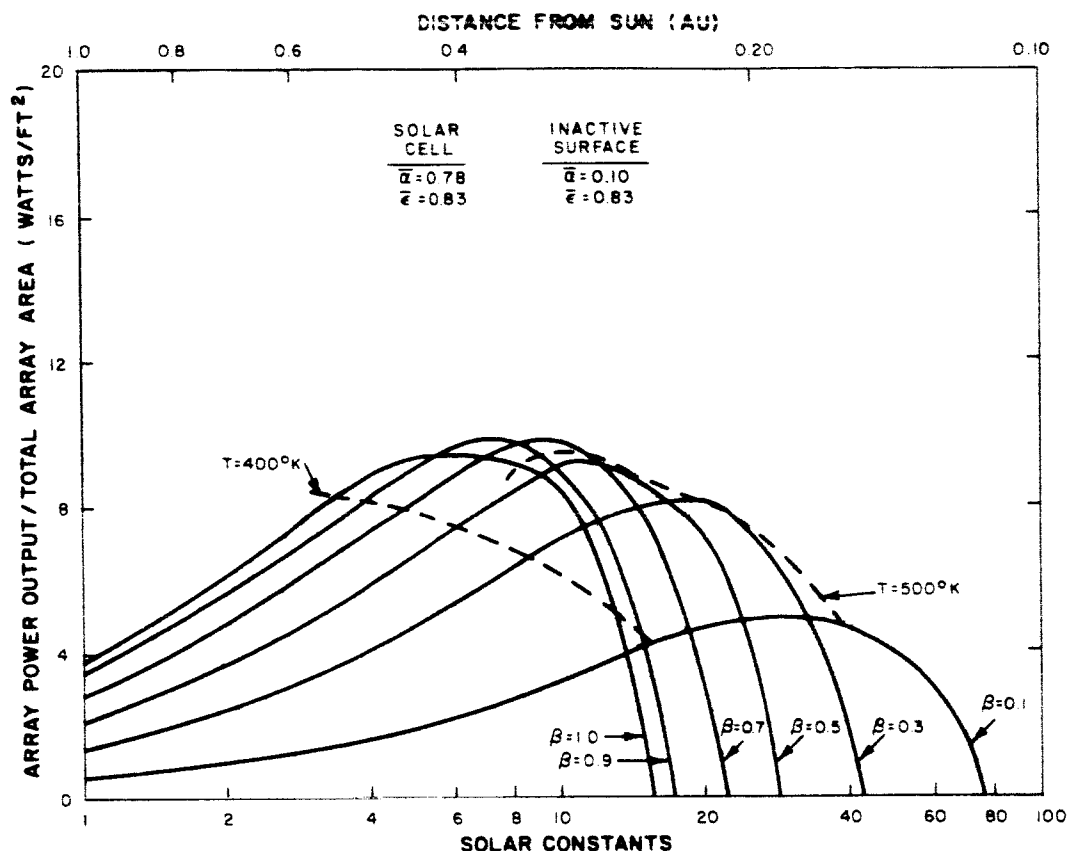


Figure 27. Array Power Output for Gallium-Arsenide Cells as a Function of Solar Intensity and Packing Fraction (β) on a Spinning Cylindrical Array

E. THERMAL CONTROL USING A HYBRID SYSTEM OF ARRAY TILTING AND CYLINDRICAL MIRROR

From both power output and thermal considerations, the method of tilting the solar array off-normal for near-sun missions is very good. However, as the angle between the array normal and the sun vector approaches 90° (as would be required for thermal control during very near-sun missions) other problems will occur. The power output characteristics of solar cells at grazing sun angles is not well known and the appropriate experimental programs would be extremely difficult to perform. Therefore, a practical approach might well be a hybrid system incorporating the benefits of an angular tilt system and a reflective system. Since the characteristics of solar cells are well known at grazing angles of up to 60° , it would be advantageous to have the array operate at normal orientation at 1 solar constant, tilting off to an angle of 60° at some chosen point, and then fully tilting and receiving reflected solar energy beyond this point.

From Figures 17 and 18 (array power output as a function of solar intensity for gallium-arsenide cells), it can be seen that the maximum power per cell area at 1 AU varies between 10.5 and 12 watts/ft² at zero tilt angle. Assuming a packing factor of 90 percent and a required power output per panel of 50 watts, the required panel area is 762 square inches.

A reasonable upper temperature limit for gallium-arsenide solar panels is 500°K. From Figure 18, it can be seen that a temperature limit of 500°K and a tilt angle limit of 60° limit the maximum number of solar constants to 10.5 (corresponding to operation at 0.31 AU). Under these conditions, the 762-square-inch solar array is generating 93 watts of electrical power.

At near-sun distances, the solar panel must travel to full tilt ($\theta = 90^\circ$) in order to preclude panel temperatures higher than 500°K. This requires that the solar array be illuminated by reflection from a cylindrical mirror. At this location (AU = 0.31) the mirror is sized for an array power output of 50 watts. The solar reflectivity of the cylinder is assumed to be 90 percent. For this situation, the required projected area of the reflector to the solar vector is given by:

$$A_p = \frac{P}{S\eta\rho} = 73.6 \text{ sq. inches}$$

where

P = required power output (50 watts);

S = solar constant at 0.31 AU (9.45 watts/in²);

η = cell efficiency (8%, equivalent to 1 solar constant at 323°K); and

ρ = reflectivity of cylindrical mirror (0.90).

If the 762-square-inch solar array is made as a square, it is 27.3 inches on a side. The following relationships can be set up from Figure 28 for a cylindrical reflector of the same length:

$$X = \frac{A_p}{L} = 2.69 \text{ inches}$$

and

$$R = \frac{X}{\cos \gamma_1 - \cos \gamma_2} = 3.95 \text{ inches}$$

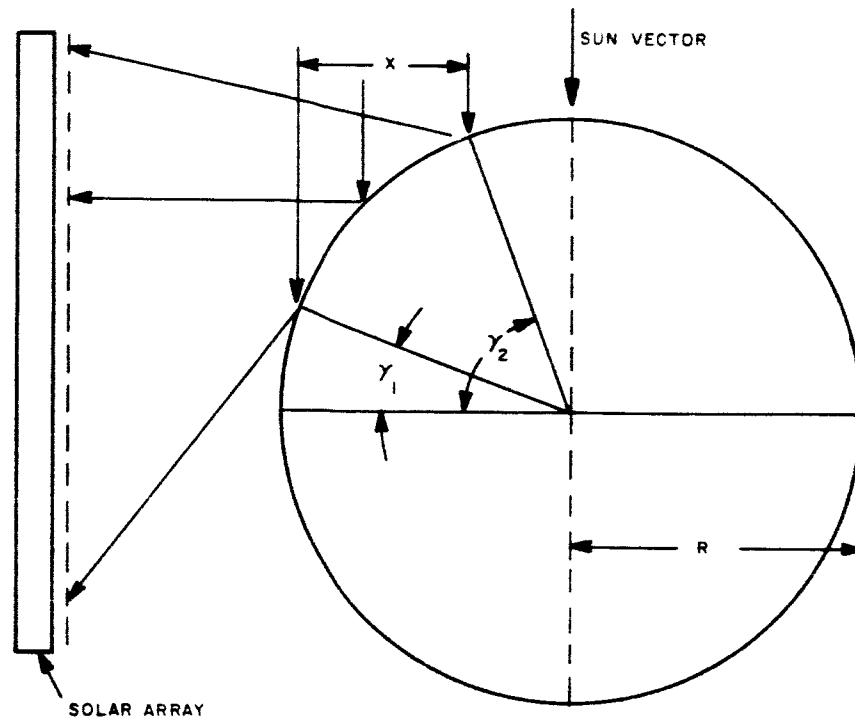


Figure 28. Cylindrical Mirror Geometry

where

$$A_p = 73.6 \text{ in}^2$$

$$L = 27.4 \text{ in.}$$

$$\gamma_1 = 20^\circ \text{ (assumed)}$$

$$\gamma_2 = 75^\circ \text{ (assumed)}$$

$$R = \text{radius of cylindrical mirror.}$$

Thus the required radius of the cylindrical mirror is 3.95 inches for an actual reflecting surface of arc $\gamma_2 - \gamma_1$.

The problem of the reflector temperature at near-sun missions was also investigated. The method used to keep the reflector reasonably cool is shown in Figure 29. The energy balance equation for this method is given by the expression:

$$R(\cos \gamma_1 - \cos \gamma_2) L \bar{\alpha}_2 S + R(1 - \cos \gamma_1) \bar{\alpha}_1 L S = \sigma T^4 \left[LR(\gamma_2 - \gamma_1) \bar{\epsilon}_2 + L(\pi R + R\gamma_1) \bar{\epsilon}_1 \right]$$

or

$$\sigma T^4 = \frac{S \left[(\cos \gamma_1 - \cos \gamma_2) \bar{\alpha}_2 + (1 - \cos \gamma_1) \bar{\alpha}_1 \right]}{(\gamma_2 - \gamma_1) \bar{\epsilon}_2 + (\pi + \gamma_1) \bar{\epsilon}_1}$$

where

$S = 90 \text{ watts/in}^2$, (solar constant);

$\gamma_1 = 20^\circ = 0.349 \text{ radian}$;

$\gamma_2 = 75^\circ = 1.309 \text{ radian}$;

$\bar{\epsilon}_1 = 0.9$ (emissivity of exposed cylinder, non-reflector area);

$\bar{\alpha}_1 = 0.9$ (solar absorptivity of exposed cylinder, non-reflector area);

$\bar{\epsilon}_2 = 0.1$ (emissivity of reflector area of cylinder);

$\bar{\alpha}_2 = 0.1$ (solar absorptivity of reflector area of cylinder);

σ = Stefan-Boltzmann constant.

Substitution of these parameter values into the energy balance equation results in a value of (T) equal to 538°K .

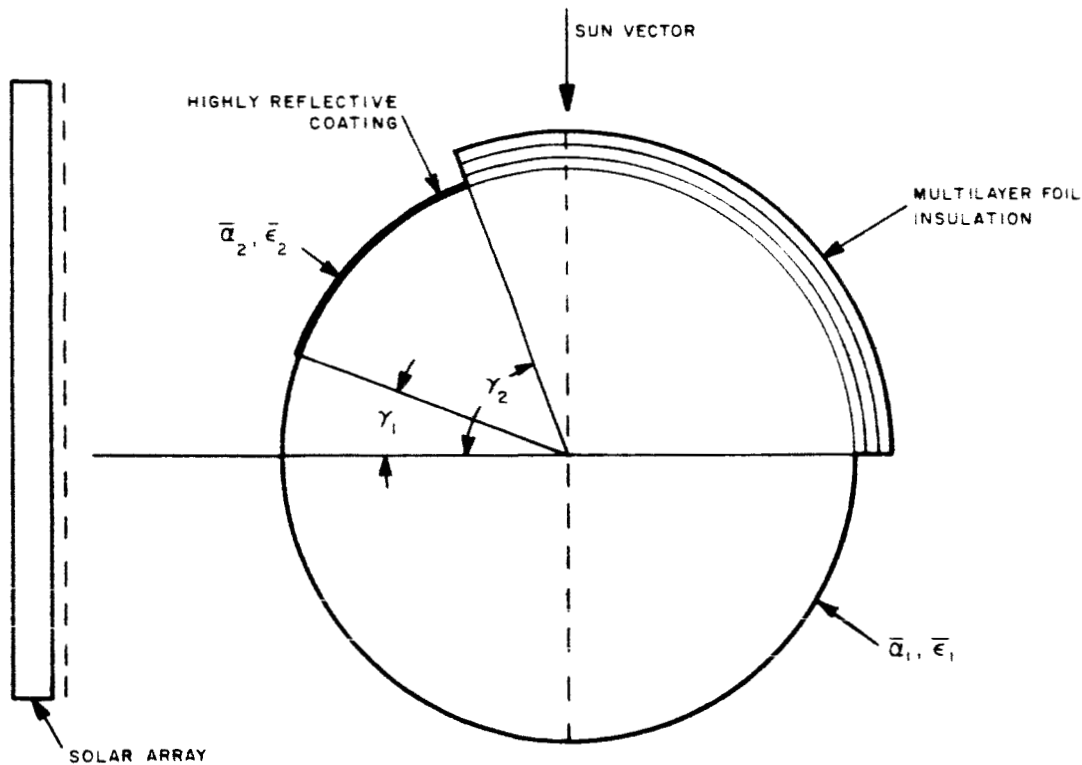


Figure 29. Cylindrical Mirror Cooling Method

The multilayer foil insulation was assumed to be perfectly adiabatic for this calculation. High temperature measurements on these foils from radioisotope thermoelectric generator (RTG) programs have given effective emissivity values of 0.002 with no degradation during life tests.

The cylinder used for this calculation was assumed to be isothermal which is reasonable for an aluminum cylinder. Weight can be saved by using a tube but wall thickness will have to be a trade-off as a function of the resulting temperature difference across the tube. The reflector temperature of 538°K should result in no material problems for the highly reflective coating. This vacuum-deposited coating has been developed to have a solar reflectivity greater than 90 percent. The coating is also characterized by low values of emissivity; thus the $\bar{\epsilon}_2$ value of 0.1 was chosen.

Figure 30 shows the geometric spacing of the system. For a solar panel 27.5 inches on a side, the following geometrical relationships can be written:

$$a \tan 60^\circ + R \cos 15^\circ + b \tan 50^\circ = 27.4 \quad (1)$$

$$a + R \sin 15^\circ = b + \frac{R \sin 20^\circ}{\tan 50^\circ} + R \cos 20^\circ \quad (2)$$

Solving equation (1) for (a),

$$a = \frac{27.4 - R \cos 15^\circ - b \tan 50^\circ}{\tan 60^\circ}$$

Substituting the expression for (a) into equation (2) and solving for (b),

$$b = \frac{R}{1 + \frac{\tan 50^\circ}{\tan 60^\circ}} \left[\frac{27.4}{R \tan 60^\circ} + \sin 15^\circ - \frac{\cos 15^\circ}{\tan 60^\circ} - \frac{\sin 20^\circ}{\tan 50^\circ} - \cos 20^\circ \right]$$

$$b = 5.8 \text{ inches (for } R = 3.95 \text{ inches).}$$

The spacing (D) between the array and the cylinder is given by:

$$\begin{aligned} D &= b + \frac{R \sin 20^\circ}{\tan 50^\circ} + R \cos 20^\circ \\ &= 10.7 \text{ inches.} \end{aligned}$$

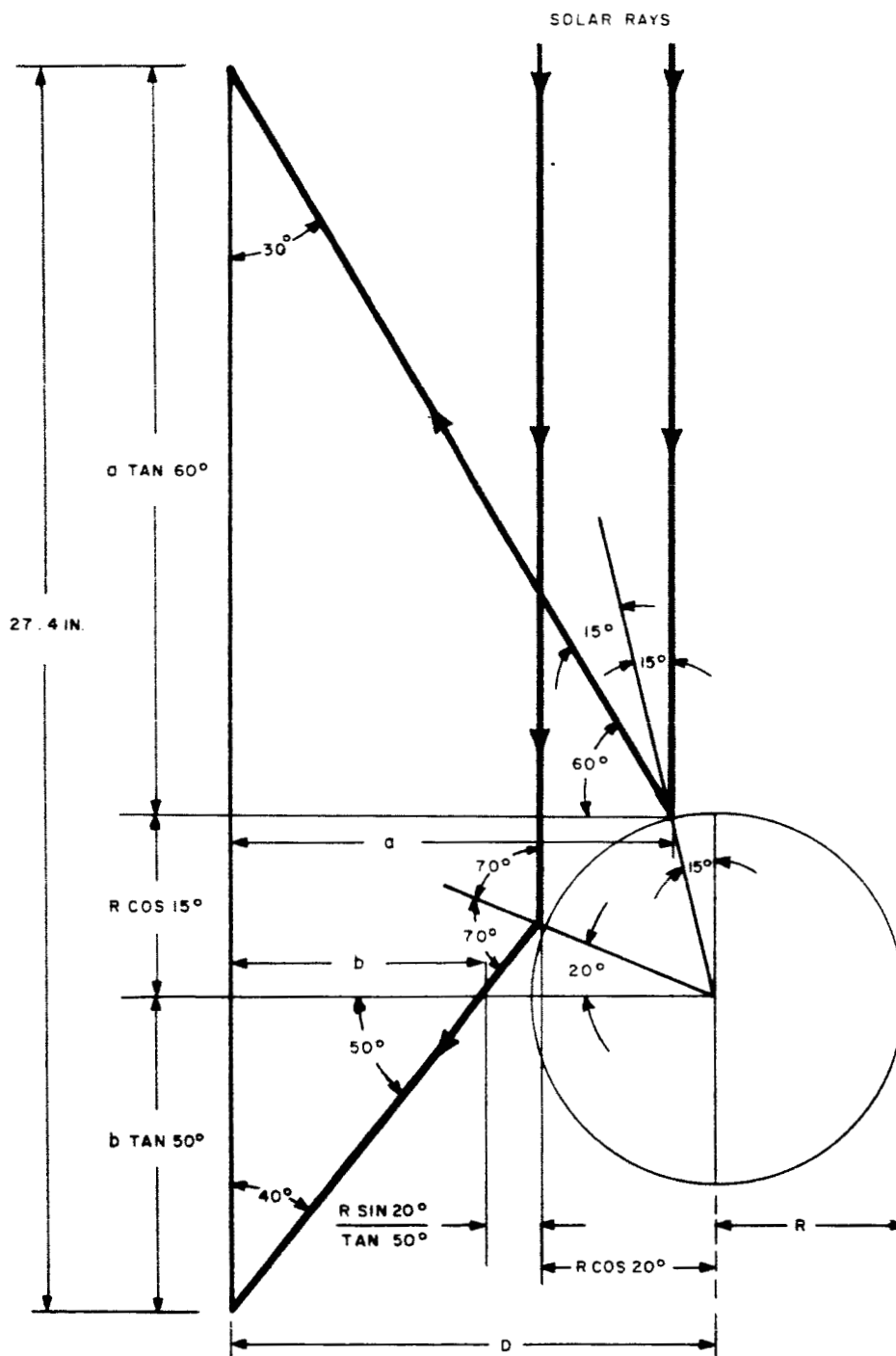


Figure 30. Cylindrical Mirror Positioning Diagram

sensing device, the tilt angle between 0.34 and 0.22 AU could be made a gradual, constant-temperature movement, hitting a switch at the 60° point which would actuate the full tilt movement.

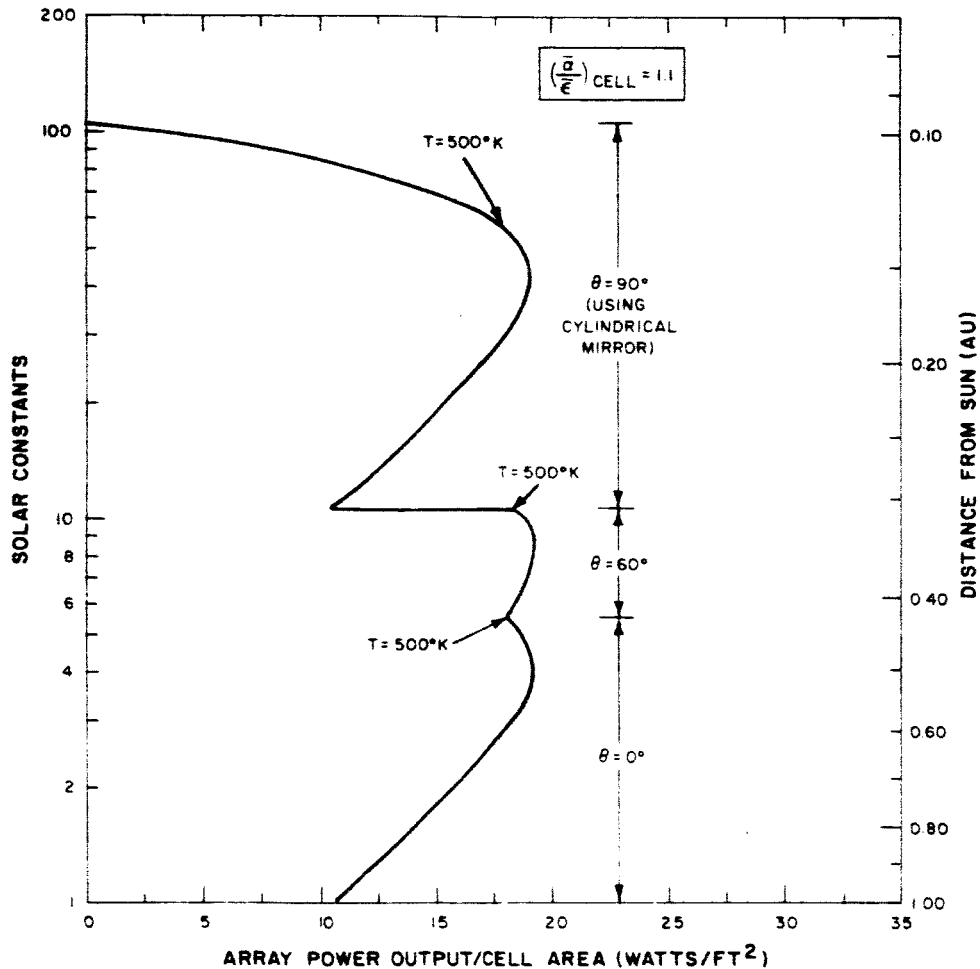


Figure 32. Array Power Output for Hybrid Gallium-Arsenide System as a Function of Solar Intensity and Array Angle, $\left(\frac{\bar{\alpha}}{\bar{\epsilon}}\right)_{\text{cell}} = 1.1$

The power output of the hybrid gallium-arsenide system is shown in Figures 31 and 32 for two different solar cell $\bar{\alpha}/\bar{\epsilon}$ values. The previously calculated power and size numbers used the solar cell $\bar{\alpha}/\bar{\epsilon}$ value of 1.1 as a base but Figure 17 shows the gain in array power output for an $\bar{\alpha}/\bar{\epsilon}$ value of 0.7 which is the lowest possible limit.

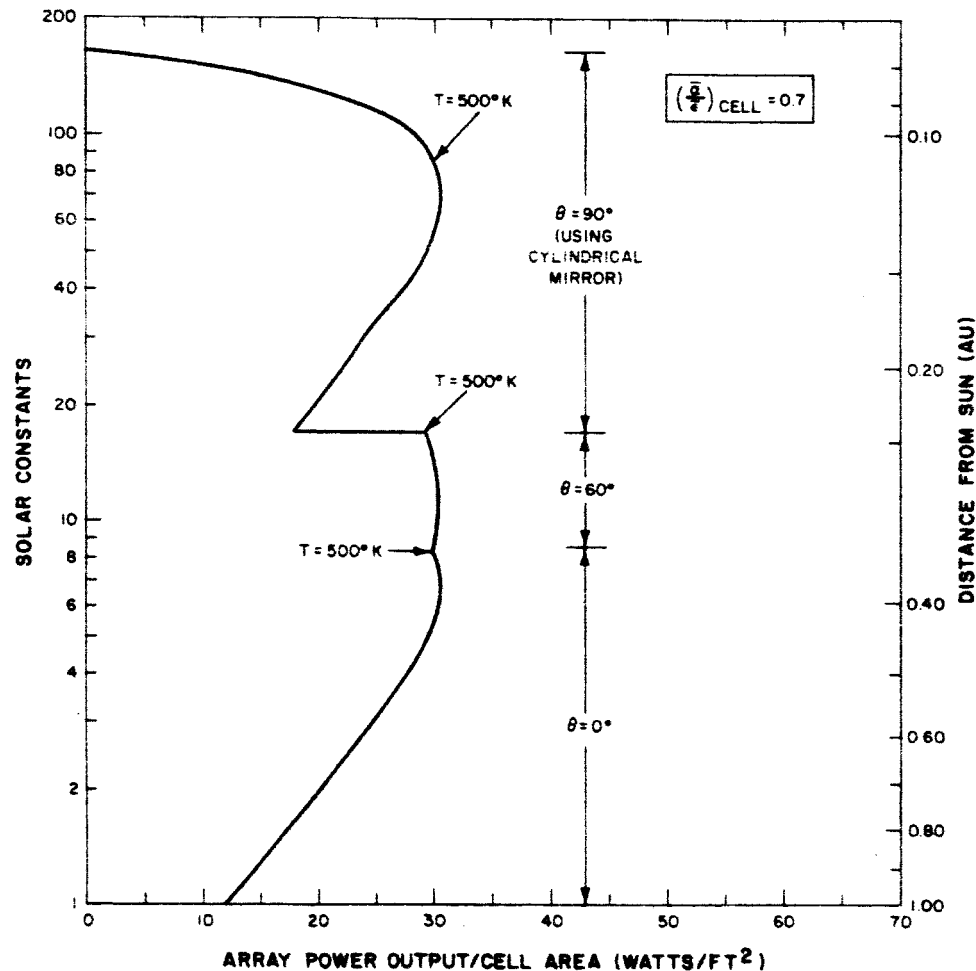


Figure 31. Array Power Output for Hybrid Gallium-Arsenide Cell System as a Function of Solar Intensity and Array Tilt Angle, $\left(\frac{\bar{\alpha}}{\bar{\epsilon}}\right)_{\text{cell}} = 0.7$

Figure 31 is based on a maximum tilt angle of 60° and a maximum allowable panel temperature of 500°K . From 1.0 to 0.34 AU the panel is oriented normal to the Sun (tilt angle of 0°). At 0.34 AU the panel temperature reaches 500°K and the ratio of power output to solar cell area is 30 watts/ft². At this time the panel tilts to an angle of 60° to the Sun, cools appreciably, but maintains the power output approximately constant. At 0.22 AU the temperature again reaches 500°K and the panel tilts to 90° . If the tilt angle were controlled by a temperature

SECTION V

SOLAR-ARRAY PARAMETERS FOR THE FOUR SOLAR PROBE MISSIONS

A. SOLAR-ARRAY PARAMETERS FOR THE 0.4-AU MISSION

The spin-stabilized Extended Pioneer solar probe is assumed to have a cylindrical solar-cell array with circular cross section. The spin axis of the probe is coincident with the cylinder axis and is perpendicular to the sun vector during the duration of the 180-day mission. Solar cells are mounted only on the lateral cylindrical surface, are in good thermal contact with the high-conductivity array substrate material, and are thermally insulated from the remainder of the spacecraft structure. A conservative value of solar cell $\bar{\alpha}/\bar{\epsilon}$ ratio of 0.95 was assumed and array output power was calculated on the basis of watts per square foot of active cell area, so that packing factor could be varied (as shown in Table 9).

Both the silicon and gallium-arsenide solar-cells considered are one-by-two centimeters in area, twelve mils thick, and have nine mils of Corning 7940 fused-silica cover glass for irradiation protection and high thermal emissivity. The charged particle flux degrades the silicon solar cell about 20 percent during this six-month mission, but does not affect the gallium-arsenide cell power output.

Applying the performance calculation procedure described in Section III, the environment-degraded output power density for gallium-arsenide and silicon solar cells was calculated at numerous points along the probe trajectory and plotted in Figure 33. The two power plots represent the output at the maximum power point of the solar cell I-V curves. In order to realize this power, a maximum power-point-tracker circuit would have to be used in the power supply subsystem. The maximum power-point tracker is a pulse-width-modulated device which allows the power-conditioning subsystem to utilize maximum power capability of the solar-cell array by forcing the subsystem to operate on that point of the array output characteristic (I-V curve) which produces the largest current-voltage product. Another feature which may be incorporated in the power supply subsystem allows operation from a point on the array I-V curve which produces just the amount of input power required to supply the load demand and power supply losses. This feature minimizes dissipation of unused power when the array capability exceeds total power demand, aiding in the reduction of system operating temperature. The solar cell operating temperature as a function of days in the trajectory is also shown in Figure 33.

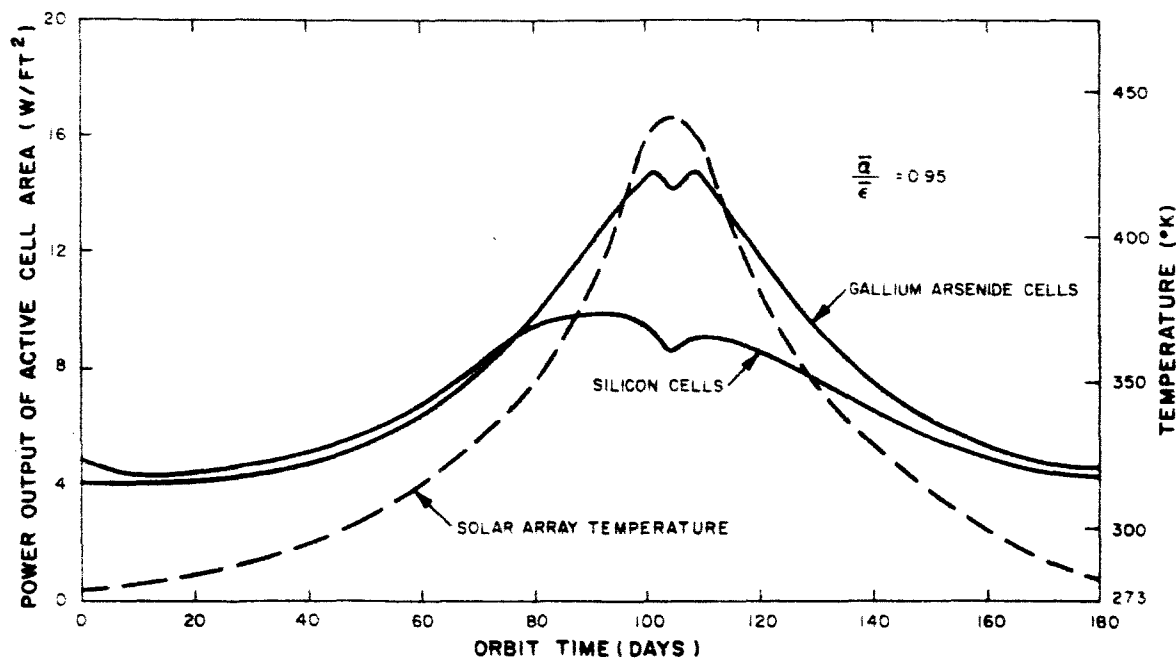


Figure 33. Maximum Power Output of Silicon and Gallium-Arsenide Solar Cells Versus Orbit Time for 0.4-AU Extended Pioneer Trajectory

Inspection of the power density curves shows that the gallium-arsenide array has its minimum power at the greatest sun-probe distance, which occurs at the day of launch. The silicon array, because of charged-particle irradiation damage to the solar cells, has a minimum output at the end of the mission (180 days). Therefore, the size of the arrays must be such that the required output power of 55 watts is supplied at the time of minimum array capability (day 0 for gallium arsenide and day 180 for silicon).

The use of a maximum power-point tracker would supply a greatly increased power demand near perihelion, if the spacecraft experiments or communications required an added number of watts at this time. Both the gallium-arsenide and silicon arrays can fulfill the mission power requirements, although the gallium-arsenide array can provide greater power at the closest sun approach.

Table 8 presents the array size (square feet of active solar-cell area), cost of solar cells, weight of array and power available at perihelion for gallium-arsenide and silicon solar arrays, designed to provide a minimum of 55 watts of output power during the 180-day mission.

The weight of the array is based on the values of 1.11 lbs/ft² for a silicon array and 1.30 lbs/ft² for a gallium-arsenide array. These values represent a reasonably good design which has been achieved in practice with a 0.9 packing factor. All array components including cover glass, cells, panel substrate, thermal emissive coating, electrical components and mounting hardware are represented in the array weights.

TABLE 8. SILICON AND GALLIUM-ARSENIDE SOLAR-CELL ARRAY
PARAMETERS FOR MINIMUM OUTPUT OF 55 WATTS
DURING 0.4-AU MISSION

	Perihelion Power (watts)	Active Cell Area on Cyl. Array (ft ²)	Cost of Solar Cells-1968 (thousands of \$)	Array Weight (lbs)
Silicon	86	12.8	29.7	14.2
Gallium Arsenide	140	13.8	64.0	17.9

Cost of the solar cells is based on a budgetary estimate for production quantities of cells manufactured in 1968, having the efficiencies specified in Section III.

Using the array power versus probe-sun distance curve (Figure 27), the total array size and packing factor were determined for the spinning cylindrical array for sun approaches of less than 0.4 AU (Extended Pioneer mission). Table 9 presents the calculated silicon and gallium-arsenide solar-cell array sizes and packing factors. The gallium-arsenide cells may be used for missions having a 0.15-AU perihelion and silicon solar cells could possibly be used for sun approaches as close as 0.2 AU.

For the silicon cells, the operating temperature was limited to 450°K at all calculated sun approaches by varying the packing factor. At this operating temperature, the efficiency of the silicon cell is two percent. Since trajectory information was not available for sun approaches closer than 0.4 AU, charged-particle irradiation damage incurred beyond 0.4 AU was neglected.

TABLE 9. ARRAY AREA AS A FUNCTION OF DISTANCE OF CLOSEST SUN
APPROACHES FOR GaAs AND SILICON SOLAR-CELL SPINNING
CYLINDRICAL ARRAYS

Closest Sun Approach (AU)	Packing Factor		Active Cell Area (ft ²)		Total Array Area (ft ²)	
	GaAs	Si	GaAs	Si	GaAs	Si
0.40	0.90	0.90	13.75	12.75	15.3	14.2
0.30	0.90	0.50	13.75	12.75	15.3	25.5
0.25	0.80	0.25	13.75	12.75	17.2	51.0
0.20	0.50	0.10	13.75	12.75	27.5	127.5
0.15	0.20	—	13.75	—	68.8	—

B. SOLAR-ARRAY PARAMETERS FOR THE 0.51-AU MISSION

The 0.51-AU Advanced Pioneer solar probe has a flat panel solar-cell array which is maintained normal to the sun vector during the entire 360-day mission. This array orientation can be used to provide a maximum power/array-area ratio because at the closest sun approach of 0.51 AU the array operating temperature is only 468°K. At this temperature, both silicon and gallium-arsenide solar cells have a power output. Silicon conversion efficiency at this temperature is about one percent and gallium-arsenide efficiency is about 3.5 percent (see Figure 5).

The same solar-cell $\tilde{\alpha}/\tilde{\epsilon}$ ratio (0.95), packing factor (0.9), and cover glass thickness (9 mils) as those of the 0.4-AU probe are specified for this mission. The silicon solar-cell power output was degraded about 25 percent by the charged-particle flux encountered over this one-year mission, while the gallium-arsenide solar-cell power output was not affected. Thermal radiation from the rear side of the solar panel was assumed at an emissivity of 0.88.

Using the solar-cell power output calculated in Section III, the power density (watts per square foot of active solar-cell area) for both silicon and gallium-arsenide solar cells versus days in the trajectory are plotted in Figure 34. Also shown is the solar-cell temperature versus time and the power density versus time for a hybrid array consisting of a 70-percent quantity of silicon cells and a 30-percent quantity of gallium-arsenide cells. All three power density curves represent the maximum power output of the array and would require the use of a maximum power-point tracker to realize this output.

Minimum power output for the silicon array occurs at the end of life (360 days) and at the greatest sun-probe distance (230 days) for the gallium-arsenide array. Consequently, the array was sized to provide the required output of 285 watts at the time minimum output occurred.

By combining both silicon and gallium-arsenide solar cells in a hybrid array, a flatter curve can be obtained for the available array power versus time data. A more sophisticated power conditioning system would be required to integrate the two contributions from the hybrid material array.

Table 10 presents the array size (square feet of active solar-cell area), cost of solar cells, weight of array and maximum available power at perihelion for the silicon, gallium-arsenide, and hybrid arrays. The data presented in this table is based on arrays designed to produce a minimum power output of 285 watts during the life of the mission. Basis of weight and cost is the same as for the 0.4-AU mission.

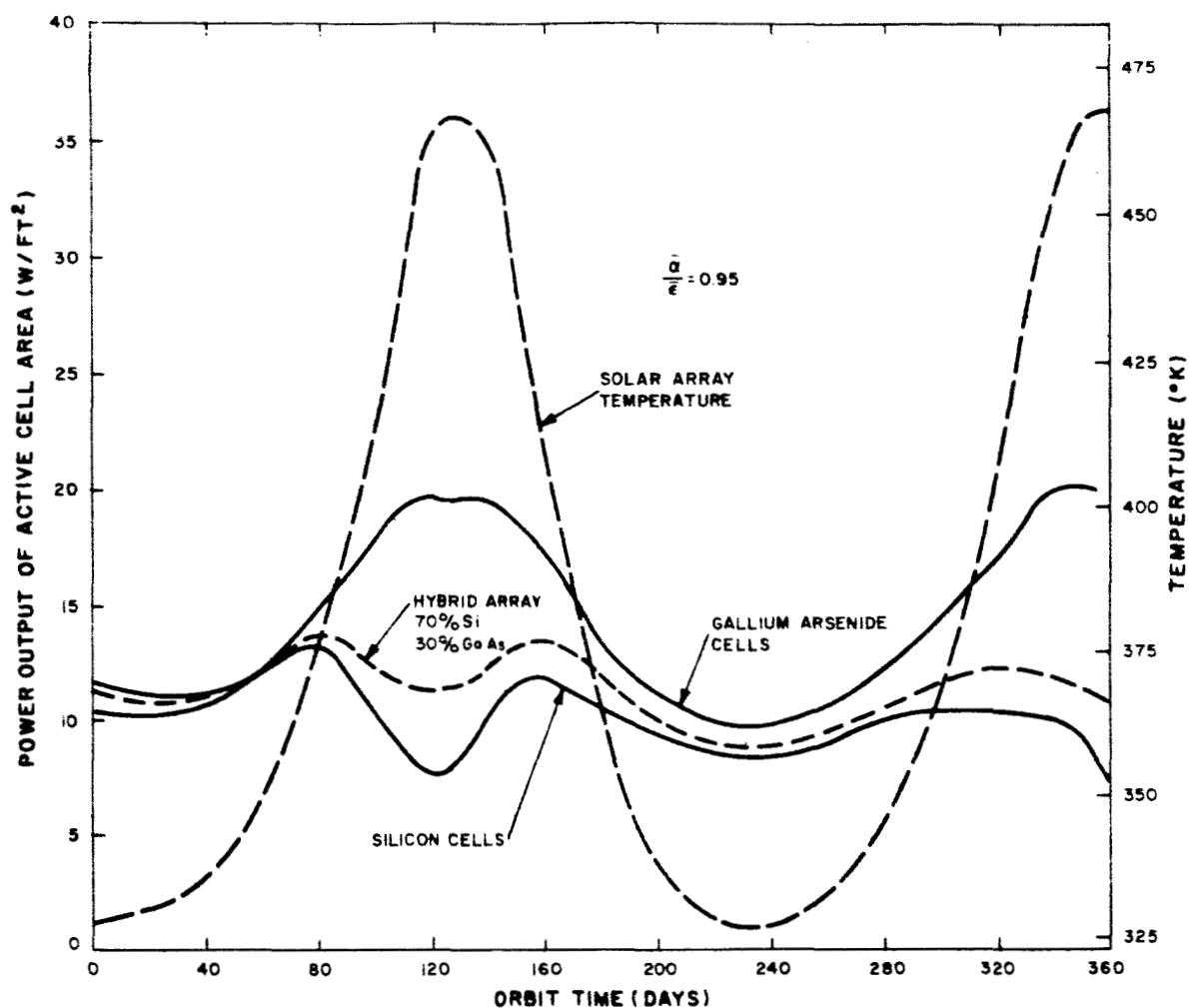


Figure 34. Maximum Power Output of Silicon and Gallium-Arsenide Solar Cells Versus Orbit Time for 0.51-AU Advanced Pioneer Trajectory

TABLE 10. SILICON, GALLIUM-ARSENIDE, AND HYBRID SOLAR-CELL ARRAY PARAMETERS FOR MINIMUM OUTPUT OF 285 WATTS DURING 0.51-AU MISSION

	Perihelion Power (watts)	Active Cell Area on Array (ft ²)	Cost of Solar Cells - 1968 (thousands of \$)	Array Weight (lbs)
Silicon Array	302	39.6	92	51.5
GaAs Array	535	28.5	132	41
Hybrid Array (70% Si, 30% GaAs)	357	31.7	96	40.9

C. SOLAR-ARRAY PARAMETERS FOR THE 0.291-AU MISSION

The 0.291-AU Advanced Pioneer solar probe uses a flat-panel solar-cell array with 9 mils of fused-silica cover glass shielding and a maximum power-point tracker in order to obtain maximum available power from the array during the entire 350-day mission. A value of $\bar{\alpha}/\bar{\epsilon}$ ratio of 0.7 is specified for the solar cells, with thermal emission from both sides of the solar cell panel.

Charged-particle flux is insufficient to degrade the shielded gallium-arsenide cell power output, but the silicon solar cell degrades about 30 percent during this one-year mission.

Figure 35 shows the gallium-arsenide and silicon solar-cell array power density versus days in the 0.291-AU trajectory. These two curves represent the power output of a normally oriented array without the employment of a temperature-control technique. The array operating temperature versus time in the trajectory is also shown.

Based on the solar-cell output power calculations described in Section III, the power density plots show that the gallium-arsenide array can readily supply the 285-watt mission power requirement with normal solar-panel orientation, but the high temperature at the near-sun approaches causes the silicon cell efficiency to drop to zero. The simplest technique which will reduce the array temperature sufficiently to allow silicon solar cells to operate during the entire mission is tilting the solar panel with respect to the sun vector. With an angle of 60 degrees between the array normal and the sun vector, the silicon array will produce a minimum of 8.5 watts per square foot of active solar cell area.

Table 11 presents the array characteristics calculated for the 0.291-AU mission. The gallium-arsenide array maintains normal orientation throughout the mission. Its size is determined by its minimum power output, which occurs at the time of launch. The silicon array has an incidence angle of 60 degrees throughout the mission. A hybrid array consisting of a 50-percent quantity of gallium-arsenide cells and a 50-percent quantity of silicon cells will provide the required 285 watts with normal orientation and the least array size and weight. A packing factor of 0.9 was assumed for each array. The array weights are 1.1 and 1.30 pounds per square foot for the silicon and gallium-arsenide arrays, respectively. Solar-cell costs are based on the guidance budgetary estimates used for the missions previously described.

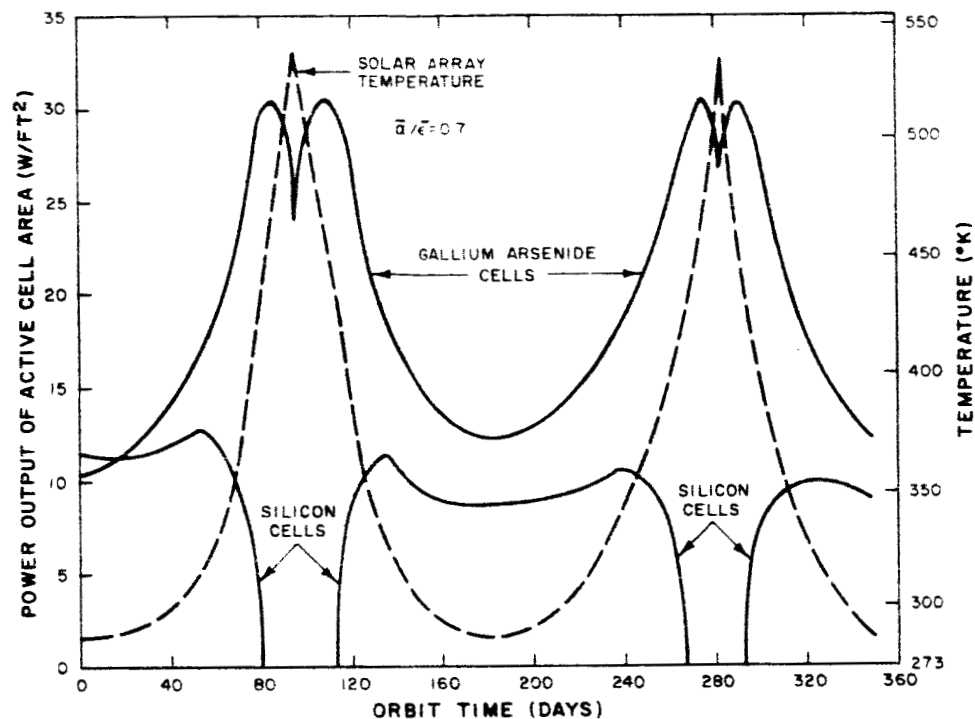


Figure 35. Maximum Power Output of Silicon and Gallium-Arsenide Solar Cells Versus Orbit Time for 0.291-AU Advanced Pioneer Trajectory

TABLE 11. SILICON, GALLIUM-ARSENIDE, AND HYBRID SOLAR-CELL ARRAY PARAMETERS FOR MINIMUM OUTPUT OF 285 WATTS DURING 0.291-AU MISSION

	Perihelion Power (watts)	Active Cell Area on Array (ft ²)	Cost of Solar Cells - 1968 (thousands of \$)	Array Weight* (lbs)
Silicon Array**	600	33.5	78 ⁺	41.3
GaAs Array***	665	27.6	129	40
Hybrid Array*** (50% Si, 50% GaAs)	328	27.2	95	36.5
* Array Weight for Packing Factor = 0.9				
** Incidence Angle (θ) + 60°				
*** Normal Orientation with Respect to Sun Vector				
⁺ Off-Angle Panel Orientation Mechanism Cost Not Included				

D. SOLAR-ARRAY PARAMETERS FOR THE 0.09-AU MISSION

The 0.09-AU Advanced Pioneer solar probe encounters the most severe environmental factors of the four missions considered in this report. Because of the close sun approach (0.09 AU), the operating temperature of the flat-panel solar array is so high (500°K), that the silicon solar-cell efficiency is completely destroyed, even with the application of the array cooling methods discussed in Section IV. With the use of the most effective of the four cooling techniques considered (the hybrid system using array-tilting and cylindrical mirror), a gallium-arsenide array is capable of supplying the required 285 watts for the duration of the 350-day mission.

The charged-particle flux encountered by the vehicle on the 0.09-AU mission is greater than that encountered on any of the other three probe trajectories, but still not enough to degrade the performance of a gallium-arsenide solar cell with 9 mils of fused-silica cover-glass shielding.

Assuming an $\bar{\alpha}/\bar{\epsilon}$ ratio of 0.7 for the array (which should be a practical value at the time of the 0.09-AU probe launch) and a packing factor of 0.9, the size of the array to supply 285 watts was determined. Using the array-tilting/cylindrical-mirror method of temperature control described previously, it can be seen from Figure 36 that the minimum array output-power density occurs at the greatest probe-sun distance (day 140). The minimum power density of 11.2 watts per square foot of active solar cell area, specifies an array containing 25.4 square feet of active cell area. The packing factor of 0.9 then defines a total array size of 28.3 square feet.

At perihelion, the array has reached a maximum operating temperature of approximately 543°K and will supply 558 watts of output power. As with the other three solar-probe missions, a maximum power-point tracker would be used to obtain the predicted power.

Array operating temperature and array output-power density are plotted as a function of time in the 0.09-AU trajectory in Figure 36. Table 12 presents the gallium-arsenide parameters for a minimum output of 285 watts during the 350-day mission. The cost of the gallium-arsenide solar cells used for this mission is based on the guidance budgetary estimate of \$7.50 per cell for 1970 production. Array weight assumes a packing factor of 0.9 and 1.30 pounds per ft² of total array area.

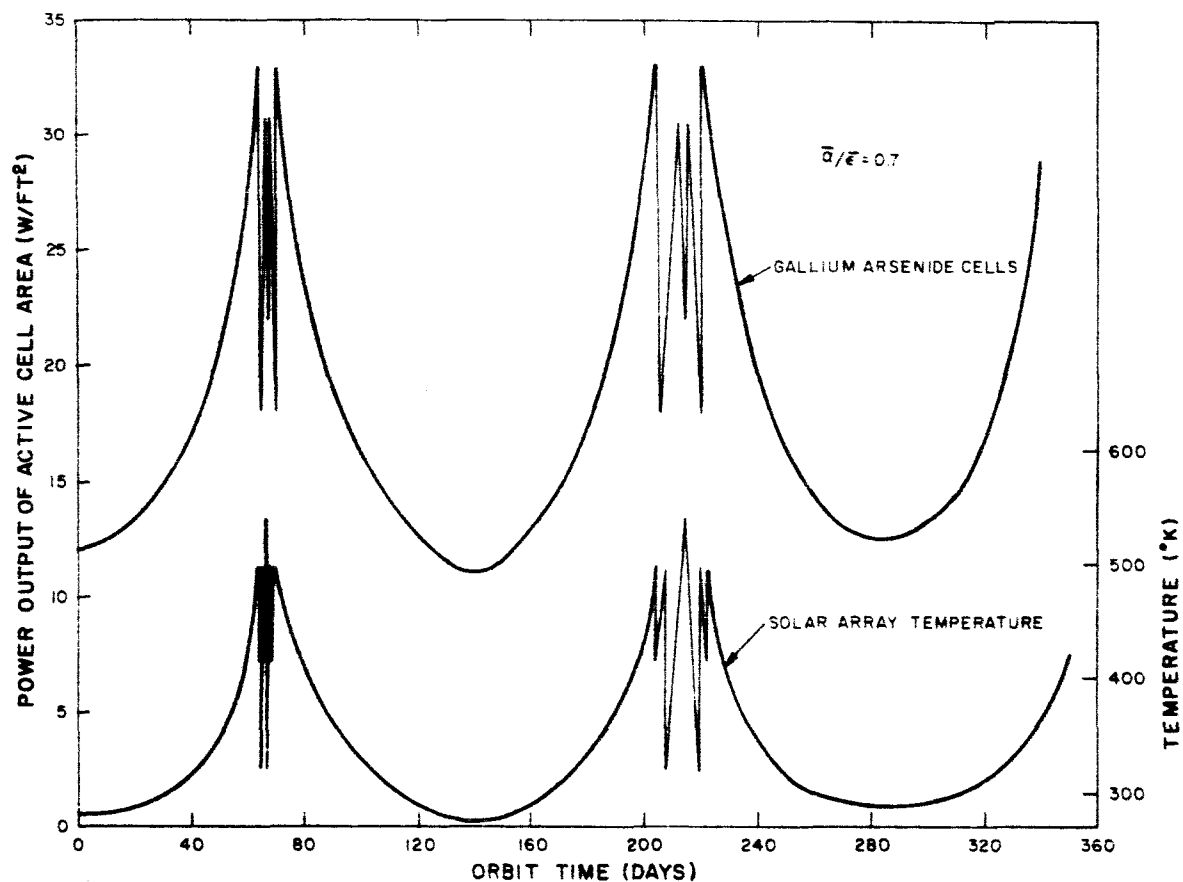


Figure 36. Maximum Power Output of Gallium-Arsenide Solar Cells Versus Orbit Time for 0.09-AU Advanced Pioneer Trajectory.

TABLE 12. GALLIUM-ARSENIDE SOLAR-CELL ARRAY PARAMETERS FOR MINIMUM OUTPUT OF 285 WATTS DURING 0.09-AU MISSION

	Perihelion Power (watts)	Active Cell Area on Array (ft ²)	Cost Of Solar Cells - 1970 (thousands of \$)	Array Weight (lbs)
GaAs Array	558	25.4	98.3	36.8
Si Array	(Environment too severe for Silicon)			

E. SUMMARY OF ARRAY PARAMETERS FOR THE FOUR SOLAR MISSIONS

A comparison of the relative merits of silicon and gallium-arsenide solar-cell arrays for the four Pioneer solar-probe missions discussed in this report is presented in Table 13. A hybrid array consisting of both gallium-arsenide and silicon solar cells is also compared to silicon and gallium-arsenide arrays for the 0.51- and 0.291-AU missions; advantages of this type array are negligible for the 0.4-AU mission and silicon solar cells will not produce power during the entire 0.09-AU mission.

The array characteristics presented in Table 13 are perihelion power output, array power density, array power-to-weight ratio, and solar cell cost-per-watt ratio.

The perihelion power output is the predicted maximum available array power output. For every array considered, this power output is greater than the design power of 55 watts for the Extended Pioneer mission and 285 watts for the Advanced Pioneer missions.

The array power density is defined as watts of array output per square foot of active solar-cell area. The values of power density shown in Table 13 are those calculated for the point in each trajectory when the solar array output is a minimum.

Array power-to-weight ratio is defined as watts of array output per pound of array weight. The array power is that power required by the mission (either 55 or 285 watts). Array weight is the total weight of the array including panel substrate, wiring, blocking diodes, shielding and bonding components, solar cells and contacts, thermal coatings and supporting hardware. The weight of thermal control equipment, (where applicable) is not included.

The solar cell cost-per-watt ratio is defined as the estimated cost of the bare solar cells purchased in production quantities in 1968, per watt of array power output, based on either 55 or 285 watts of array power. Cost of cells for the 0.09-AU mission is based on an estimate for 1970 production.

Each array compared in the table consists of 1 x 2 centimeter solar cells, 12 mils thick, having 9 mils of fused-silica cover-glass shielding. Efficiency of the silicon cells is 10.5 percent for a cover-glassed, module-assembled cell at 303°K air-mass-zero conditions. Efficiency of the gallium-arsenide cells is 8.6 percent for a cover-glassed cell at 303°K air-mass-zero conditions. The array packing factor, defined as the ratio of total active solar-cell area to total array area, is 0.09 for each array in Table 13.

All power predictions were obtained by using the calculation procedure described in Section III. Consequently, these predictions are limited in accuracy by the validity of the basic assumptions made. Greater confidence in the ability to design optimum solar-cell arrays for the severe-environment solar-probe missions can be realized when the results of presently unreported experimental data such as the effects of high-illumination intensity, high temperature, and extreme ultraviolet irradiation are obtained.

	GaAs	Si	GaAs	Si	30% GaAs 70% Si	GaAs	Si	50% GaAs 50% Si	GaAs	Si
Perihelion (AU)	0.4	0.4	0.51	0.51	0.51	0.291	0.291	0.291	0.09	0.09
Minimum Power Required During Mission (watts)	55	55	285	285	285	285	285	285	285	285
Perihelion Power (watts)	140	86	535	302	357	665	600	328	558	
Minimum Array Power Density 1. (watts/ft ² , active solar cell array) 2. (watts/ft ² , total array)	4.0 3.6	4.3 3.9	10.0 9.0	7.2 6.5	9.0 8.1	10.3 9.3	8.5 7.65	10.5 9.45	11.2 10.1	
Array Power-to-Weight Ratio (watts/pound of array)	3.1	3.9	6.9	5.5	7.0	7.1	6.9*	7.8	7.7*	
Solar Cell Cost-per-Watt Ratio (\$1000/watt)	1.17	0.54	0.46	0.32	0.34	0.45	0.27**	0.33	0.35**	

* Does not include temperature controlling mechanism weight.
** Does not include temperature controlling mechanism cost.

*** Does not include temperature controlling mechanism weight.**

**** Does not include temperature controlling mechanism cost.**

SECTION VI

DEVELOPMENT PLAN FOR THE GALLIUM-ARSENIDE SOLAR ARRAY

Investigation conducted during the gallium-arsenide solar-cell study program has shown that, for the set of solar-cell properties known and extrapolations used, the use of gallium-arsenide solar cells is very promising for near-sun probes. The Development Plan presented here defines the logical, experimental effort required to produce solar-array power supplies for use in solar missions. Some of the first areas to be investigated include determination of short- and long-term properties of solar cells, cover glasses, and adhesives (if used) at a variety of solar intensities, temperatures, and electromagnetic and particle radiations.

Because the vast majority of solar-array programs have been concerned with orbits in the vicinity of earth, very little test data has been reported for near-sun environmental simulation; some so-called high-intensity simulation tests assumed linearity of the very factors whose linearity was to be investigated.

Some areas of uncertainty can be explored initially in relatively inexpensive short-term measurement and study programs using cells now available. Other areas of uncertainty will require considerable effort in material development, cell production-line reinstatement, and cell development. Four limited programs to determine existing cell performance are recommended for immediate investigation; these programs constitute Phase I of the Development Plan. RCA is currently preparing a proposal for submission to NASA-ARC recommending task A of Phase I. The results of all of Phase I will determine whether further effort in the subsequent phases is warranted.

Phase II of the Development Plan consists of the intensive investigation and development of the gallium-arsenide material, solar cell, and associated array components (cover glass, optical bandpass filter, reflective and anti-reflective coatings, transparent adhesives, substrate materials, blocking diodes, etc.). Also included will be a development to minimize the irreversible damage done to some existing gallium-arsenide cells when maintained at temperatures of 475°K to 575°K for moderate durations. Pilot production of high-efficiency gallium-arsenide solar cells and ancillary components capable of sustained high temperature operation would hopefully result from the work performed during Phase II effort; the selection of covers, filters and adhesive techniques which yield a minimum of overall environmental degradation is the balance of the Phase II goal.

Phase III is the solar-array design, fabrication, and test portion of the Development Plan. During this phase, a solar-probe mission is specified, a solar-array system is designed, and the solar panels are fabricated, assembled with the necessary environmental control components, and subjected to qualification-level environmental testing. The output of the Phase III program would be a proof-of-principle panel employing a gallium-arsenide solar array with a thermal-control mechanism. This panel would be submitted to NASA.

Phase IV of the Development Plan follows the award of a hardware contract for the design, production, and testing of flight model solar-cell arrays for use on a particular solar mission.

The Development Plan schedule (Table 14) is based on series-sequencing of phases and, to a large extent, series-sequencing of tasks within each phase. This was done to minimize risk (as presently understood) at the expense of time. When the major development problems are more fully analyzed, an accelerated schedule can be defined. Thus, it is planned to use the results of the Phase I (Task A) effort to define an "accelerated" Development Plan compatible with earlier launches.

The following paragraphs present detailed descriptions of each phase of the development plan.

A. PHASE I: INVESTIGATION OF SOLAR-CELL AND SOLAR-CELL-ASSEMBLY CHARACTERISTICS

In this phase it is proposed to perform a limited amount of testing on the small stock of gallium-arsenide cells which are currently available. The intent of the phase is to obtain sufficient data of reasonable significance from the available gallium-arsenide cells.*

1. Testing of Solar-Cell Performance Characteristics

An accurate measure of high-intensity, high-temperature output characteristics of existing silicon and gallium-arsenide solar cells can be obtained by plotting the I-V curves of the cells at intensity increments up to at least the equivalent of 10 suns. A calibration technique must be applied that will define the relative intensity level. I-V curves at each intensity level should be plotted for several temperatures up to the point where the solar-cell efficiency approaches

* Once the inventory is consumed, the start-up of a production line will have to be undertaken, and material and cell development work reactivated, before more cells are available.

zero. Air-mass-zero I-V curve short-circuit currents, and series resistance measurements of the cells will be recorded before and after the high-intensity testing to detect possible performance degradation.

Solar cells with different grid spacing configurations will be tested and compared with theory to determine the optimum grid spacing as a function of solar irradiance.

The result of this measurement program would be a calculation procedure, based on measured data, which would permit the accurate extrapolation of silicon and gallium-arsenide solar-cell-output characteristics to the high-temperature, high-intensity, near-sun environment.

2. Determination of Temperature Effect on Filter and Cover-Glass Assembly and Determination of Filter Characteristics on Cell Temperature

In order to accurately determine the feasibility of utilizing gallium-arsenide solar cells for solar probe missions three effects should be examined: These are:

- (a) The effects of high temperature on the absorptivity and emissivity of the gallium-arsenide cell complete with filters and cover glass. This should be done for multiple temperatures from 273°K through 573°K. This should also be done for silicon cells up to about 473°K. The effect of angle of incidence on the absorptivity and emissivity of the cell assembly at elevated temperatures should also be determined. This experimental information would increase the accuracy of the temperature determination of the solar array. For solar-probe missions, accurate determination of solar-cell temperature is essential for power output predictions.
- (b) Another area of unknown effect at high temperatures is the stabilization and adhesion of multilayer anti-reflective coatings and cutoff filters on the cover glass. The adhesion of anti-reflective and filter coatings is a basic requirement at elevated temperatures. Poor adhesion at elevated temperatures would result in higher than expected cell temperatures. This test would be designed to substantiate this adhesion reliability and, if failures occur, to explore the failure mechanism.
- (c) An accurate performance evaluation of the effect of optimizing cutoff and bandpass filters for gallium-arsenide cells is also desirable. This would be done for two or three near-sun missions. The effect of cutoff and bandpass filters on solar cell temperature could then be verified. With the results verified from such a study, the optimum cutoff and bandpass wavelength for various missions would be determined. For near-earth missions this filter variance has a negligible effect on cell temperature. For near-sun missions this is probably not the situation and the degree of effect should be definitely determined.

3. Annealing of Charged-Particle Irradiation Damage in Solar Cells

Investigation conducted during the study program has determined that proton and electron bombardment of silicon solar cells in the missions studied produce extensive damage (up to 35-percent power decrease with silicon solar cells having 9 mils of fused-silica shielding); however, the damage to gallium-arsenide solar cells is negligible if these cells are protected with the same 9 mils of fused-silica shielding. Nevertheless, both types of cells should be investigated in the area of annealing of defects; this takes place at a rate directly related to temperature.

Recent reports have described the partial annealing of electron damage to silicon cells as a result of storing the solar cells at high temperatures (473°K) after room-temperature bombardment of the cells.

Recommendations are made for the following tests:

- (a) Electron bombardment of gallium-arsenide and n-on-p silicon solar cells while the cells are maintained at selected temperatures: (323, 373, 423, 473, 523, and 573°K; the last two values are for gallium-arsenide only). The bombardment should be carried out at three different rates, in order to permit extrapolation from the usual rapid bombardment of solar cells in the laboratory to the much slower, actual-environment process.
- (b) Proton bombardment of gallium-arsenide and n-on-p silicon solar cells, with cell temperature and bombardment rate variables as above. Results of this program would show: (1) whether silicon could not have usefulness, and (2) whether the reported high-temperature annealing may be treated as a net decrease in radiation-induced degradation rates.

4. Revision of Development Plan

Should the utility of gallium-arsenide solar cells continue to be encouraging, Phase II of the Development Plan will be recommended and Phases II, III, and IV will be redefined based upon the results of Phase I.

The Electronic Components and Devices Division of RCA is no longer engaged in research and development of gallium-arsenide solar cells. Therefore, the gallium-arsenide solar-cell production facilities have been dismantled and personnel reassigned. As a result, the schedule for the Development Plan shows the time required to re-organize and re-equip for this activity. With the successful completion of test work in Phase I, a detailed Development Plan (with cost included) for Phase II will be submitted as part of the Phase II effort.

B. PHASE II: DEVICE AND MATERIALS DEVELOPMENT

1. Solar Cell Development

The goal in this phase of the Development Plan is to produce gallium-arsenide solar cells and modules exhibiting long-term stable operation at temperatures approaching 573°K. Efforts towards increasing the power conversion efficiency of the cells will be undertaken. Optimum grid-size and spacing will be redetermined and production processes developed. Investigations of vapor deposition and pressure contacting of cover glass to the solar cell will be performed for the purpose of eliminating the cover-to-cell adhesive. All production processes will be determined and production equipment will be installed and operated. The result of this part of Phase II will be a pilot production of reproducible gallium-arsenide solar cells capable of operation in a solar probe mission.

2. Auxiliary Component Development

The following auxiliary components for the solar modules will be developed:

- (a) Cover glass to solar-cell adhesive,
- (b) Cover glass,
- (c) Optical filter coatings,
- (d) Thermal coatings exhibiting high emissivity and low absorptivity characteristics for the inactive area of the solar panel surface, and
- (e) Solar cell interconnecting leads and solder (selection based on the combination which results in stable low-resistance values and at high and low temperatures).

3. Environmental Testing of Solar Cells, Solar Modules and Module Components

Environmental testing will be performed on the solar cells, cover glasses, optical filters, and cover-glass adhesives. These tests will be performed individually and with the components assembled in modules. Where applicable, optical transmission and current-voltage relationships will be measured both before and after the following environmental tests:

- (a) High temperature/vacuum test,
- (b) Charged particle irradiation/thermal-vacuum tests (accelerated-annealing effects on cells and cover glasses included),
- (c) Ultraviolet irradiation/thermal-vacuum tests (accelerated), and
- (d) Vibration, acceleration, and shock tests on modules.

4. Revised Development Plan for Phases III and IV

The Development Plan for Phases III and IV will be revised to reflect the results of Phase II.

C. PHASE III: SOLAR PANEL DESIGN, DEVELOPMENT, AND TEST

1. Mission Definition

The following items will be defined:

- (a) Trajectory/time relationship.
- (b) Solar irradiance versus time profile,
- (c) Temperature versus time profile,
- (d) Charged particle flux versus time profile, and
- (e) Spacecraft thermal, mechanical, and electrical interface.

2. Analysis and Design Optimization

- (a) Solar-cell size, thickness, grid spacing, and efficiency range
- (b) Cover glass material and thickness

Consideration will be given to the following factors:

- (1) Transmissivity versus time in environment,
- (2) Weight effect of thermal expansion coefficient on thermal stresses,
- (3) Radiation shielding for cells,
- (4) Radiation degradation of transmissivity, and
- (5) Self-adhesion to cells.

(c) Cover-glass/solar-cell adhesive

Consideration will be given to the same material and thickness factors as for the cover glass. In addition, the adhesion strength and cell corrosion effect will be analyzed.

(d) Optical filter

Consideration will be given to the following factors:

- (1) Anti-reflection wavelength,
- (2) Cut-on wavelength,
- (3) Cut-off wavelength,

- (4) Optical reflectivity and transmissivity shift with angle of incidence, and
 - (5) Total reflection angle.
 - (e) Solar cell to substrate adhesive

Consideration will be given to the thermal stress influence of material and thickness, and to the long-term thermal and radiation effects on flexibility of adhesive.
 - (f) Substrate

Consideration will be given to weight, thermal conductance, and the expansion effect on solar cells over the specified temperature range.
 - (g) Electrical design of array
 - (h) Array diode and harness design
 - (i) Design of temperature-control coatings for the panel
 - (j) Design of the array thermal control subsystem
 - (k) Thermal model analysis of solar-array/spacecraft interfaces.
 - (l) Design specifications
 - (m) Drawings
3. Fabrication of Full- or Partial-Scale, Solar-Array Pre-Prototype with Thermal Control Subsystem
 4. Qualification Level Environmental Test of Solar-Array Pre-prototype

Tests will determine the current-voltage characteristics under several selected solar intensities, angles of incidence, and temperatures before and after the following environments:

 - (a) Thermal-vacuum,
 - (b) Ultraviolet irradiation during thermal vacuum, and
 - (c) Vibration, acceleration, and shock.
 5. Design and Fabrication of Prototype Solar-Array System
 6. Qualification Level Environmental Test of Prototype Solar Array

The solar-array prototype will be subjected to the following environments:

 - (a) Thermal-vacuum,
 - (b) Ultraviolet irradiation during thermal-vacuum, and
 - (c) Vibration, acceleration, and shock.

7. Delivery of Prototype Solar-Array System
8. Design of Special Test Equipment (STE)
9. Procurement, Fabrication, and Assembly of Special Test Equipment (STE)
10. Revised Development Plan for Phase IV

D. PHASE IV: DESIGN, FABRICATION, AND TEST OF FLIGHT-MODEL SOLAR-ARRAY SYSTEM

Phase IV of the Development Plan will consist of the following operations:

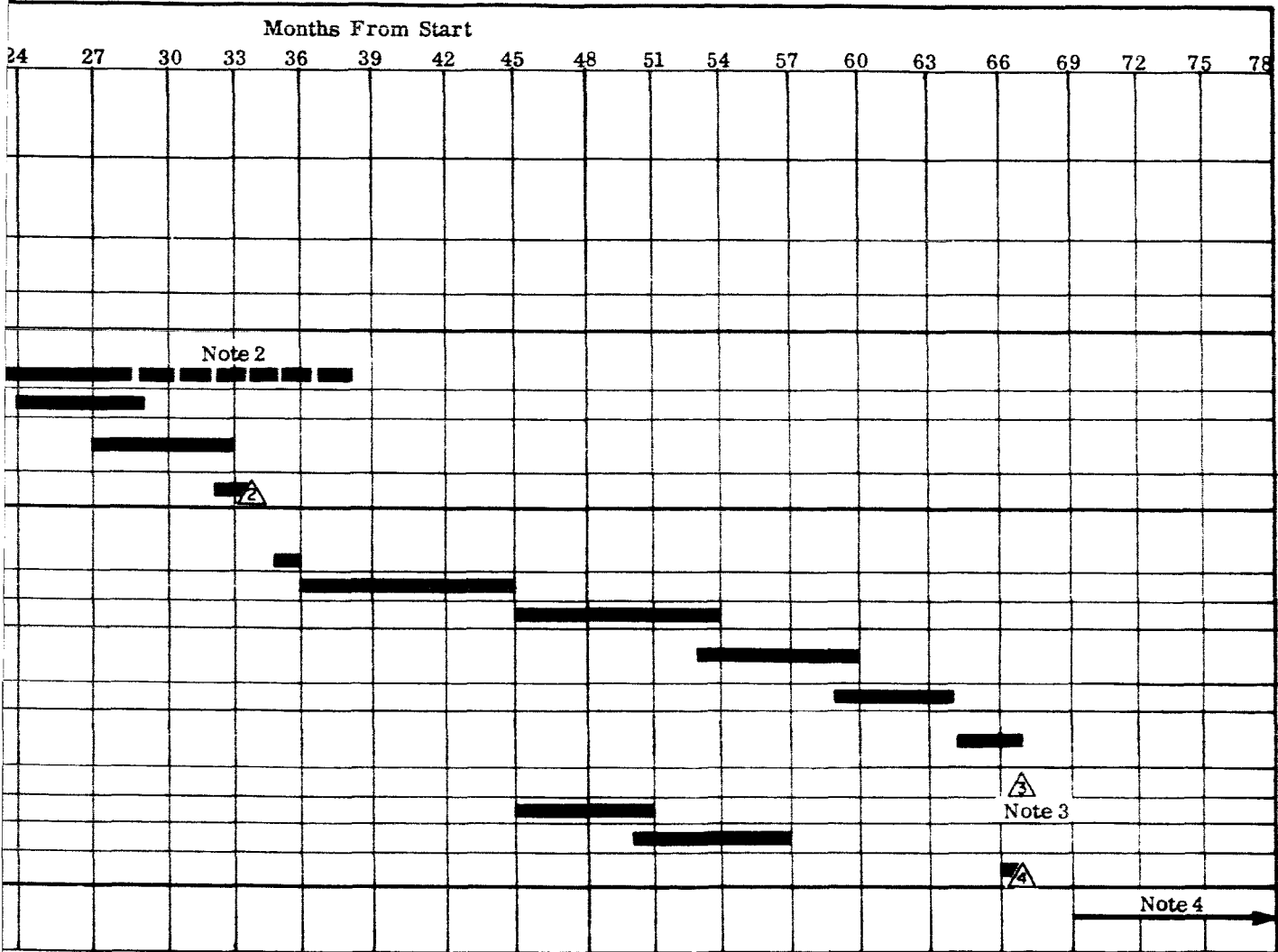
1. Final design,
2. Preparation of final purchase specifications for components and assemblies,
3. Procurement of components,
4. Fabrication of components,
5. Assembly of solar panel subsystem,
6. Assembly of thermal control subsystem,
7. Performance testing of subsystems,
8. Assembly of solar-array systems,
9. Environmental acceptance testing of solar-array systems,
10. Delivery of solar-array systems,
11. Design of ground support equipment (GSE),
12. Procurement of GSE components,
13. Fabrication of GSE,
14. Testing of GSE, and
15. Delivery of GSE.

TABLE 14. DEVELOPMENT PLAN

	0	3	6	9	12	15	18	21
PHASE I - Preliminary Evaluation of Existing Devices								
1. Testing of Solar-Cell Performance Characteristics at High Solar Intensities and a Variety of Temperatures								
2. Determination of Temperature Effect on Filter and Cover Glass Assembly and Determination of Filter Characteristics on Cell Temperature								
3. Annealing of Charged-Particle Irradiation Damage in Solar Cells								
4. Revised Development Plan								
PHASE II - Device and Materials Development								
1. Solar Cell Development								
2. Auxiliary Component Development								
3. Environmental Testing of Solar Cells, Solar Modules, and Module Components								
4. Revised Development Plan for Phases III and IV								
PHASE III - Solar Panel Design and Test								
1. Mission Definition								
2. Analysis and Design Optimization								
3. Fabrication of Pre-prototype Solar Array								
4. Qualification Level Environmental Test of Pre-prototype Array								
5. Design and Fabrication of Prototype Solar Array System								
6. Qualification Level Environmental Test of Prototype Array								
7. Delivery of Prototype Solar Array System								
8. Design of Special Test Equipment (STE)								
9. Procurement, Fabrication and Assembly of STE								
10. Revised Development Plan for PHASE IV								
PHASE IV - Design and Test of Flight Model Solar Array System								
LEGEND:	NOTES:							
△ Phase I completed	1. From the completion of each phase to the start of a subsequent phase or							
△ Phase II completed	2. Included in Solar Cell Development is the time required to re-equip a p							
△ Delivery of prototype	and cell improvement; and to set-up a pilot production line. Two time							
△ Phase III completed	the other estimate (dotted line) shows the estimate which applies if mat							
	maintaining schedule for the tasks is based upon the optimistic schedule es							
	3. The only item of hardware delivery shown on the Development Plan is							
	for testing will be made available at the request of NASA-ARC.							
	4. Phase IV time span is undefined at this time since the number of flight							

44-1


SCHEDULE



One month is allocated for an approval cycle.

Production facility; to conduct basic cell material development periods are shown: one gives an optimistic estimate (solid line); material and device problems are greater than foreseen. The re-estimate.

the Prototype Solar Array System. However, all samples used

models is not known.

REFERENCES AND BIBLIOGRAPHY

REFERENCES

1. Memorandum from J.R. Swain, NASA-ARC, "Selection of Solar Flare Model Envelope," (July 30, 1963)
2. Robley D. Evans, "Principles For the Calculations of Radiation Dose Rates in Space Vehicles," MIT Report No. 63270-05-01, Prepared Under NASA Contract No. NAS 5-664, (July 1961)
3. W.L. Brown, J.D. Grabbe, and W. Rosenzweig, "Results of the Telstar Radiation Experiment," The Bell System Technical Journal (July, 1964)
4. J.J. Wysocki and E. Davidson, "Proton Irradiation of Silicon and Gallium-Arsenide Solar Cells at 17.6 Mev," RCA Laboratories (Nov., 1962) (Company Private)
5. "Development of Improved Gallium-Arsenide Solar Cells," Electronic Components and Devices Division (ECD) of RCA, Mountaintop, Pennsylvania, Final Report Prepared Under NASA Contract NAS 5-9600
6. "Commercial Communications Satellite," Final Report by Bell Telephone Laboratories and the Astro-Electronics Division of RCA (April 1, 1965)
7. "Applications Report on Manufacturing Methods Program for Gallium-Arsenide Solar Cells," Electronic Components and Devices Division of RCA, Somerville, New Jersey, Technical Document Report No. ML-TDR-64-164 (July, 1964)
8. D. Berman and E. L. Ralph, Heliotek Division of Textron Electronics Inc. "Improved Solar Cells for Use in Concentrated Sunlight," report presented at Eighteenth Annual Power Sources Conference, Atlantic City, N. J.

BIBLIOGRAPHY

E. L. Ralph and P. Berman, Heliotek Division of Textron Electronics Inc., "Silicon Cells For Use in Concentrated Solar Energy," report presented at Seventeenth Annual Power Sources Conference, Atlantic City, New Jersey.

"Photovoltaic Space Power Systems," Summer Course at University of Pennsylvania, (1962), Course notes by S.H. Winkler, Astro-Electronics Division of RCA, Princeton, New Jersey.

J.J. Wysocki, "The Effect of Series Resistance on Photovoltaic Solar Energy Conversion," RCA Review (March, 1961).

APPENDIX

OPTIMUM GRID SPACING

Solar-cell optimizations have been primarily concerned with near-earth environments. For the solar-probe missions the level of sun irradiance increases as the inverse square of the distance from the Sun. For the 0.09-AU mission the sun irradiance is 123 times the near-earth level. This large increase can have a marked effect on solar-cell power output levels, and will result in a high current developed in the diffused layers of the cell. It can be easily seen that as this current level increases over its 1-AU value, much more power is dissipated in the cell (I^2R), and less power is supplied to the load. This is due to the sheet resistance of the diffused layer of the cell. This resistive loss can be minimized by placing a conductive grid structure over the solar cells. Use of the grid structure reduces the length of the conduction path and consequently decreases the sheet resistance in direct proportion to the number of grids. It was first thought that there would be an optimum grid number for the cell for each perihelion. Upon observation of the maximum power output versus orbit time (Figure 34) the limiting power for the gallium-arsenide cell was found to occur at 1 AU. Thus, the design point for the optimum grid number was chosen at the beginning of the mission.

The effect of high sun irradiance is presented in a report by Berman and Ralph.⁸ For sun irradiances of 1 to 5 Langleys, an 11 to 15 gridded cell was found to be optimum. However, when an 11 and 26 gridded cell were illuminated with 42 watts/cm², the efficiency and power output did not vary markedly. The 26 gridded cell was more efficient than the 11 gridded cell, but the difference was less than 1 percent even at the higher illuminations.

Based on Berman and Ralph's work on high-intensity multi-gridded cells and in view of the fact that the limiting power of gallium-arsenide cells occurs at 1 AU, it appears that the 1 × 2 cm cell should have 7 to 15 grid lines for optimum operation.